

T-2734

Carbon Dioxide Gasification
of
Ponderosa Pine Char

ARTHUR LAKES LIBRARY
COLORADO SCHOOL of MINES
GOLDEN, COLORADO 80401

by
Timothy Graham Bradley

ProQuest Number: 10782456

All rights reserved

INFORMATION TO ALL USERS

The quality of this reproduction is dependent upon the quality of the copy submitted.

In the unlikely event that the author did not send a complete manuscript and there are missing pages, these will be noted. Also, if material had to be removed, a note will indicate the deletion.



ProQuest 10782456

Published by ProQuest LLC (2018). Copyright of the Dissertation is held by the Author.

All rights reserved.

This work is protected against unauthorized copying under Title 17, United States Code
Microform Edition © ProQuest LLC.

ProQuest LLC.
789 East Eisenhower Parkway
P.O. Box 1346
Ann Arbor, MI 48106 – 1346

A thesis submitted to the Faculty and the Board of Trustees of the Colorado School of Mines in partial fulfillment of the requirements of the degree of Master of Science (Chemical and Petroleum-Refining Engineering).

Golden, Colorado

Date April 14, 1983

Signed: Timothy Graham Bradley
Timothy Graham Bradley

Approved: Michael S. Graboski
Michael S. Graboski
Thesis Advisor

Golden, Colorado

Date April 27, 1983

Philip F. Dickson
Philip F. Dickson
Head of Department
Chemical and Petroleum-
Refining Engineering

ABSTRACT

Powdered Ponderosa pine char was gasified with CO_2 in the temperature range 800°C to 1130°C . The apparent activation energy was found to be 34.2 kcal/mole. To determine the effect of thermal annealing on the gasification rate, char was pretreated at a temperature higher than the gasification temperature. A pretreatment activation energy of -19.8 kcal/mole and a true activation energy of 53.9 kcal/mole was determined for CO_2 gasification of the subject char.

Gasification rates for pine char pellets are significantly less than those for powdered chars at equivalent conditions. The activation energy for the gasification of pellets and powders are very close. The small difference in activation energy indicates that heat and mass transfer effects are insignificant in the gasification of pellets. It is postulated that as a result of the pelletization process, the surface area of pellets falls below the surface area of powders. This loss of surface area leads to a reduced reaction rate.

TABLE OF CONTENTS

ABSTRACT	iii
LIST OF FIGURES	vi
LIST OF TABLES	viii
ACKNOWLEDGEMENTS	ix
INTRODUCTION	1
PREVIOUS WORK	3
GASIFICATION REACTION THERMODYNAMICS	7
GASIFICATION KINETICS	19
DIFFUSION	32
GASIFICATION MODELS	40
EXPERIMENTAL EQUIPMENT	45
EXPERIMENTAL PROCEDURE	50
CHAR PRODUCTION	50
POWDER GASIFICATION	51
PELLET GASIFICATION	52
GAS DIFFUSION	52
RESULTS	54
GASIFICATION OF POWDERED CHAR	58
GASIFICATION OF POWDERED CHAR IN CO ₂	58
GASIFICATION OF POWDERED CHAR IN	63
CO ₂ /CO MIXTURES	
GASIFICATION OF PELLETS	71
DIFFUSION	75

HEAT TRANSFER	84
CONCLUSIONS	87
RECOMMENDATIONS FOR FUTURE WORK	89
REFERENCES CITED	90
APPENDICES	
A NOMECLATURE	94
B POWDER GASIFICATION DATA	96
C PELLET GASIFICATION DATA	100
D CO ₂ ADSORPTION DATA	101
E MERCURY INTRUSION POROSIMETER DATA	108
F EFFECTIVE DIFFUSIVITY CALCULATION	123

LIST OF FIGURES

Figure 1	Updraft Gasifier	4
Figure 2	Downdraft Gasifier	6
Figure 3	Air Gasification of Dry Wood - Gas Composition	12
Figure 4	Adiabatic Air Gasification of Dry Wood - Low Heating Value	13
Figure 5	Adiabatic Air Gasification of Wood - Energy in Product Gas	14
Figure 6	Oxygen Gasification of Dry Wood - Product Gas Composition	16
Figure 7	Adiabatic Flame Temperature	17
Figure 8	Oxygen Gasification of Wet Wood - Product Gas Composition	18
Figure 9	Low Heating Value vs Equivalence Ratio	20
Figure 10	Reaction Rate as a Function of C_{H_2O} and/or C_{CO_2}	28
Figure 11	Influence of Burnout on the Gasification Rate of Poplar Wood in Steam-Argon Mixture	31
Figure 12	Effect of Char-Preparation Temperature on Rate Constant in Hydrogen	33
Figure 13	Schematic of Experimental Equipment	46
Figure 14	Experimental Reactor	48
Figure 15	Pellet Press Dies	49
Figure 16	Char Make	56
Figure 17	Fractional Conversion vs Resident Time	61
Figure 18	$-\text{RATE}/P_{CO_2}$ vs Temperature ⁻¹	62

Figure 19	$-\text{RATE}/P_{\text{CO}_2}$ vs Temperature ⁻¹	65
Figure 20	Reaction Rate vs $1/P_{\text{CO}_2}$	67
Figure 21	Calculated Rate vs Temperature ⁻¹ at Different P_{CO_2}	69
Figure 22	Calculated Rate vs Temperature ⁻¹ at Different P_{CO_2}	70
Figure 23	Rate vs Temperature ⁻¹ for Different Pellet Diameters	72
Figure 24	Ratio of Experimental Rate to Calculated Rate vs Temperature - $\frac{1}{2}$ " Pellets	74
Figure 25	CO ₂ Adsorption vs Time - $\frac{1}{2}$ " Pellet	77
Figure 26	Cumulative Pore Volume and Surface Area vs Pore Size	81
Figure 27	Incremental Pore Volume vs Pore Size	82
Figure 28	Incremental Surface Area vs Pore Size	83
Figure 29	Radial Temperature Gradient vs Temperature for $\frac{1}{2}$ " & $\frac{3}{4}$ " Pellets	85

List of Tables		Page Number
Table 1	Gasification Reactions	8
Table 2	Typical Analysis for Dry, Sulfur and Ash Free Wood	10
Table 3	Activation Energy of Carbon-CO ₂ Reaction	29
Table 4	Apparent Activation Energy and Frequency Factor for Steam Gasification	30
Table 5	Effective Diffusivity for CO ₂ -N ₂ in Graphite	38
Table 6	Effective Diffusivity of CO ₂ in Ar Calculated from Overall Rate	39
Table 7	Calculated and Experimental Residence Times for Overall Char Conversion	43
Table 8	Ponderosa Pine Feedstock Analysis	55
Table 9	Proximate and Ultimate Analysis of Biomass Chars	57
Table 10	Rate Constants for a Number of Temperatures	68
Table 11	Effective Diffusivity of CO ₂ in Char	78
Table 12	Mean Pore Sizes for Different Chars	80

Acknowledgments

I wish to thank Dr. Michael S. Graboski for his guidance and encouragement as my thesis advisor. Special thanks to my family, Kathrine, Adam, Mollie and Mary for their patience and support.

The financial support from the Solar Energy Research Institute, Department of Energy, Contract DE-FG02-80CS84002 is gratefully acknowledged.

Many thanks to the various people who assisted in this program at one point or another.

INTRODUCTION

In the 19th century wood was the dominant energy source in the United States. Today the largest volume use of wood on a worldwide basis is still for energy (firewood). In the developed countries, wood for energy on an industrial scale has been almost completely replaced by fossil fuels. But, as the price of fossil fuels increases and their availability becomes uncertain, there is renewed interest in wood energy.

It has been estimated that even without counting any wood harvested for conventional forest products, about 560 million tons are available for energy production in the United States. That is the equivalent of 9.5 quads of energy, or about 12 percent of the energy required by the United States in 1980⁽¹⁾. While many energy users are able to utilize wood directly by combustion, many industrial processes are limited to gaseous or liquid forms of fuel. Two major objections to wood as an energy source are the energy density of the material and its available form. Pelletization of wood products solves the problem of energy density as the energy density of pelletized wood approaches that of coal⁽²⁾. To convert the pelletized wood to a more usable form, an applicable technology is gasification.

Wood as a gasification feed compares well with coal and other fossil fuels. The typical heating value of a dry wood material is 8500 BTU/lb, in comparison to 10,000 BTU/lb for lignite coal. Pollution problems associated with gasification are minimized when using wood, as the sulfur and ash content of wood is lower than that of coal. The principle advantage of wood as a gasification feedstock is that it is a renewable resource.

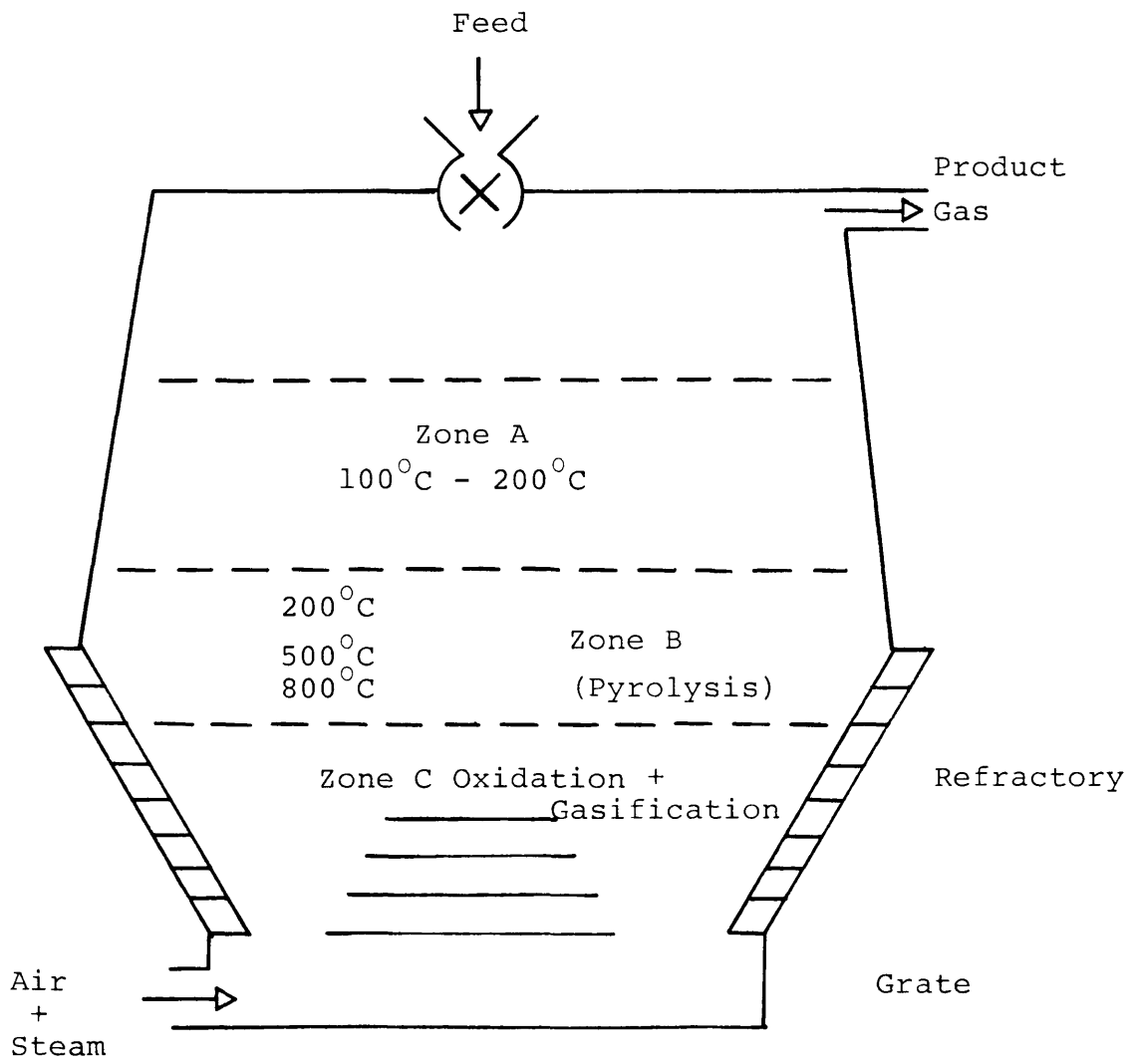
A research program supported by the Department of Energy has set out to investigate the pyrolysis and gasification kinetics of densified biomass. The work presented here demonstrates the effects of temperature and pellet physical properties on CO₂ gasification kinetics. The data gained in this research will be useful for gasifier design and scale up.

PREVIOUS WORK

Gasification is a process which converts a solid fuel into easily handled fuel gases. Typically this is a two stage process. The gasifier feed is first pyrolyzed and the resultant char is gasified. Pyrolysis of the gasifier feed produces CO, H₂, CO₂, hydrocarbons, condensibles and a carbonaceous residue or char. Gasification of the char can occur by a number of reactions to produce a fuel gas or a synthesis gas. A number of gasifier configurations are available. These include fixed bed, entrained bed and fluid bed gasifiers. Fixed bed systems are relatively simple and have been popular since the early 1900's.

Fixed bed gasifiers may be designed to operate in either an updraft or a downdraft mode. The flow scheme for an updraft gasifier is illustrated in Figure 1 (3). The gasifier feed descends through the three zones illustrated and the air (or oxygen) ascends through the oxidation zone, the pyrolysis zone and finally the drying zone before being taken off, cleaned as necessary and used as a fuel gas.

FIGURE 1
Updraft Gasifier⁽³⁾



The reactions occurring are:

Zone A - Drying at 100-200°C

Wet wood + Heat → dry wood + steam

Zone B - Pyrolysis at 200-500°C

Dry wood + Heat → Char + CO + CO₂ + H₂

+ hydrocarbons

+ condensibles

Zone C - Oxidation of Char at 1100-1500°C

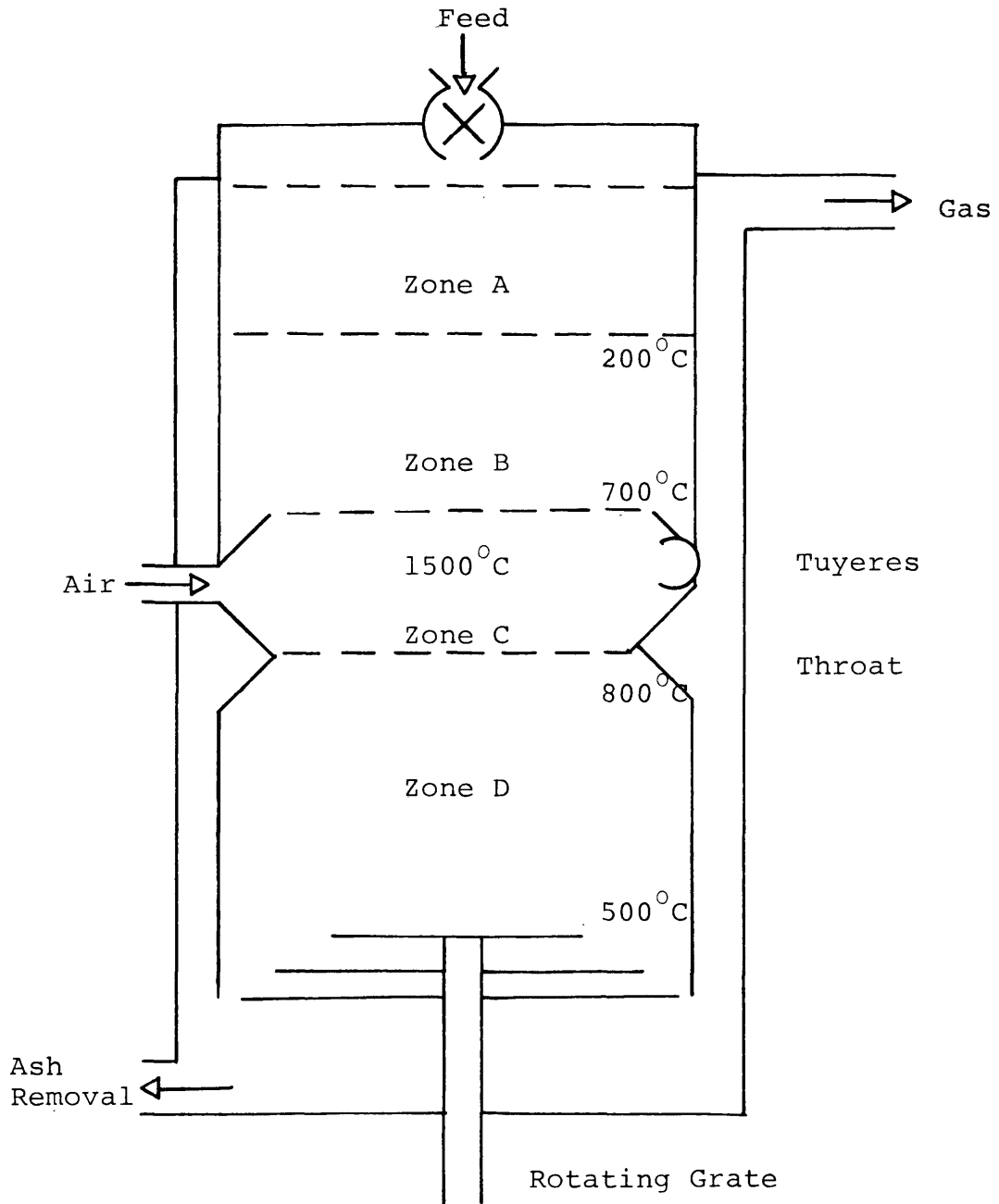
Char + O₂ + H₂O* → CO + H₂O + CO + Heat

(*Steam either added or in feed)

The first two processes are driven by the heat given out in the oxidation zone. Oxidation of carbon to CO₂ is the sole source of heat to drive the process and explains why the overall process efficiency of this gasification process will not exceed about 70%. The efficiency is limited as part of the fuel input is required to maintain the high temperatures of the oxidation and gasification zone.

In the downdraft design the air (or oxygen) enters the gasifier with the feed. While the updraft gasifier will always produce tars from wood, the downdraft design is configured so that the tars and other gases all have to pass through the hot oxidation zone, C. Figure 2 illustrates how the gases produced by the combustion and cracking of the

FIGURE 2
Downdraft Gasfier

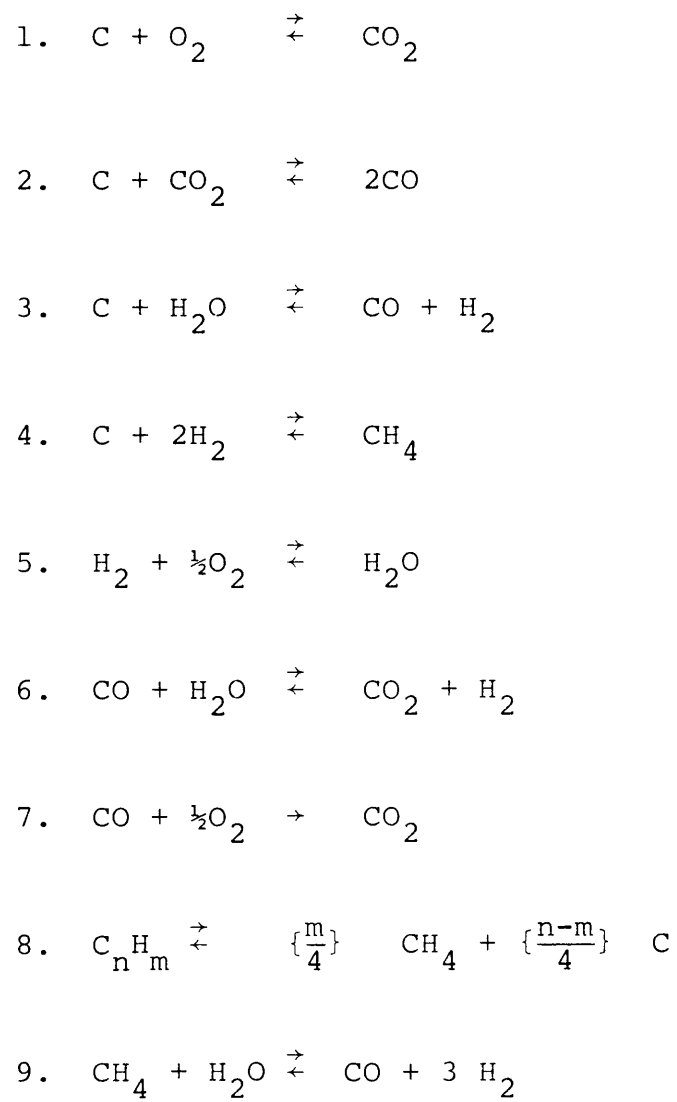


tars are then passed along with solid carbon into the reaction zone, D. This zone serves to reduce carbon dioxide and water vapor to carbon monoxide and hydrogen by means of the Boudouard and water gas reactions. These two reactions are endothermic and eventually they cool the char and ash to below 600°C . The reaction then ceases and fixes the final gas composition. In both up and downdraft units, the size of the reactor is defined by the char- CO_2 and steam gasification kinetics.

Gasification Reaction Thermodynamics

The process chemistry associated with wood gasification is reasonably complex and dependent on reactor design, operating conditions and feedstock characteristics. Many of the possible reactions are listed in Table 1⁽⁴⁾. Reactions 1 through 4 involve the gasification of the fixed carbon in the wood. Reaction 1 is the oxidation of carbon to carbon dioxide which is highly exothermic. The carbon is further gasified by CO_2 and steam via reactions 2 and 3. These two reactions are highly endothermic. Finally, the carbon may be gasified by hydrogen to produce methane. Reaction 4 is exothermic and unfavorable at high temperature.

Table 1



The oxidation reactions 5 and 7 are exothermic and essentially irreversible. Reaction 6, the water-gas shift reaction, is reversible and exothermic. Upon rapid heating, the volatile matter in the wood decomposes to release methane and higher hydrocarbons as in reaction 8. Methane and higher hydrocarbons may be steam reformed to carbon monoxide and hydrogen as shown in reaction 9.

A few gasifiers, such as the downdraft or fluidized bed with recycle, will approach equilibrium. For these systems, equilibrium predictions are useful in modeling gasifier performance. For updraft systems, the product gas is in a highly non-equilibrium state because the pyrolysis products remain intact. Equilibrium models are not useful for these systems. A number of equilibrium calculations have been done by Desoriers⁽⁵⁾. The calculations were based on a typical analysis for dry, sulfur free and ash free wood shown in Table 2. Carbon as graphite is the only solid product considered. To aid in describing wood pyrolysis, gasification and combustion, the concept of equivalence ratio is used. The equivalence ratio (ER) is defined as the oxidant to fuel weight ratio divided by the stoichiometric ratio.

$$ER = \frac{\text{weight oxidant/weight dry wood}}{\text{stoichiometric oxidant/wood ratio}} \quad 10$$

Complete combustion of the typical wood defined in Table 2 with oxygen requires 1.476 grams O₂ per gram of wood or 6.364 grams air per gram of wood.

Table 2

Typical Analysis for Dry, Sulfur and Ash Free Wood

Composition	C	52.5 wt %
	H	6.16
	O	41.24
	N	0.10
High Heating Value (HHV)	-22.21 kJ/kg	(-9550 BTU/lb)
Low Heating Value (LHV)	-20.90 kJ/kg	(-8987 BTU/lb)
Heat of Formation	- 3.74 kJ/kg	(-1609 BTU/lb)

Formula

C_6 basis	$C_6 H_{8.39} O_{3.54} N_{0.1}$	(FW = 137.27)
C_1 basis	$C H_{1.4} O_{0.59} N_{0.017}$	(FW = 22.86)

Equilibrium calculations for dry wood gasified in air are illustrated in Figures 3, 4 and 5. Dry gas composition as a function of the equivalence ratio is shown in Figure 3. An equivalence ratio of zero corresponds to pyrolysis. The principal products at an equivalence ratio of zero are hydrogen and solid carbon, followed by H_2O , CO_2 , CO and a trace of CH_4 . As the equivalence ratio is raised to the end of the carbon stability region, ($ER = 0.275$), gasification is taking place and solid carbon is consumed. Principal products now are H_2 and CO . Further addition of air results in consumption of H_2 and CO until combustion conditions at $ER = 1.0$ are reached. The low heating value (LHV) as a function of the equivalence ratio is demonstrated in Figure 4. The initial decrease in LHV is due to the decrease in the mole fraction of CH_4 . Further decreases in LHV are due to the consumption of CO and H_2 as the equivalence ratio is raised to the combustion point. In Figure 5 the sensible, chemical and total energy is plotted against the equivalence ratio. Note that in Figures 3, 4 and 5 there is an inflection point for each curve at $ER = 0.255$, corresponding to total carbon uptake. This is the point that an air blown gasifier should be operated.

Equilibrium calculations similar to those for air blown gasification have been made for oxygen gasification. Figure 6 illustrates the dry gas composition as a function of the

FIGURE 3
Air Gasification of Dry Wood 1 atm
Gas Composition⁽⁵⁾

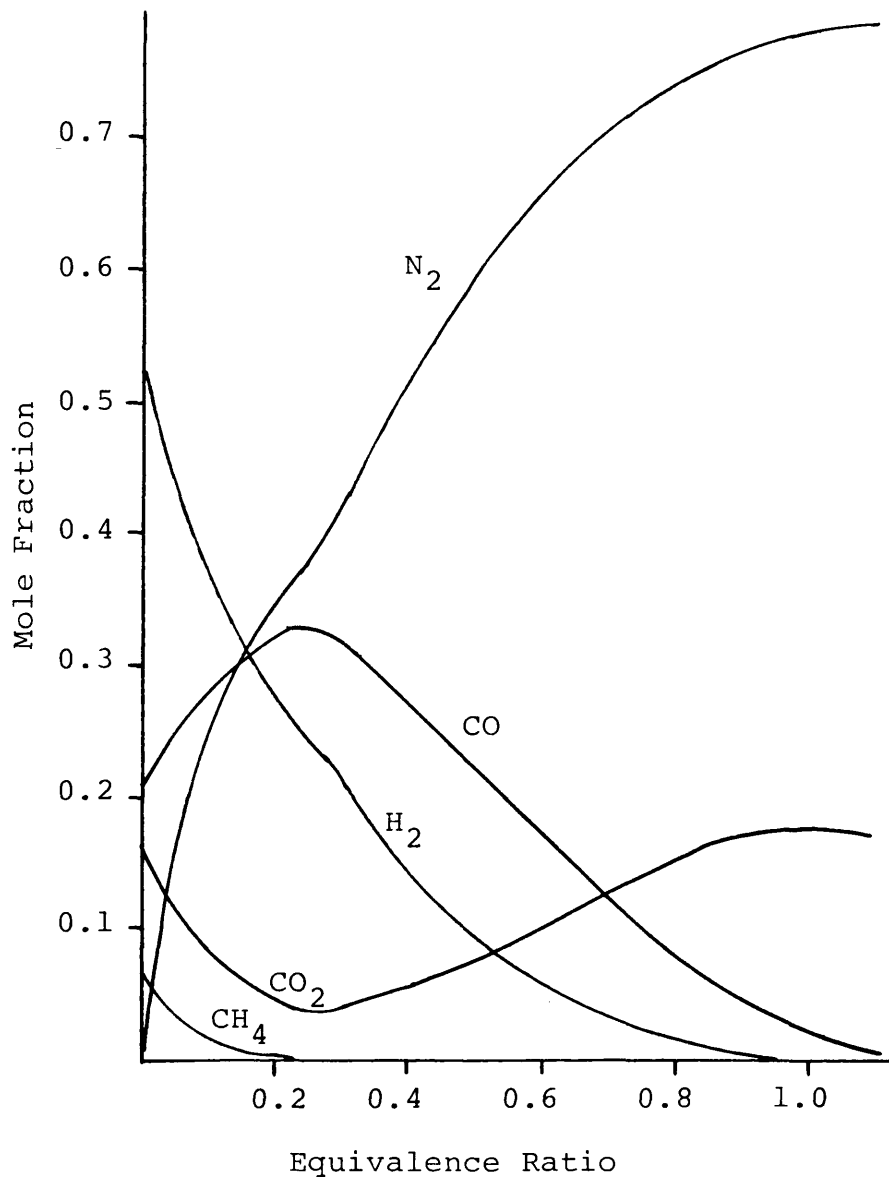


Figure 4
Adiabatic Air Gasification of Dry Wood @ 1 atm
Low Heating Value⁽⁵⁾

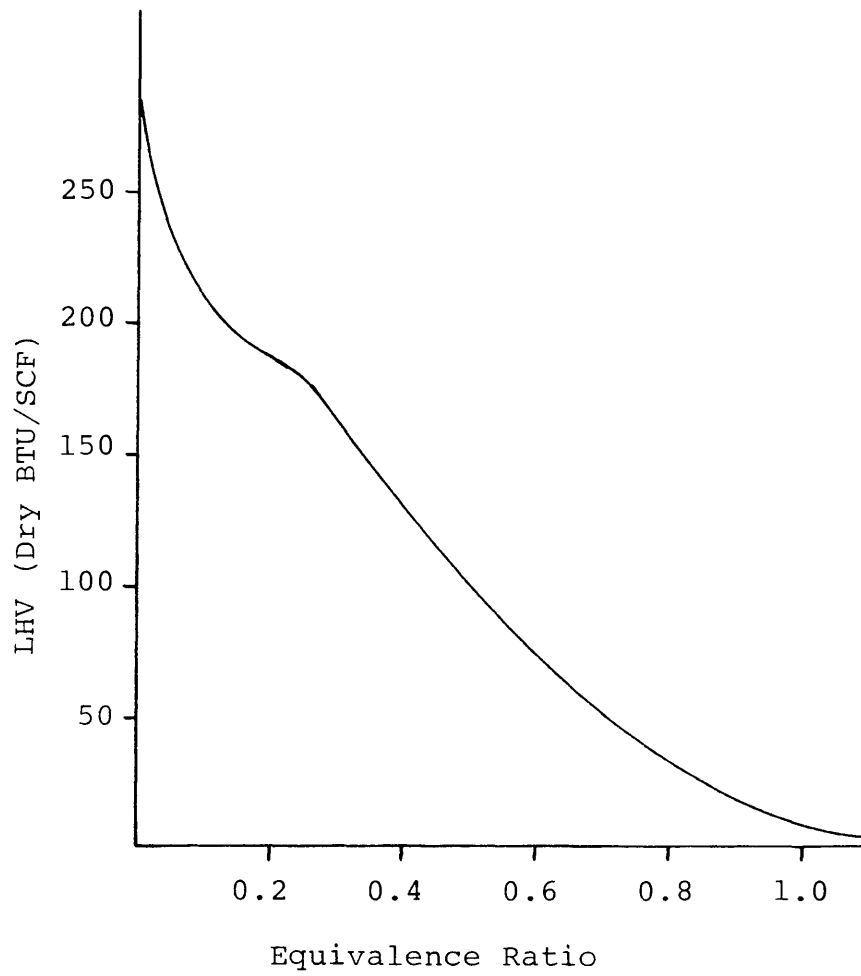
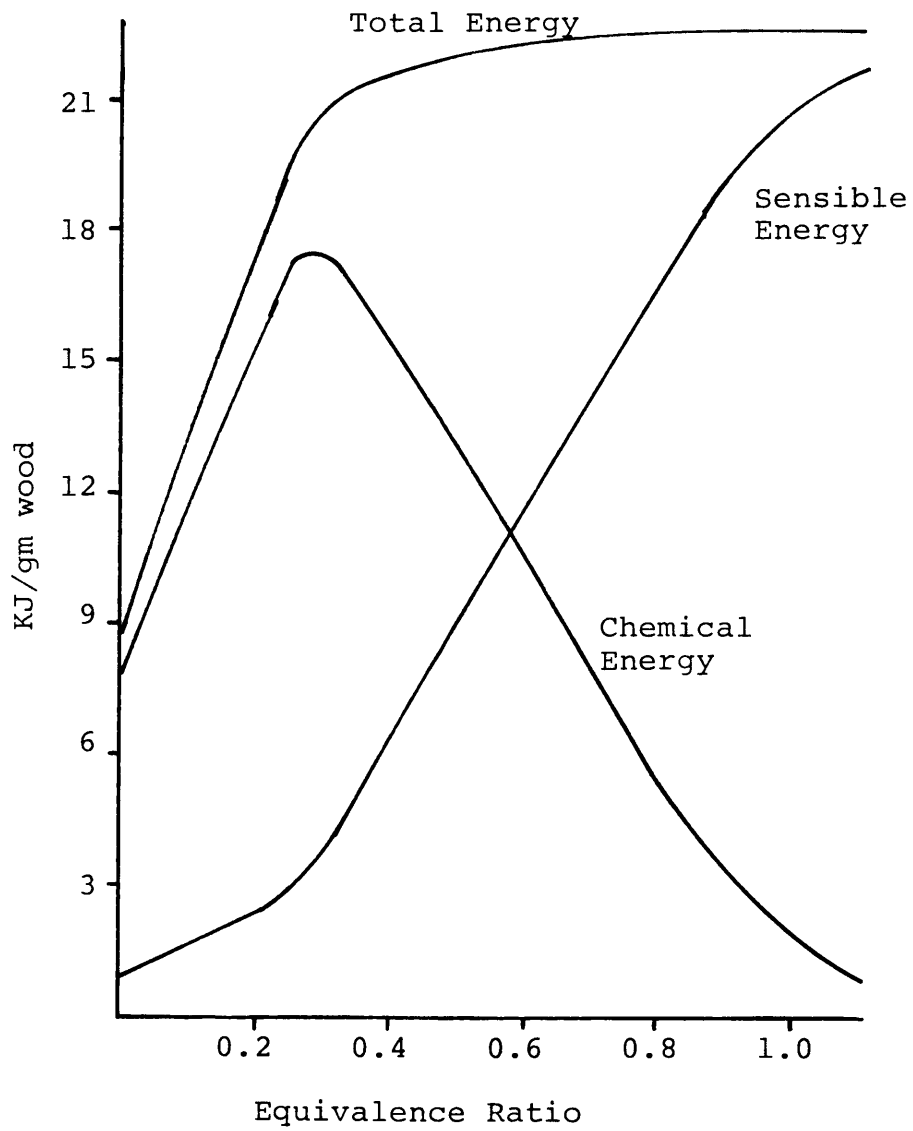


Figure 5
Adiabatic Air Gasification of Wood
Energy in Product Gas⁽⁵⁾
1 atm



equivalence ratio. Figures 3 and 6 would be identical if the diluent nitrogen from the air is neglected.

The water in wet wood used for gasification has a significant effect on the reaction process. Figure 7 illustrates the effect of water on the calculated adiabatic flame temperature for both oxygen and air blown gasification. For a given equivalence ratio, as the gasifier feed is switched from dry wood to wet wood, the adiabatic flame temperature decreases. Water or the resultant steam is not just a diluent; the gasification of carbon by steam is strongly endothermic and will depress the adiabatic flame temperature. As would be expected, the presence of water has a strong effect on the composition of the product gas. In Figure 8, the dry gas composition for the oxygen gasification of wet wood is shown. Notable is the initial high concentration of methane and carbon dioxide. The gasification of carbon by hydrogen to produce methane is unfavored at high temperatures; thus, as the equivalence ratio increases, the adiabatic flame temperature increases and methane production drops off. While methane production is decreasing, hydrogen production increases. The mole fraction of hydrogen reaches a maximum just as methane production ceases. The changes in product gas composition due to the presence of water in the gasification process is reflected in the low heating value of the gas.

FIGURE 6
Oxygen Gasification of Dry Wood at 1 atm
Product Gas Composition⁽⁵⁾

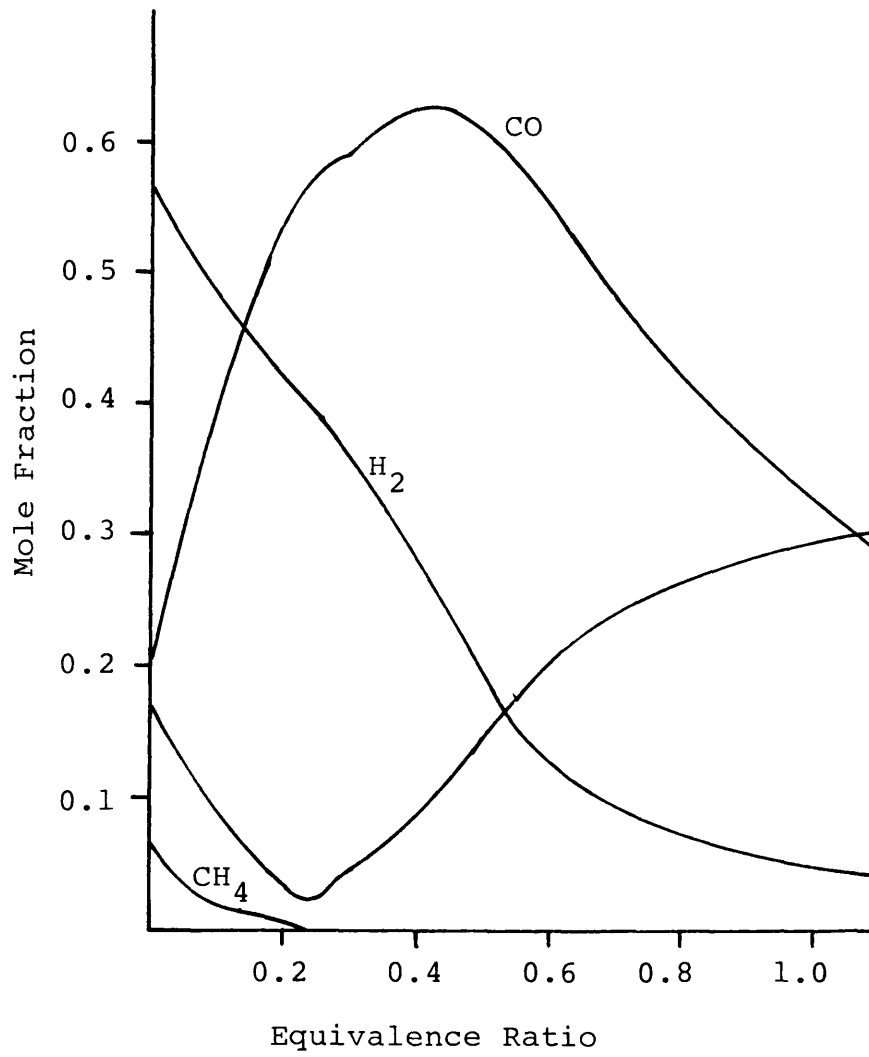
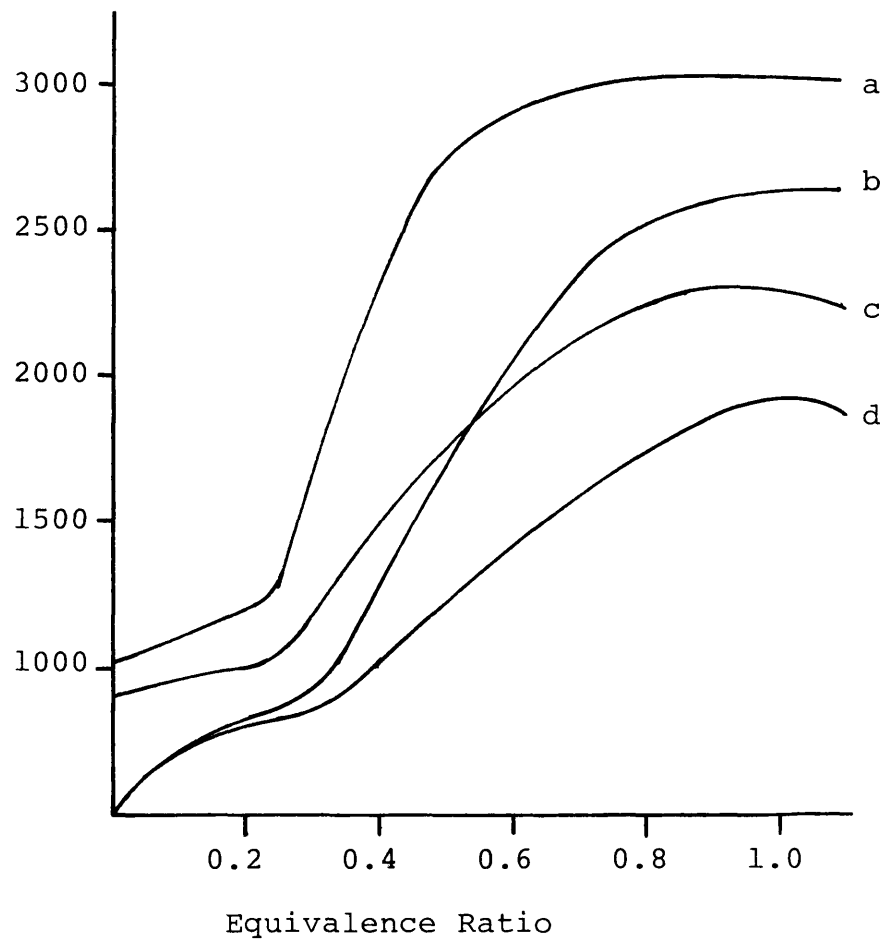


FIGURE 7
Adiabatic Flame temperature⁽⁵⁾



- a oxygen and dry wood
b oxygen and 0.8 gm H₂O/gm wood
c air and dry wood
d air and 0.8 gm water/gm wood

FIGURE 8
Oxygen Gasification of Wet (80%) Wood at 1 atm
Product Gas Composition⁽⁵⁾

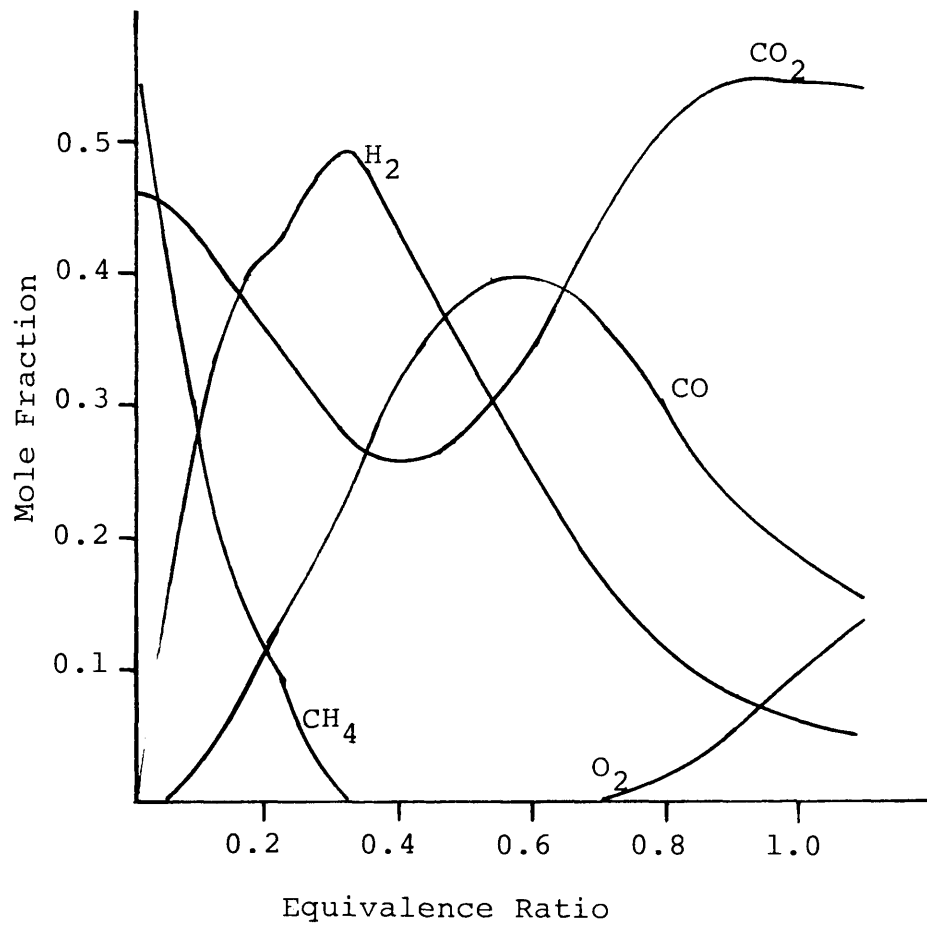


Figure 9 compares the low heating value for the product gas from air blown, oxygen and oxygen with water gasification. The initial high methane content in the product gas from oxygen blown gasification of wet wood yields a product with a high LHV. As the equivalence ratio increases, the LHV for oxygen gasification of wet wood drops below the LHV for oxygen gasification of dry wood. The LHV for air blown gasification is lower than the LHV for either of the two oxygen systems due to dilution by nitrogen.

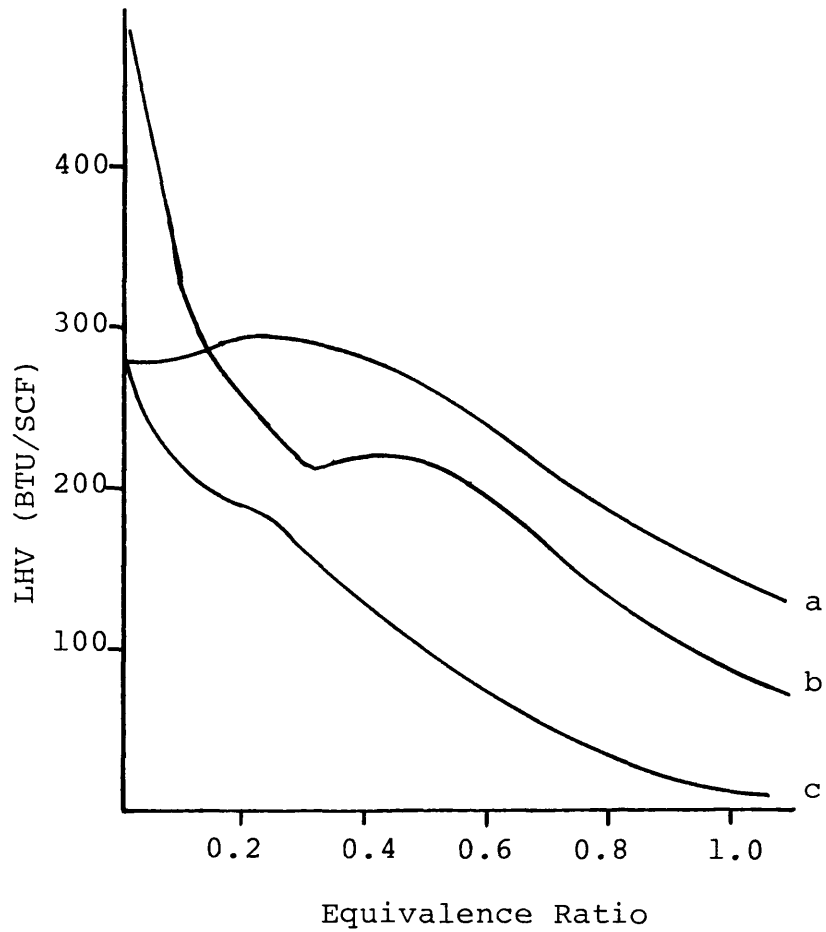
Gasification Kinetics

The simplest rate expression applicable to high temperature gas solid reactions was developed by Langmuir (for single site mechanisms); Hinshelwood later extended the model to dual site mechanisms⁽⁶⁾. Three assumptions are inherent in the Langmuir-Hinshelwood mechanism:

1. The surface is homogenous with uniform distribution of active sites.
2. There is no interaction among adsorbed species.
3. Surface migration is either nonexistent or so rapid that only adsorption and desorption can be rate-controlling.

For the char-CO₂ reaction, several rate expressions of the Langmuir-Hinshelwood type have been proposed by various investigators on the basis of the concepts of adsorption and

FIGURE 9
Low Heating Value vs Equivalence Ratio ⁽⁵⁾



- a Oxygen and dry wood
- b Oxygen and 0.8 gm water/gm wood
- c Air and dry wood

desorption of gases on solid surfaces. These rate expressions are of the following general form:

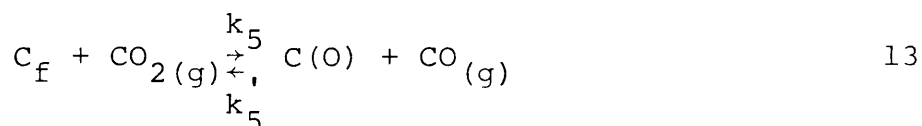
$$- \text{Rate} = \frac{k_1 A^X}{k_2 + k_3 A + k_4 B} \quad 11$$

for a reaction of the type



where k_1 , k_2 , k_3 and k_4 represent the rates of the various steps in adsorption, desorption and reaction involved in the proposed reaction mechanism, and A and B are the concentration of the reactant and product gases respectively.

Many mechanisms have been proposed for the char- CO_2 reaction. The one proposed by Menster and Ergun⁽⁷⁾ is as follows:



The rate expression for this mechanism is:

$$- \text{Rate} = \frac{dX/dt}{1-X} = \frac{k_c \text{CO}_2}{1 + k_{c1} \text{CO}_2 + k_{c2} \text{CO}} \quad 15$$

$$k_c = k_5 \quad k_{c1} = \frac{k_5}{k_6} \quad k_{c2} = \frac{k_5}{k_6}$$

Carbon monoxide will have an inhibiting effect on the char- CO_2 reaction as reaction 14 is irreversible. Moreover, the

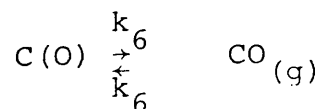
order of the reaction with respect to the CO_2 concentration will tend toward unity at low partial pressure and to zero at high partial pressures of CO_2 . At sufficiently high total pressure, equation 15 will reduce to the following expression:

$$-\text{Rate} = \frac{k_c^*}{1 + k_c^* \text{PCO}/\text{PCO}_2}$$

$$k_c^* = k_c/k_{c2} \quad k^* = k_{c1}/k_{c2}$$

Reaction 13 represents an oxygen exchange reaction in which a carbon dioxide molecule dissociates at an active site, C_f , on the carbon surface, releasing a molecule of carbon monoxide and forming a solid carbon-oxygen complex, $C(O)$. This reaction, considered reversible, results only in the exchange of oxygen with the solid and does not result in gasification of solid carbon. The actual carbon gasification occurs in reaction 14, with the dissociation of the carbon-oxygen surface complex from the bulk carbon matrix, leading to the formation of carbon monoxide and to the generation of a new active center on the solid carbon surface. Menster and Ergun have shown that the oxygen exchange reaction (14) is correct by employing tracers in the studies.

In a more recent analysis, reaction 14 has been postulated to be reversible⁽⁸⁾.



Assuming that the total number of active sites plus carbon-oxygen complexes is constant and assuming further that under steady-state conditions the net rate of formation of carbon-oxygen complexes is zero, the following rate expression has been derived:

$$- \text{rate} = \frac{k_5 n_t P_{\text{CO}_2} \left[1 - (k_5^1 k_6^1 / k_5 k_6) (P_{\text{CO}}^2 / P_{\text{CO}_2}) \right]}{1 + (k_6^1 / k_6) + (k_5^1 / k_6) P_{\text{CO}} + (k_5 / k_6) P_{\text{CO}_2}} \quad 18$$

where n_t is the concentration of total free active sites plus oxygen-carbon complexes in moles/moles solid carbon. Equation 18 is analogous to equation 15 with the following identities:

$$\begin{aligned} k_c &= k_5 n_t \\ k_{c1} &= \frac{k_6^1}{k_6} + \frac{k_5^1}{k_5} \\ k_{c2} &= k_5 / k_6 \end{aligned}$$

To satisfy thermodynamic equilibrium requirements, the term $(k_5^1 k_6^1 / k_5 k_6)$ in equation 18 should be equal to the equilibrium constant, $k_{5,6}$, for the overall reaction given by reaction 11. Generally though, gasification reactions are far from equilibrium and the simpler form of equation 16 is applicable.

A number of other mechanisms for the char- CO_2 reaction have been proposed. Goldberg and Yavorskii⁽⁹⁾ have investi-

ated two different mechanisms for the inhibition of the char-CO₂ reaction by CO. The first, mechanism A, is described by the following sequence of reactions:



Mechanism B is represented by:



If all the conditions for a Langmuir scheme are satisfied for both mechanisms, then rate equation 15 is applicable for both mechanisms. It is not possible, then, to make a choice between the mechanisms on the basis of only one type of dependence of the rate of gasification on the pressures of CO and CO₂. Based on an evaluation of the pre-exponential factors derived from experimental data and from statistical thermodynamics, mechanism B is found to fit within the framework of the simple Langmuir system.

The rate expression in the form of equation 15 is attractive from a mechanistic view, but, its applicability for design purposes is limited because of the requirement of more than one arbitrary rate constant. For practical purposes, empirical rate expressions which involve the use of only one or two rate constants to account for the effect of concentration on individual reactions are useful. The rate constants of these empirical expressions are deter-

mined comparatively easily from experimental time-conversion data. The general empirical expression⁽¹⁰⁾ for a volumetric reaction without mass transfer limitations may be expressed in the following form:

$$\frac{dX}{dt} = k_v \cdot \alpha_v(X,T) \cdot A^n \cdot s^{m-1} \cdot (1-X)^m \quad 23$$

where X is the conversion of carbon in the char-gas reaction, k_v is the volumetric reaction rate constant having a dimension of $L^{3(m+n-1)}/\text{mole}^{m+n-1} \cdot \theta$ and $\alpha_r(X,T)$ represents the relative available pore surface area of particles and is a function of carbon conversion and temperature. For reactions at one atmosphere and 850°C to 1080°C Dutta et al⁽¹¹⁾ expressed gasification rates with a correlation having the form:

$$- \text{Rate} = \frac{dX/dt}{(1-X)} = a k_v C \quad 24$$

where C is the carbon dioxide concentration and "a" is a parameter that reflects the relative available internal char surface area. For initial gasification rates, where a=1 by definition, the rate equation reduces to:

$$\frac{dX/dt}{(1-X)} = \frac{k_v}{RT} \quad 25$$

The application of this type of rate law is dangerous over a wide range of gas compositions.

In their study of char gasification by CO₂ and H₂O, Groenveld and van Swaij⁽¹⁶⁾ utilized rate expression 26.

$$- \text{Rate} = k C_s (C_{\text{CO}_2} + C_{\text{H}_2\text{O}})^{0.7} \quad 26$$

This equation is limited to atmospheric pressure and treats the complex concentration dependency using a fractional power exponent. The experimental activation energy is 51.9 kcal/gm-mole. Reaction rate is a function of C_{H_2O} and/or C_{CO_2} is shown in Figure 10. In their work with coal, Wen et al⁽¹⁷⁾ correlated their rate with a power-law rate expression

$$\frac{dx}{dt} = a k^n C^n (1-x) \quad 27$$

where "a" represents the relative available pore surface area. Activation energies for different particle sizes are shown in Table 3.

Graboski⁽¹⁸⁾ has shown that the kinetic behavior of different carbons in steam and CO₂ are similar and that the steam reaction is 3 to 5 times faster. Therefore steam kinetics are useful for the relative ranking of materials of variable reactivity in CO₂. In a study of biomass gasification processes, Rensfelt et al⁽¹⁹⁾ compared the apparent activation energy and frequency factor for a number of carbon sources. A first order rate expression was used to interpret their steam gasification results. The experimental values for activation energy, frequency factor and relative rates are shown in Table 4. Rensfelt's study points out the importance of the carbon source in terms of reactivity. Under similar conditions, most biomass materials gasify at rates an order of magnitude greater than coals. For large particles, mass transfer then might be more important for biomass than for coals. Within the study the effect of burnout on gasification rate was determined. Their relationship between burnout and gasification rate is illustrated in Figure 11 for the gasification of poplar wood in a steam-argon mixture. Recasting Rensfelt's data in terms of $-\text{rate} = \frac{1}{\bar{w}_0} \frac{dW}{dt}$ greatly reduces the strong effect of inventory on kinetics thus simplifying the correlation.

FIGURE 10
Reaction Rate as a Function
of C_{H_2O} and/or C_{CO_2} (16)

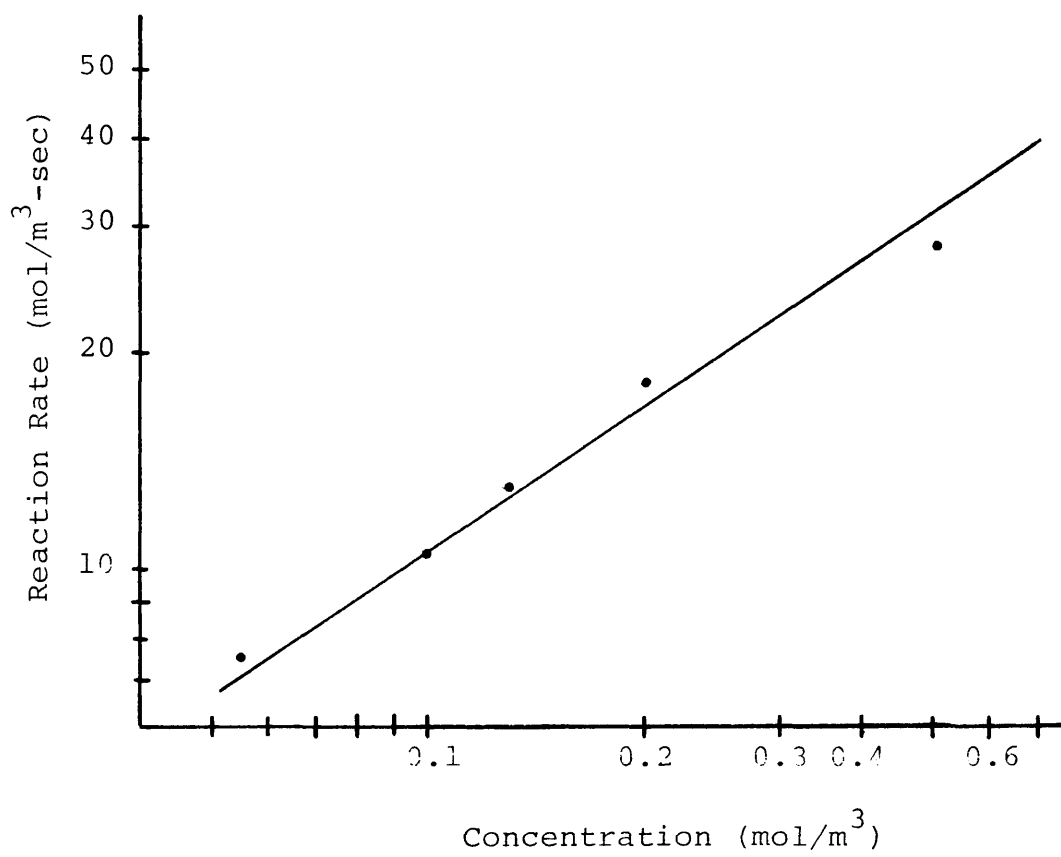


Table 3

Activation Energy of Carbon - CO₂ Reaction (17)

Temperature Range °C	Activation Energy E kcal/mole	Type of carbon
850-1100	59.26	coal char 300 microns
850-1100	75	coal char 50 microns
850-1100	59.2	coal char 325 microns

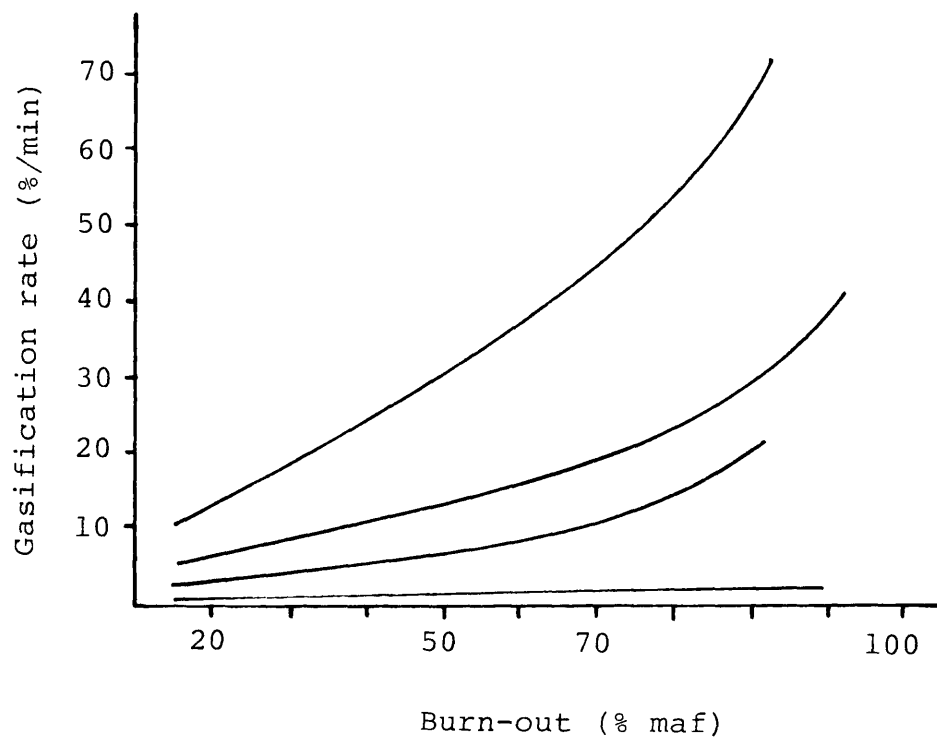
Table 4

Apparent Activation Energy and Frequency
Factor for Steam Gasification⁽¹⁹⁾

Carbon Source	Activation Energy kcal/mole	Frequency Factor min ⁻¹	-Rate*
Solid waste	59.5	3.9×10^{10}	0.319
Poplar wood	43.5	1.2×10^8	0.941
Straw	43.5	5.9×10^7	0.463
Bark	42.5	9.1×10^7	1.096
High moor peat	40.4	5.1×10^6	0.139
Coal	48.8	5.9×10^7	0.048

*steam, 1 atm, 900°C

FIGURE 11
Influence of Burn-out on the
Gasification Rate of Poplar Wood in
Steam-Argon Mixture, $X_{\text{H}_2\text{O}}=0.73$ (19)



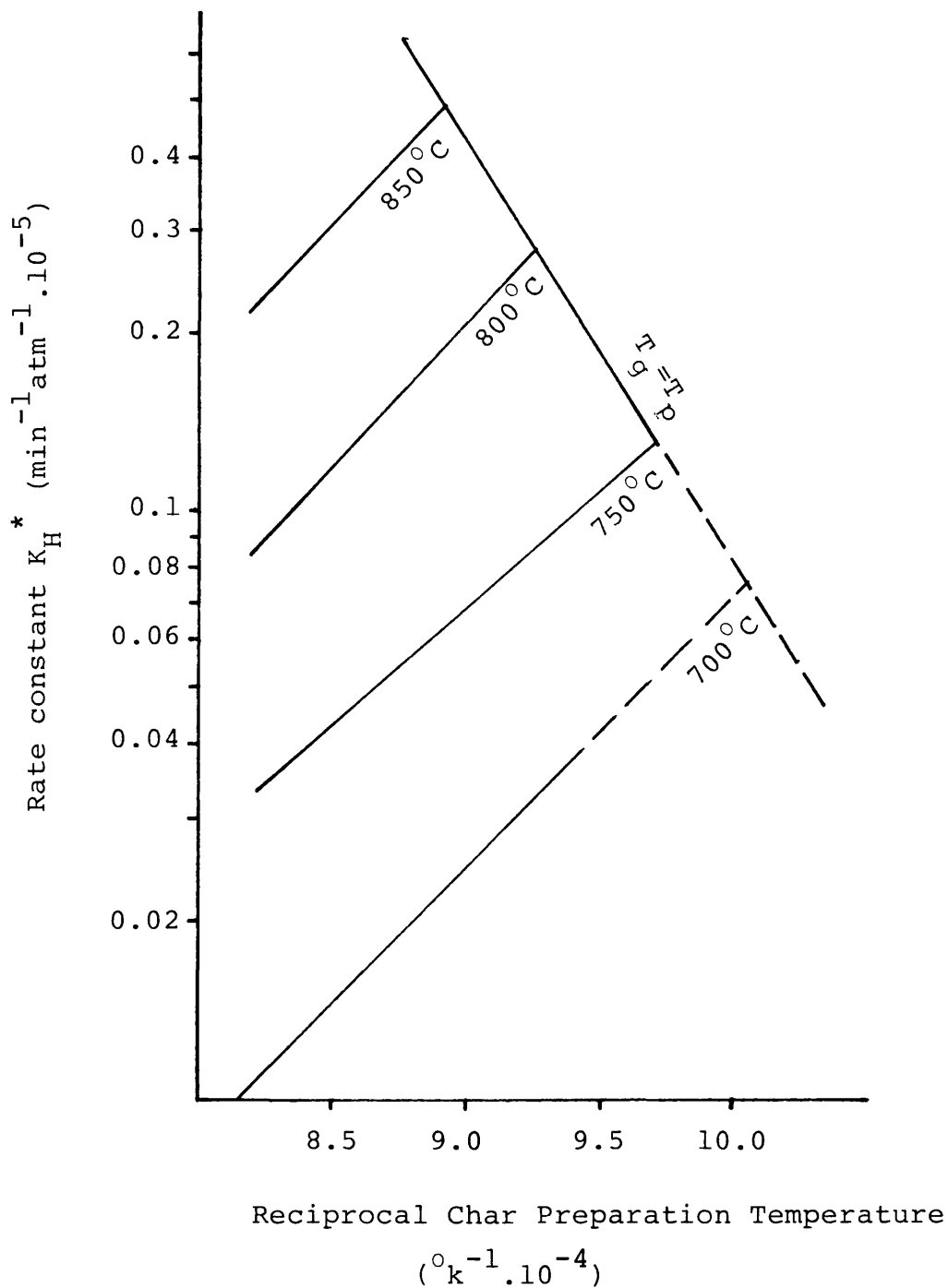
When reviewing gasification rates from various sources, there is often a large discrepancy in the reported activation energy for a given gasification condition. Variations in carbon source will often be the cause of discrepancy. Preparation conditions also have an effect on the reaction rate.

In Figure 12, the effect of char-preparation temperature on the rate constant for coal char gasification in hydrogen is illustrated. The char reactivity decreases with increasing preparation temperature, relative to the temperature of subsequent gasification in hydrogen is illustrated. Johnson⁽⁸⁾ models this pretreatment effect in terms of a thermal annealing contribution to the apparent activation energy. Apparent activation energy is then the sum of the true activation energy and the pretreatment activation energy.

Diffusion

In the study of char-gas reactions, information on gas diffusion at elevated temperatures is desirable when developing models for reactions involving structures such as pellets. Reactions between porous solids and gases are usually interpreted in terms of idealized models based on sharply defined reaction zones in the particle. The homogeneous and shrinking core models represented the extremes

FIGURE 12
Effect of Char-Preparation Temperature
on Rate Constant in Hydrogen (8)



that might be encountered within the limits of very rapid and very slow diffusion of the reacting gases. Diffusion can be shown to be important due to the boundary layer and internal structure. Boundary layer gasification occurs only at very high temperatures ($>1500^{\circ}\text{C}$). For large particles or particles with small pores, diffusion within the solid can be important at lower temperatures. Diffusion within the solid is an important factor in the temperature dependency of the global rate. Under severe diffusion limitations, the activation energy appears to be halved.

For gasification reactions with many carbons it has been shown that intraparticle diffusional effects are of minor importance below 1000°C and that the chemical reaction rate is controlling⁽¹²⁾. Above 1000°C then, a knowledge of effective diffusivity could be useful when interpreting rate data. One approximation of effective diffusivity employed by Desai and Yang⁽¹³⁾ relates effective diffusivity to Knudsen diffusivity by the relationship:

$$D_e = \frac{D_g}{\lambda} \varepsilon^2 \quad 28$$

where ε is the total porosity of the char and λ is an experimentally determined tortuosity constant.

Yang and Liu⁽¹⁴⁾ have measured diffusivities for CO₂/N₂ in graphite using a Wicke-Kallenback type diffusion apparatus and also calculated diffusivities from reaction rate data using the Stefan-Maxwell flux equations. For their carbon sample, a nuclear grade graphite was used. The sample had a porosity of 17.7% with a bimodal pore size distribution; micropores centered at 40Å diameter with a porosity of 4% and macropores at 2000Å diameter with a porosity of 13.7%. To calculate effective diffusivity using the diffusion cell, equation 29 is integrated to give equation 30.

$$N_A = -D_e C_T \frac{dX_A}{dz} + X_A (N_A + N_B) \quad 29$$

$$D_e = \frac{N_a \alpha L}{C_T \frac{1-n}{1-\alpha X_{A2}} \frac{1-\alpha X_{A1}}{1-\alpha X_{A1}}}$$

The flux N_A , can be calculated as the product of X_{A2} and the flowrate of B, divided by the cross-sectional area of the sample. The effective diffusivities of CO₂-N₂ in graphite are shown in Table 5.

Effective diffusivity was also calculated from overall rate data assuming a Langmuir-Hinshelwood rate equation. Using the rate equation, the Stefan-Maxwell flux equations and a mass balance written in cylindrical coordinates, equations 15 and 16 can be derived.

$$\frac{D_e}{r} \frac{d}{dr} \left(\frac{r}{1+X_A} \frac{dX_A}{dr} \right) = \frac{K_1 X_A}{K_2 - K_3 X_A} \quad 31$$

$$R_d = \frac{D_e}{1+X_{AS}} \frac{dX_A}{dr} \Big|_{r=R} \quad (2\pi R L C_T) \quad 32$$

The subscripts, A and C pertain to the species CO_2 and A_r respectively. The subscript s indicates molar concentration at the surface. Values of R_d , k_1 , and k_3 were measured experimentally. Equation 31 was solved numerically and a trial technique was used to guess the missing condition. From the numerical solution, effective diffusivity is calculated using equation 32. The effective diffusivities calculated from rate data can be found in Table 6.

Effective diffusivity as a function of Knudsen diffusivity and porosity has been determined for wood char by Groenveld and van Swaaij⁽¹⁶⁾. For an unreacted char particle ($\epsilon = 0.75$) the effective diffusivity varies between 0.14-0.2 D_K . For a porosity of 0.75 to 0.84 the effective diffusivity follows equation 33. Above a porosity of 0.84, the effective diffusivity equals the product of the Knudsen diffusivity and the porosity.

$$D_e = D_x (7.69\epsilon - 5.62) \quad 33$$

The Knudsen diffusivity is the controlling diffusivity in smaller pores. These studies show that for a variety of

carbons, diffusion limitations will be present due to the microstructure of the solid. Further, they suggest that carbons containing both micro and macropores will have kinetics dominated by the micropores in the temperature region below that required for boundary layer gasification.

Table 5

Effective Diffusivity for CO₂-N₂ in Graphite (21)

Temperature °K	D _e CO ₂ -N ₂ CM ² /sec 10 ⁴	D _e N ₂ -CO ₂ CM ² /sec 10 ⁴	D _k [*] CO ₂ CM ² /sec 10 ⁴
291	7.75	6.57	99.8
380	10.47	8.74	114.0
480	12.66	11.69	128.0
593	15.61	14.29	142.0

* 40Å pores

Table 6

Effective Diffusivity of CO₂ in Ar
Calculated from Overall Rate

Pellet diameter in.	Bulk Gas %CO ₂ in Ar	R _d gm/min	D _e cm ² /sec
3/16	10	0.65.10 ⁻³	7.01.10 ⁻³
5/16	10	1.18.10 ⁻³	7.50.10 ⁻³
7/16	10	1.71.10 ⁻³	7.28.10 ⁻³
5/16	20	1.88.10 ⁻³	7.32.10 ⁻³
5/16	30	2.45.10 ⁻³	8.00.10 ⁻³

Temperature 1143°C

Pressure 1 atm

Sample cyclindrical graphite 1.5 inches long

Knudsen diffusion D_k = 1.98.10⁻² cm²/sec

Gasification Models

A common feature of gas-solid reactions is that the overall process involves several steps: a) mass transfer of reactants and products between the bulk gas phase and the internal surface of the reacting particle; b) diffusion of gaseous reactants or products through the pores of a solid reactant; c) adsorption of gaseous reactants on solid reactant sites and desorption of reaction products from solid surfaces; d) the actual chemical reaction between the adsorbed gas and solid. For the gasification of a fine powder, mass transfer is insignificant and the previously described kinetic equations adequately describe steps c) and d). Global gasification rates for a large particle or pellet may be mass transfer dependent and would require a more sophisticated model that takes into account mass transfer. It is conceivable that heat transfer may also be significant in the gasification of a large particle. The decision to include heat transfer effects in a model would depend on a knowledge of the thermodynamics of the reactions involved, the intrinsic kinetics and the thermal diffusivity of the char.

In the development of their char particle gasification model, Groenveld and van Swaij⁽¹⁶⁾ assumed that no temperature gradients exist, transport of the reaction products out

of the pellet has no influence on the diffusion of the reactants, discounted external mass transfer and utilized a pseudo-steady state approximation for the concentration of the gaseous reactants in the pellet. The kinetic rate expression used is similar to equation 23 when the pore surface area term (α_v) is unity. Concentration of the reactant gas in the pellet is given by:

$$D_e(x,t) \frac{d^2 C_A(x,t)}{dx^2} + \frac{a}{x} \frac{d C_A(x,t)}{dx} - R_A = 0 \quad 34$$

and the concentration of carbon within the pellet is given by equation 35.

$$\frac{d C_s(x,t)}{dt} = -R_A \quad 35$$

Effective diffusivity, $D_e(x,t)$, is described as the product of initial diffusivity and some function of porosity. Porosity is calculated using relationship 36.

$$\varepsilon = 1 - (1 - \varepsilon_0) C_s / C_s(0) \quad 36$$

The term a in equation 34, is a geometric factor that equals 0 for a slab, 1 for a cylinder and 2 for a sphere. This set of equations was solved using the method of Baker and Oliphant (20), a three point backwards difference scheme using a linearization in C_A for the rate equation. In Table

7 experimental and calculated residence times are presented for a number of reaction temperatures and overall char conversions. For the experimental conditions presented, the model accurately describes the data. Investigation of higher reaction temperatures would provide a more rigorous test of the model. As the temperature is increased, the overall conversion rate would be expected to shift from a dependence on intrinsic kinetics to a dependence on mass transfer. If the model could accurately predict residence times overall the increased temperature range, it would be very useful for design purposes.

A model consisting of mass and energy balance equations together with the Stefan-Maxwell relations has been developed by Amundson and Srinivas(21). This model assumes that reactions 2, 3, 4 and 6 (Table 1) take place. The mass balance for the species i within the particle at steady state is given by:

$$-\nabla N_i + \sum_{j=1}^4 \alpha_{ij} r_j = 0 \quad 37$$

The consumption of carbon is given by equation 38.

$$\frac{dp}{dt} = -12 (r_2 + r_3 + r_4) \quad 38$$

The terms r_2 , r_3 , and r_4 are the reaction rates for gasification reactions 2, 3 and 4 respectively. At the surface of

Table 7

Calculated and Experimental Residence
Times for Overall Char Conversion (16)

Temperature °K	Overall Conversion	Residence Experimental	Time (sec) Calculated
1028	10.9%	21600	20170
1113	3.4%	4500	3690
1118	18.0%	20940	19340
1153	12.2%	5400	5390
1173	39.0%	20460	20620
1198	12.9%	2700	2610
1223	40.0%	13920	12460

Carbon source: Wood char particles 4x2x2 cm

the particle the energy balance is given by equation 39.

$$\frac{d}{dt} \left(\frac{m}{12} C_p T_p \right) = hA(T_b - T_p) - A \sum_i N_i h_i \quad 39$$

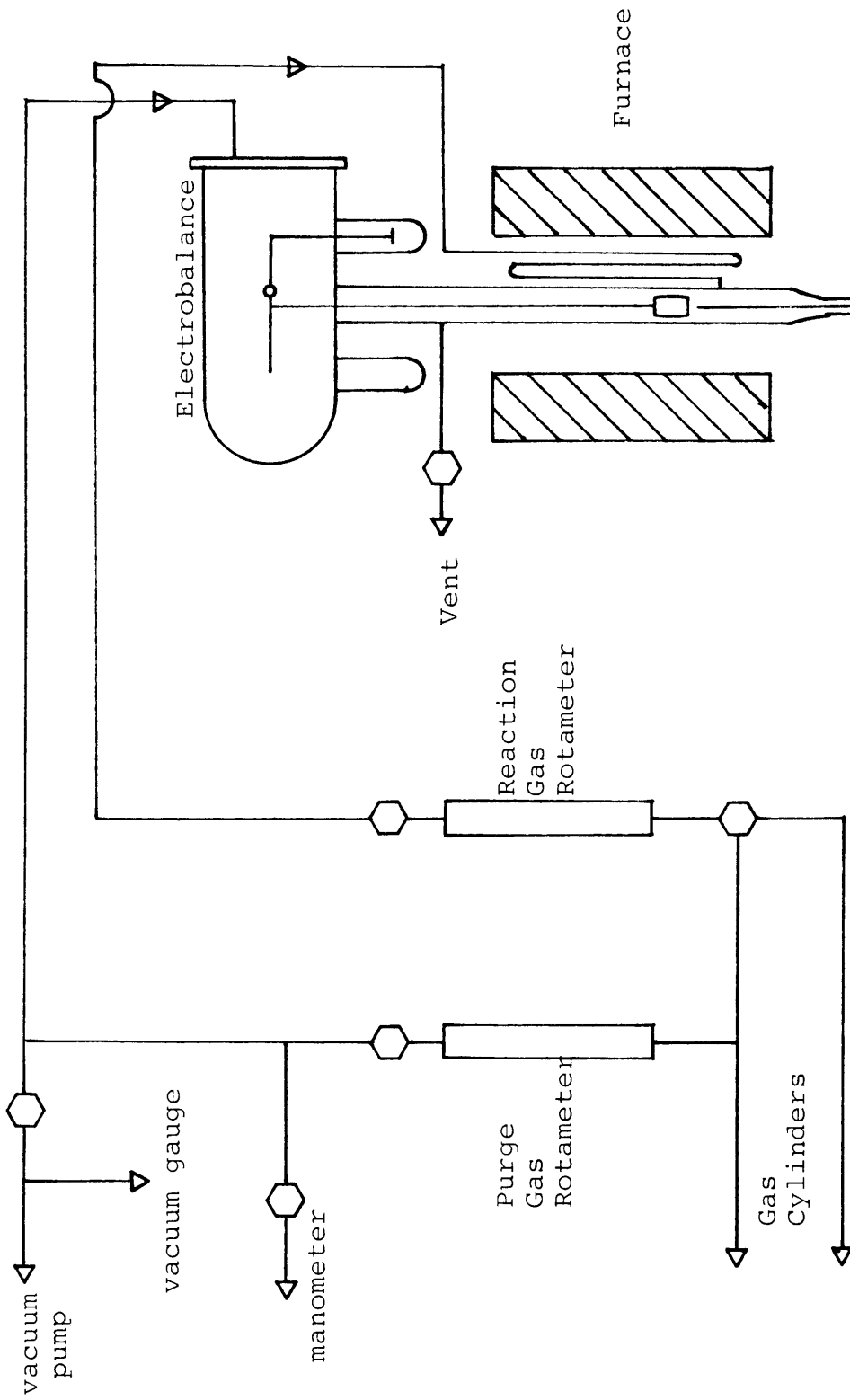
The energy balance assumes a zero temperature gradient within the pellet. While the authors do not test their model against experimental data, a comparison is made with a set relations for coal char gasification presented by Johnson (22). At small particle sizes the two models agree well, but as particle size increases the two models diverge. This is attributed to diffusion effects which are included in Amundsen and Srinivas' work.

A number of other investigators have presented models for char gasification. Hayes (23) has developed a model similar to Amundsen and Srinivas; a general method of solution is utilized which allows for any number of reactions and any number of components. Debelak et al (24) present a model that takes into account the influence of particle structure changes on the rate of coal char gasification with CO_2 . Many modeling studies in the literature have not been experimentally confirmed. A model that accurately describes the global rate in terms of chemical kinetics and heat and mass transport can be used in a differential mass balance that describes reactor. For the successful design of a gasifier, it is necessary that the application limits of the model be experimentally determined.

Experimental Equipment

A schematic of the gasification test reactor is shown in Figure 13. The reactor consists of a Cahn 2000 electro balance and a 20 inch quartz reaction tube. A quartz thermal baffle, $8\frac{1}{2}$ inches long, is used as a connection between the electro balance and reaction tube. Heat to the system is supplied by a split shell furnace. The furnace has a 10 inch hot zone and is capable of operating at temperatures up to 1200°C . Reaction temperature is determined by a type K thermocouple while power to the furnace is provided by a solid state Omega controller. Because of the large length to diameter ratio of the reaction zone and the provision for gas preheating, the thermocouple temperature correction is found to be negligible. Internal diameter of the quartz reaction tube is one inch; pellets with diameters up to $\frac{3}{4}$ inch can be gasified without difficulty.

Nitrogen is used as a purge gas in the electrobalance to prevent contamination of the balance. Flowrate of the purge and reaction gases is controlled by a pair of rotameters. Reaction gas enters the reactor at the bottom of the hot zone after first being preheated in a quartz loop alongside the reaction tube. Purge, product and excess reaction gases exit the system from a quartz line located above the hot zone. Gas from the exit line may be vented



Schematic of Experimental Equipment

FIGURE 13

or collected for analysis. Figure 14 shows the experimental set-up.

Pellets are produced using a heated pellet die and a Carver press. Four pellet dies with $1/8$, $3/16$, $1/2$ and $3/4$ inch internal diameters were machined from a 2 inch O.D. cylinder of stainless steel. The bottom plunger has a length of $1/2$ inch and the body length of each die is $4 \frac{3}{4}$ inch. The top plunger is also $4 \frac{3}{4}$ inch long so that any pellet formed can be pressed from the die. Temperature of the pellet die is determined with a type K thermocouple. The pellet die is heated using a nozzle heater. Representative pellet dies are shown in Figure 15. Pellets are pyrolyzed in a pyrolysis unit designed by Herman (25). Pyrolyzed pellets may be used as is or crushed and sized with a 200 mesh screen for powder gasification.

FIGURE 14
Experimental Reactor

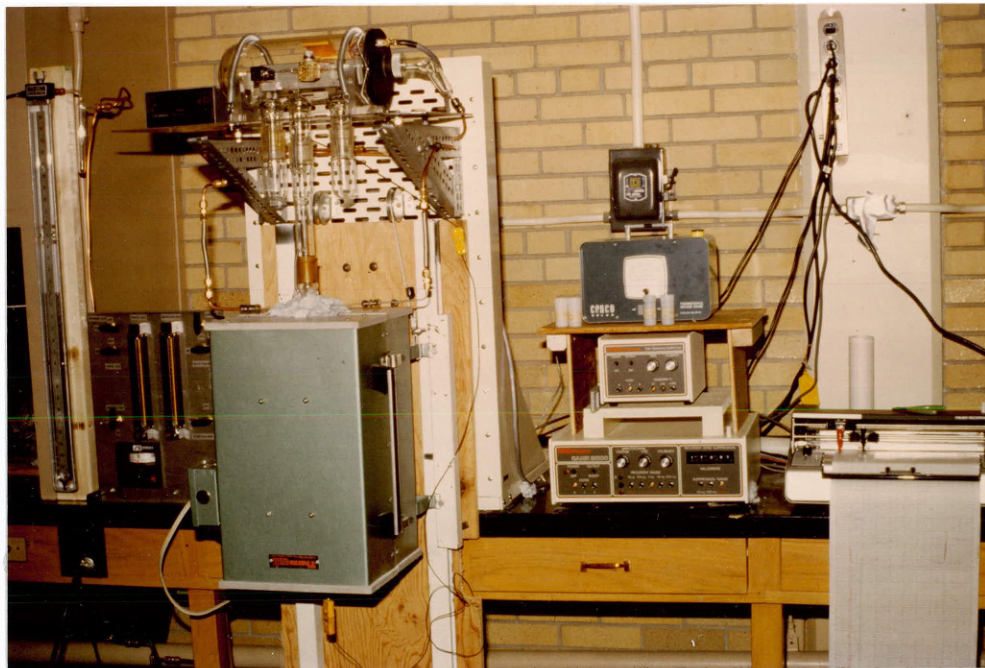
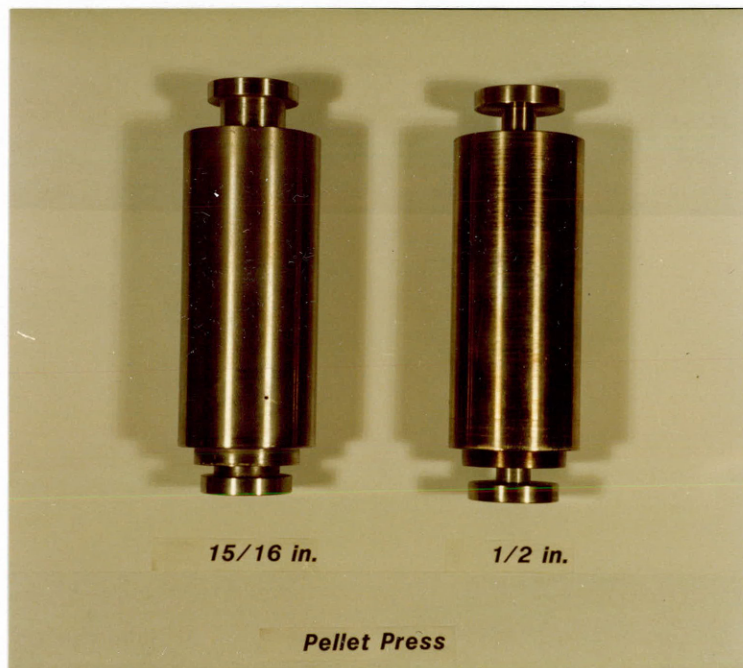


FIGURE 15
Pellet Press Dies



Experimental Procedure

Char Production

All of the char used in this study was produced by the pyrolysis of wood pellets made of -20 mesh Ponderosa pine chips. To make a pellet, the pine chips were charged to a pellet die held at 120°C and then pressed in a Carver press. Cycle time and pressure were adjusted to yield a density of ~ 1.2 gm/cc for the pellet. To prepare a pellet for pyrolysis, a hole was drilled through the pellet axis with a number 58 bit. Nichrome wire was then threaded through the pellet so that it could be suspended for pyrolysis and gasification. Next, the pellet was pyrolyzed in the pyrolysis unit at 800°C. The pyrolyzed pellet can then be used for gasification as is or ground to a -200 mesh powder for gasification.

Powder Gasification

To measure the intrinsic kinetics of the char-CO₂ reaction, 5 to 10 mg samples of powdered char were gasified at different temperatures and reaction gas compositions. The fine particle size and small sample size were selected so that heat and mass transfer effects would be insignificant. Also, the small sample size made it possible to neglect any effect of the product gas on the composition of the bulk gas phase. To gasify a char powder, the sample was placed on a platinum pan suspended in the quartz reaction tube at the midpoint of the hot zone. The gasifier was then sealed and evacuated. Once the sample was outgassed, the reactor was filled with nitrogen at atmospheric pressure. As the reactor was heated to the desired temperature, the system was purged with a constant flow of nitrogen. When the temperature set point was reached and the sample came to constant weight, the gas flow in the reaction gas line was switched from nitrogen to carbon dioxide. Onset of gasification was very distinct as the reaction gas moves through the reactor in a plug flow manner. Sample weight versus time was recorded and from this data the reaction rate was calculated. Once sufficient data has been collected, the reaction was stopped by switching the reaction gas back to nitrogen.

To study the effect of gas composition on the char-CO₂ reaction, gas mixtures of varying CO-CO₂ ratios were made up in high pressure sample cylinders. Mix composition was controlled by the partial pressure of each gas. Additionally, the composition of each mixture was checked by gas chromatography. The gasification procedure was the same as previously described.

Pellet Gasification

Gasification of pellets was carried out in essentially the same manner as powder gasification. The platinum pan was removed and the pellet was suspended from the balance with a section of nichrome wire. Evacuation and purging with nitrogen then followed. Gasification may be carried to completion or stopped at different conversion fractions.

To determine whether there is a temperature gradient within a pellet during gasification, a pellet was mounted on a fine thermocouple and gasified. The thermocouple was positioned such that the bead is at the mid-point of the pellet axis. The temperature difference between the surface and the center of the pellet was then measured.

Gas Diffusion

To measure the effective diffusivity of CO₂ in a wood

char pellet, a pellet was suspended in the reactor and evacuated as for gasification. Next the system was purged with nitrogen and the temperature set at some point between ambient and the onset of gasification. Once the temperature stabilizes, the reaction gas was switched from nitrogen to carbon dioxide and the weight gain recorded as a function of time until constant weight. When the diffusivity measurement had been repeated at a number of temperatures, the pellet can be gasified further and the diffusion measurements repeated. In this manner the effect of char conversion on diffusivity was noted.

Results

Ponderosa pine from the U. S. Forest Service sawmill in Golden, Colorado was used for this study. The wood obtained, in the form of 1/2 - 1 inch chips, was milled to -20 mesh chips. These fine chips were then densified by pelletization. The pellets produced were similar in nature to commercial pellets, where it is desired to increase the bulk energy density of wood to the level of other solid fuels. An analysis of the feedstock is shown in Table 8.

Primary pyrolysis of the pellets was carried out in a heated quartz tube swept by nitrogen.⁽²⁵⁾ The maximum attainable temperature in the pyrolysis unit was 800°C. As char make is a function of pyrolysis temperature (Figure 16), further pyrolysis occurred when the sample was heated to a gasification temperature greater than 800°C. To complete pyrolysis then, each was brought up to the gasification temperature in a nitrogen atmosphere and held until the sample came to constant weight. Proximate and ultimate analysis for char pellets of different diameters and pyrolysis temperatures are shown in Table 9.

Table 8

Ponderosa Pine Feedstock Analysis (25)

Proximate Analysis

Volatile matter	78.90 wt %
Fixed carbon	15.70
Ash	1.69
Moisture	3.71

Ultimate Analysis*

Carbon	50.17 wt %
Hydrogen	6.04
Oxygen	43.58
Nitrogen	0.16
Sulfur	0.05

Gross heating value* 8,647 BTU/lb

*moisture, ash free basis

FIGURE 16
Char Make (25)

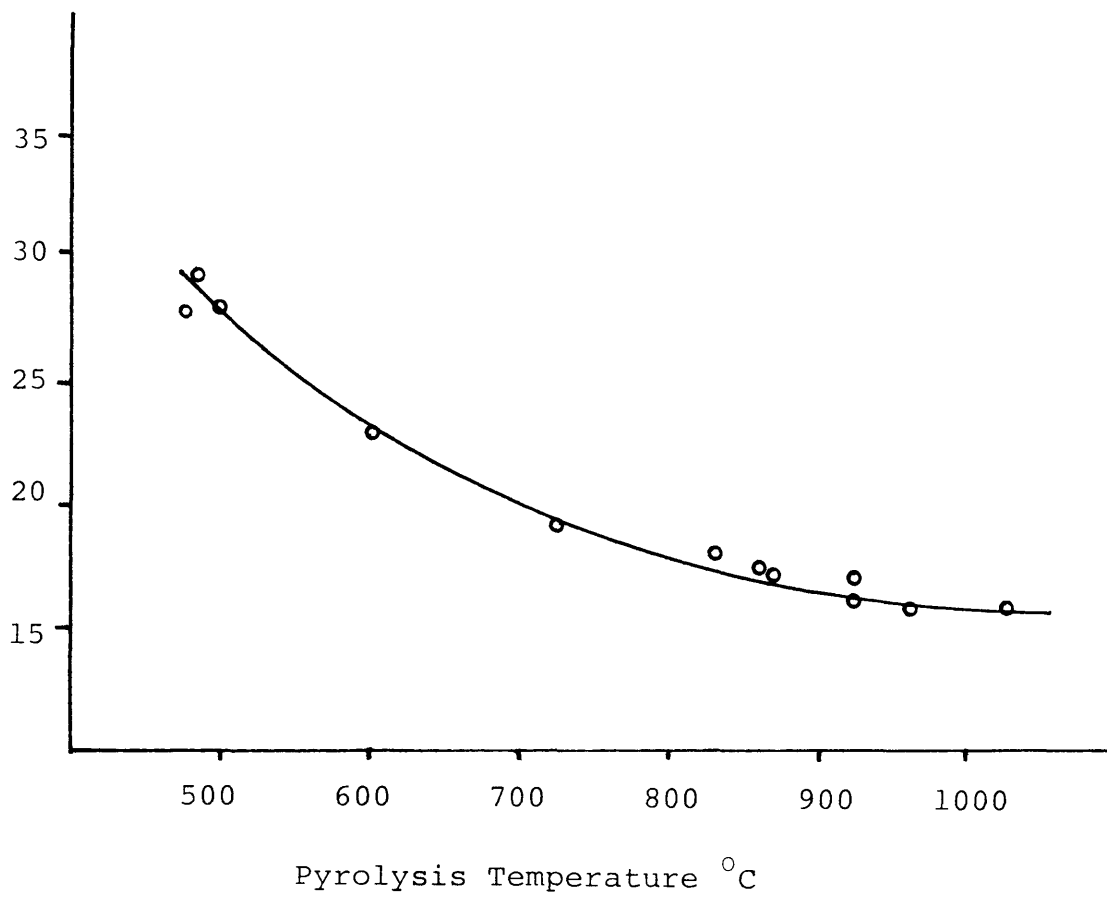


Table 9

Proximate and Ultimate Analysis of
Biomass Chars (25)

Proximate Analysis*				
Pyrolysis	Pellet	Volatile	Fixed	
Temperature °C	diameter, in	matter %	Carbon %	
870	1/2	8.73	91.27	
935	15/16	3.07	96.93	
950	2/4	2.15	97.85	
970	3/8	9.11	90.89	
Ultimate Analysis*				
Pyrolysis	Pellet	Carbon	Hydrogen	Oxygen
Temperature °C	diameter in.	wt %	wt %	wt %
730	3/8	93.36	2.53	4.11
925	1/2	96.00	1.15	2.70
935	15/16	97.29	1.44	1.26
950	3/4	95.44	1.27	3.29
965	3/8	93.08	1.50	5.42

* moisture, ash free basis

Gasification of Powdered Chars

Fine powdered char (-200 mesh) was used to study the intrinsic kinetics of the gasification reaction with CO_2 . The use of a very thin layer of fine char particles eliminated the effects of heat and mass transfer. The platinum pan had a diameter of approximately one half inch. As the gas flow in the reactor was upward, the lifting force on the pan had to be taken into account when determining reaction rate. To compensate for the lifting force on the pan, each reaction was allowed to go to completion and the final weight used as the tare weight.

Gasification of Powdered Char in CO_2

In the study of gas solid reaction kinetic of fine particles, the reaction rate depends on temperature, composition and pretreatment temperature. To determine the magnitude of the temperature effect on the reaction rate, powdered char samples were gasified in CO_2 at atmospheric pressure over the temperature range of 850° to 1115°C . Figure 17 shows the effect of residence time on fractional conversion for a series of reaction temperatures where the reaction temperature and pretreatment temperatures are the same.

The general rate law which describes the data is given as follows:

$$-r = - \frac{1}{W_0} \frac{dW}{dt} = f(T)g(C) \quad 40$$

Integrating equation 24 at constant temperature and composition results in equation 25.

$$X_A = \frac{W_0 - W}{W_0} = f(T)g(C) \quad 41$$

Equation 41 adequately describes the zero order dependency of the observed rate on carbon inventory up to high conversions. These data suggest that the available surface area for reaction remains essentially constant.

Following Menster and Ergun (7), it is postulated that the reaction rate follows an expression far from equilibrium of the form:

$$-r = \frac{k_1 P_{CO_2}}{1 + k_2 P_{CO_2} + k_3 P_{CO}} \quad 42$$

For a pure CO₂ atmosphere as in Figure 17, the data may be correlated in terms of the principle activation energy k₁. The experimental value for this activation energy (Figure 18) is 34.2 kcal/mole. While this result is within the range of values reported in the literature, it is lower than the 51.9 kcal/mole activation energy found by Groenveld and van

Swaij⁽¹⁶⁾ for the gasification of powdered wood char and the 59.3 kcal/mole activation energy for coal char determined by Dutta et al⁽²⁶⁾. It is interesting to note that the CO₂-char activation energy is very similar to the H₂O char activation energy of 51.2 kcal/mole determined by Kosowski et al⁽²⁷⁾ for jack pine char. Possibly indicating a similarity in the gasification mechanism and the distribution of active sites.

Figure 18 also shows that if the pretreatment temperature exceeds the reaction temperature, a predictable reduction in reaction rate occurs. This pretreatment or thermal annealing effect is the result of a graphitization process whereby the amorphous carbon (char) seeks a lower energy state in the form of graphite. The gasification rate of graphite is less than that of amorphous carbon so that the global gasification rate for char decreases as the proportion of carbon present as graphite increases. This thermal annealing effect can be correlated in terms of a contribution to the apparent activation energy. The rate constant is then expressed as the product of a frequency factor and two exponential terms as shown in equation 43⁽⁸⁾.

$$k = A \cdot \exp\left(-\frac{E_p}{RT_p}\right) \cdot \exp\left(-\frac{E_g}{RT_g}\right) \quad 43$$

FIGURE 17
Fractional Conversion vs Residence Time

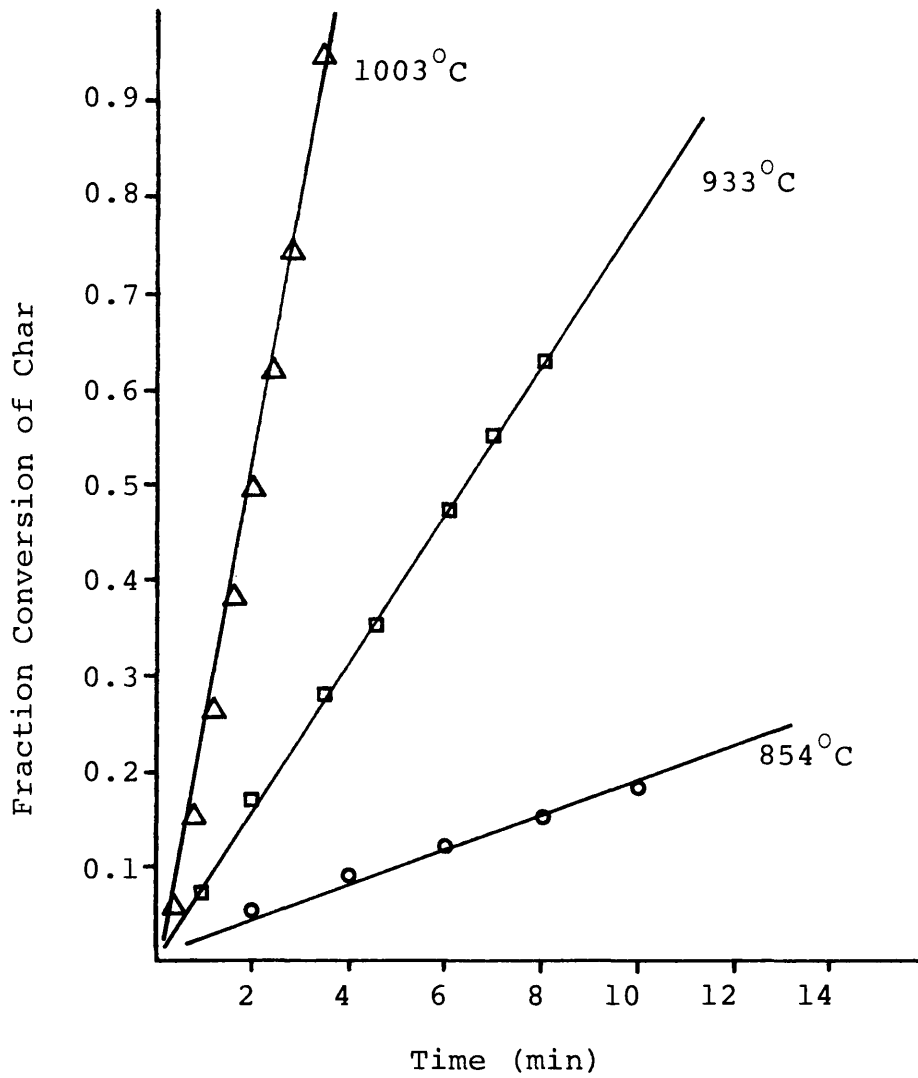
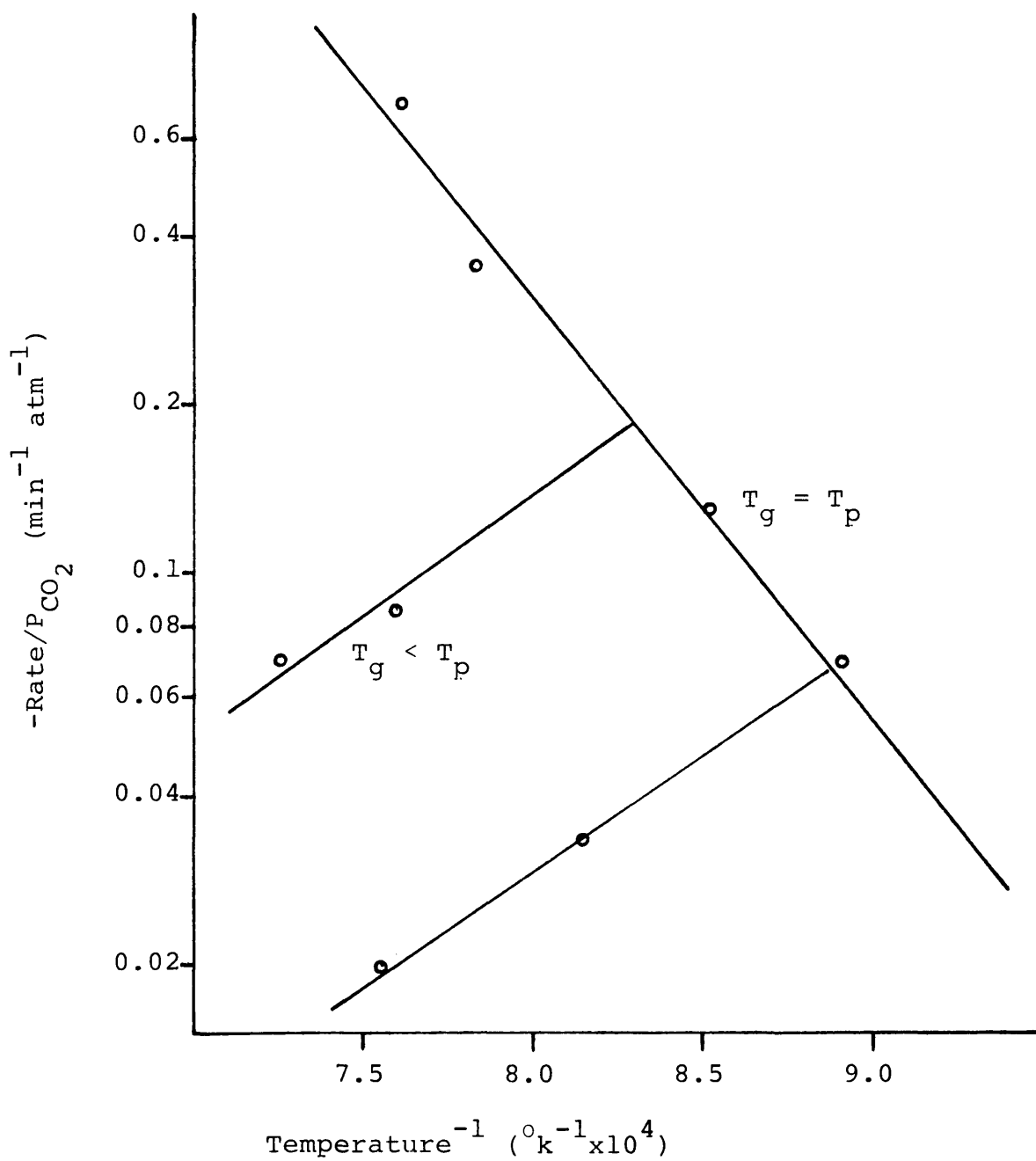


FIGURE 18
 $-\text{RATE}/P_{\text{CO}_2}$ vs Temperature⁻¹
 $P_{\text{CO}_2} = 0.81 \text{ atm}$



The first exponential term is the pretreatment effect where the rate constant is decreased as the pretreatment temperature increases above the gasification temperature. When the pretreatment temperature equals the gasification temperature the apparent activation energy is equal to the sum of true activation energy and the pretreatment activation energy. In this study the true activation energy was found to be 53.9 kcal/mole and the pretreatment activation energy is -19.8 kcal/mole.

Gasification of Powdered Char in CO₂/CO Mixtures

Previous investigations have shown that the CO₂-char reaction is not only temperature dependent, but is also dependent on the partial pressure of CO₂ and CO in the reaction gas. To investigate this relationship, powdered char was gasified with four CO₂/CO mixtures. The composition of these gas mixtures ranged from 17.9 mole %CO to 69.0 mole %CO. In Figure 19, $-\text{rate}/P_{\text{CO}_2}$ is plotted versus the inverse temperature. Data points include gasification in a CO₂ atmosphere and in different CO₂/CO mixtures. Figure 19 is very similar to Figure 18.

Equation 42 suggests that carbon monoxide and carbon dioxide retard the rate of reaction. As the experiment allowed only two independent variables, temperature and

P_{CO_2} , and there are three dependent variables in equation 42, only the most important retardation effect can be retained. Over the temperature range of interest, it was found that only carbon monoxide retardation was significant in the rate expression. Dropping the $k_2 P_{CO_2}$ term is equivalent to assuming that reaction 11 is irreversible. The resulting rate equation is then:

$$-r = \frac{k_1 P_{CO_2}}{1 + k_3 P_{CO}} \quad 43$$

Substituting P_{CO_2} and P_t for P_{CO} and inverting, equation 24 becomes:

$$-\frac{1}{r} = \frac{1}{k_1 P_{CO_2}} + \frac{k_3 P_t}{k_1 P_{CO_2}} - \frac{k_3}{k_1} \quad 44$$

FIGURE 19
-Rate/ P_{CO_2} vs Temperature⁻¹

$P_A = 0.81 \text{ atm}$

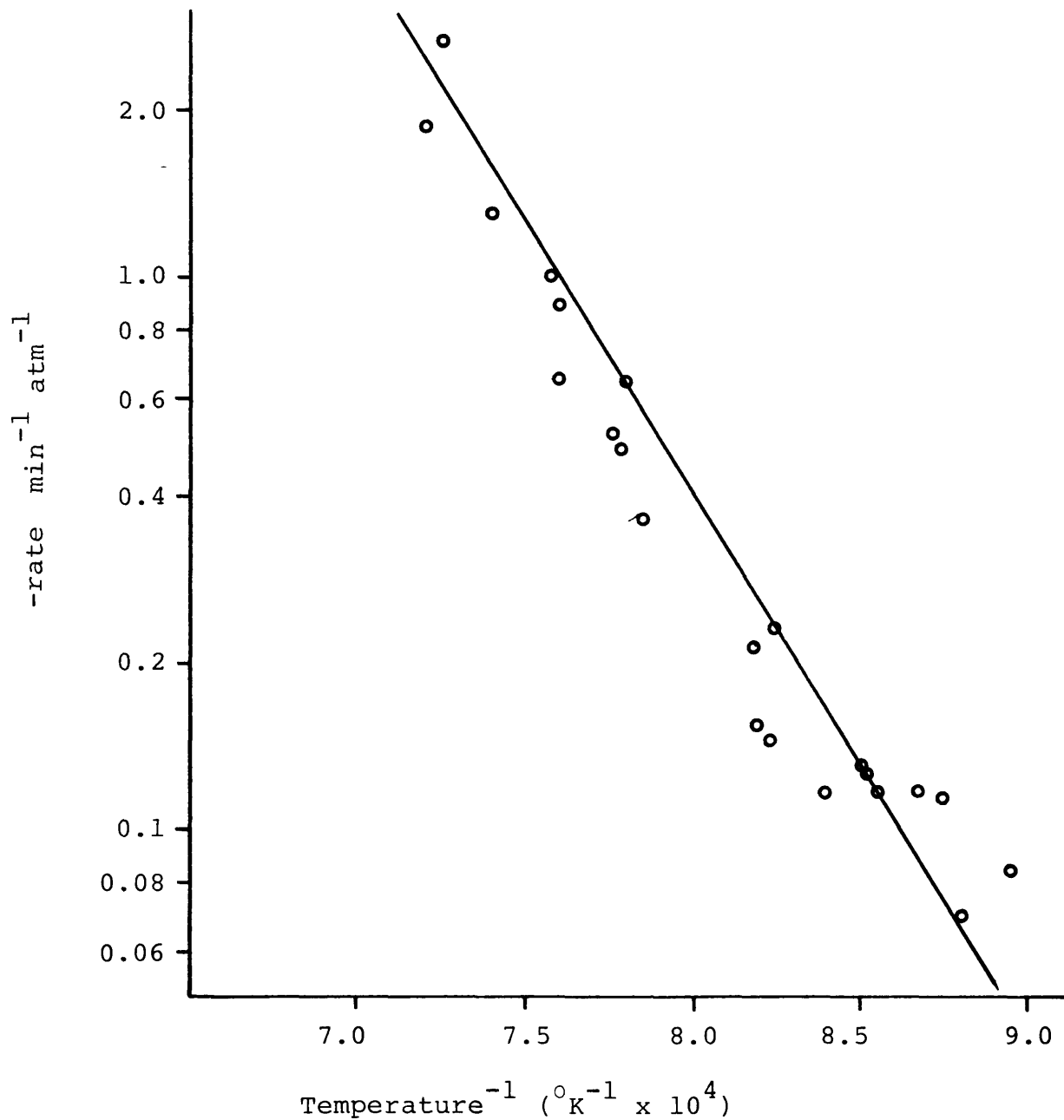


Figure 20 represents the relationship of reaction rate and P_{CO_2} for various temperatures. To construct Figure 20, the rate data for the different CO_2/CO mixtures was fitted to an exponential function of temperature. Reaction rate could then be calculated for a number of temperatures and the results plotted as a set of isotherms for inverse reaction rate versus one over the partial pressure of CO_2 . From the slope and intercept of each isotherm, values of k_1 and k_3 could be calculated (equation 44). In Table 10 the calculated rate constants are presented for a number of temperatures. The rate constants for the different temperatures can be fitted to the Arrhenius equation and the activation energies determined. The apparent activation energy (k_1) was found to be 35.9 kcal/mole and the retarding activation energy (k_3) is -41.0 kcal/mole. The frequency factors for k_1 and k_3 are $7.57 \cdot 10^5 \text{ min}^{-1} \text{ atm}^{-1}$ and $2.87 \cdot 10^{-8} \text{ atm}^{-1}$ respectively. Using these rate constants, Figures 21 and 22 were constructed to compare the calculated rate curves against the experimental data.

The values for k_1 and k_3 were arrived at through the use of three different curve fits. In the first, the experimental rate data was fitted to an exponential equation using the least squares regression method. The coefficient of determination for each curve fit was 0.9 or greater.

FIGURE 20
Reaction Rate vs $1/P_{CO_2}$
at Various Temperatures

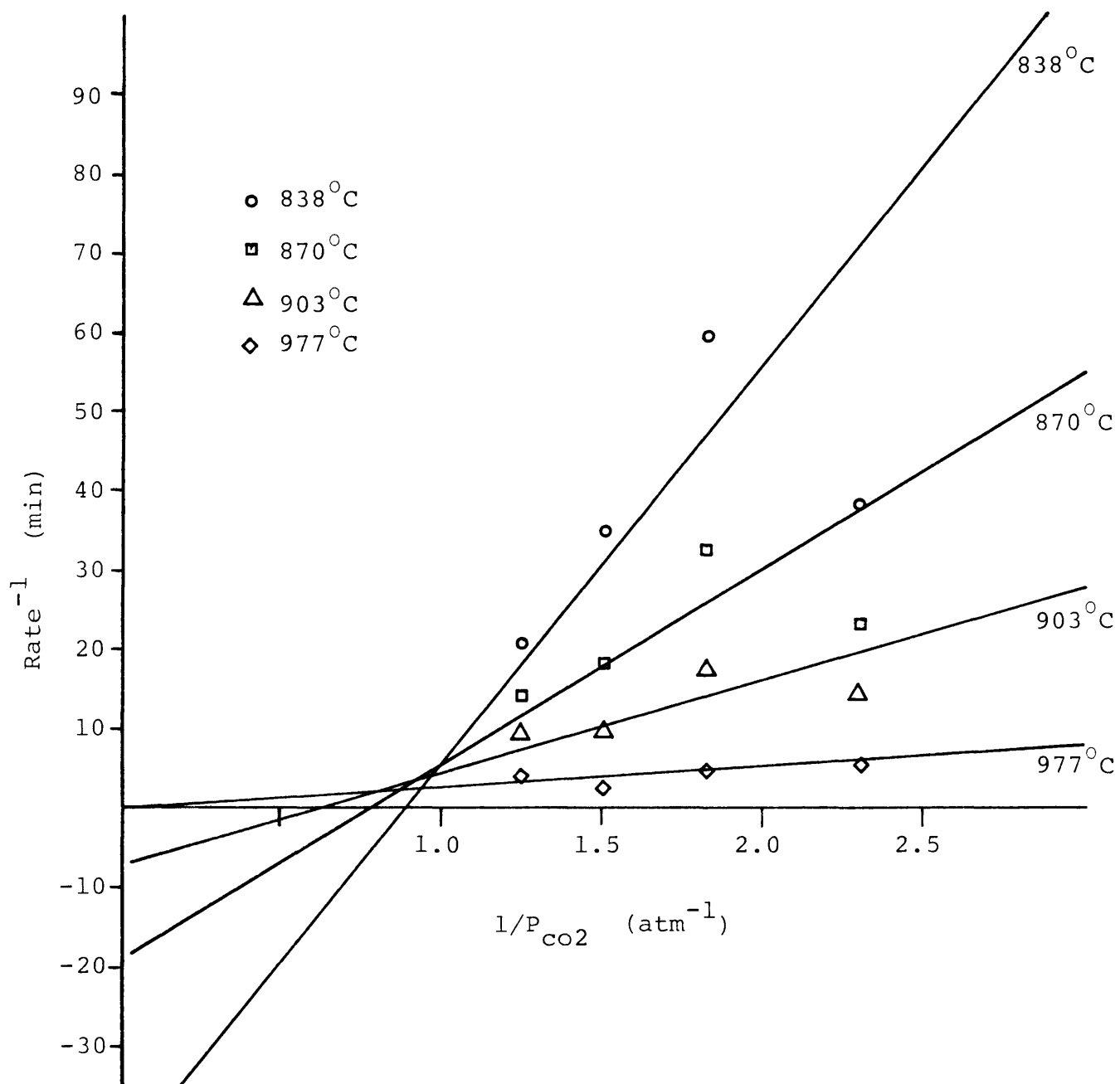


Table 10
Rate Constants for a Number of Temperatures

Temperature °C	k_1	k_3
1150	2.478	-0.996
1060	1.022	-0.592
977	0.363	-0.065
903	0.164	1.169
870	0.106	2.020
838	0.071	3.279

$$k_1 = 7.57 \times 10^5 \text{ min}^{-1} \text{ atm} \exp \frac{-7.13 \cdot 10^4}{T^\circ \text{K}}$$

$$k_3 = 2.87 \cdot 10^{-8} \text{ atm}^{-1} \exp \frac{8.15 \cdot 10^4}{T^\circ \text{K}}$$

$$-r = \frac{k_1 P_{\text{CO}_2}}{1 + k_3 P_{\text{CO}}}$$

FIGURE 21
Calculated Rate vs Temperature⁻¹
at Different P_{CO2}

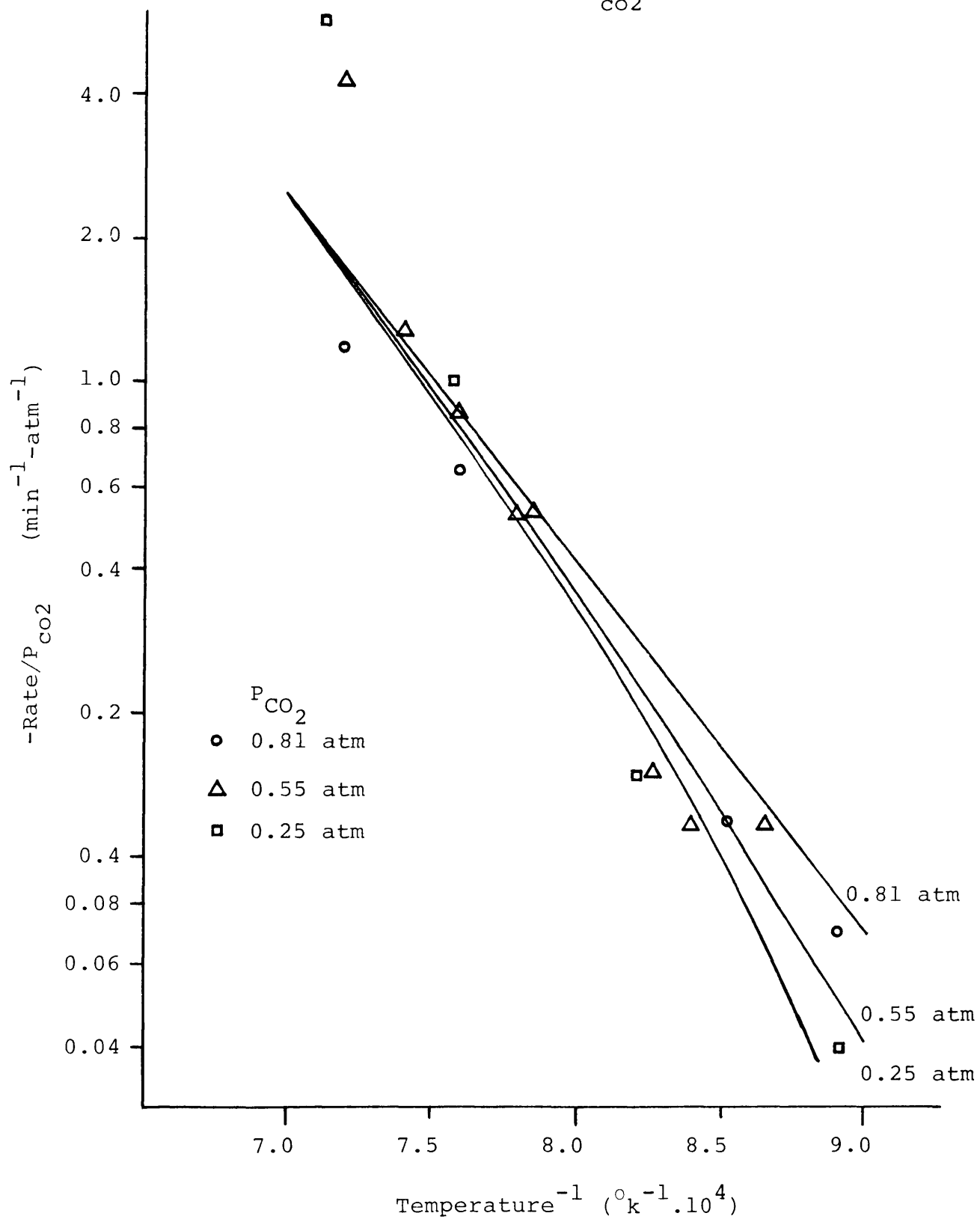
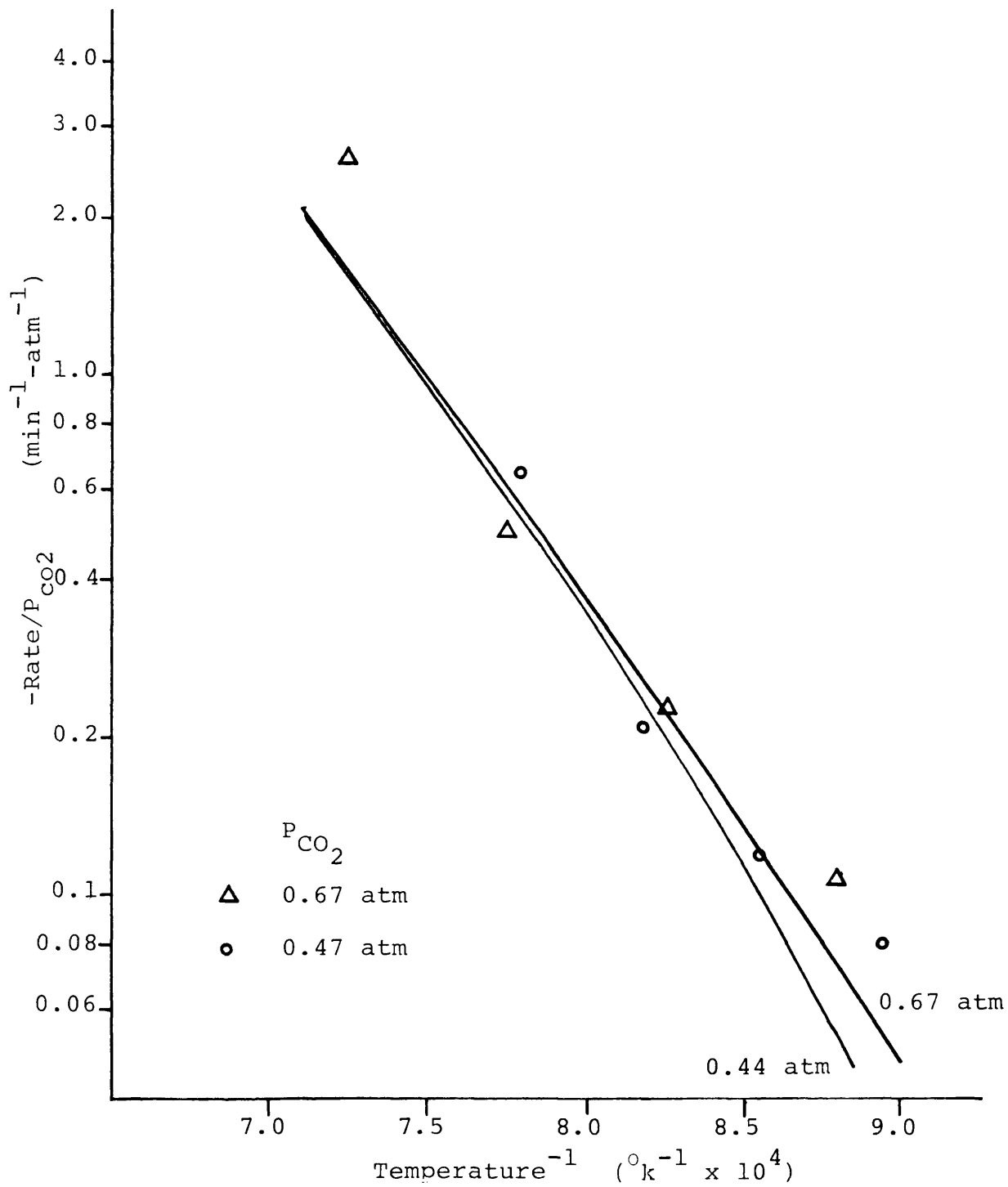


FIGURE 22
Calculated Rate vs Temperature⁻¹
at Different P_{CO2}

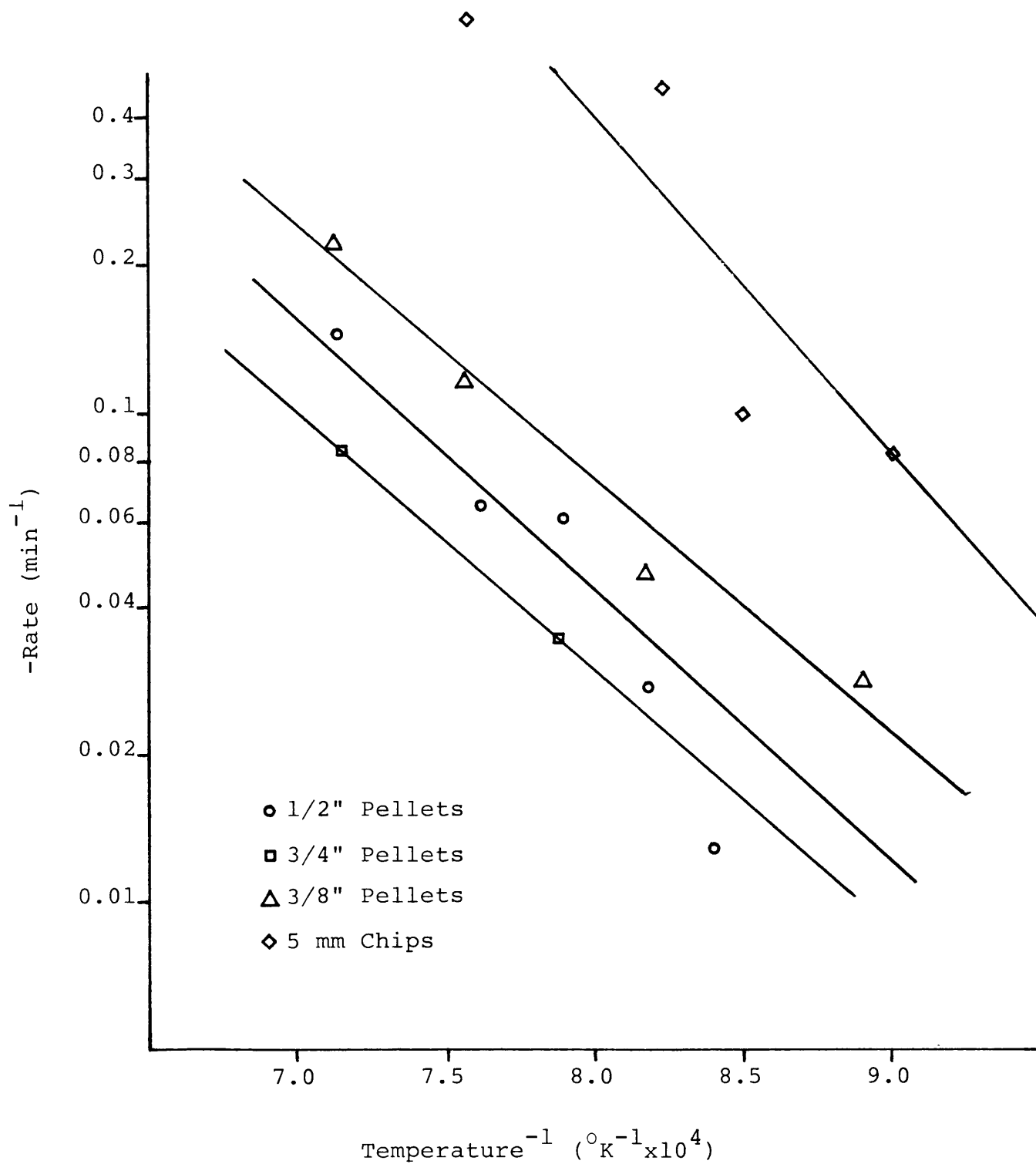


The greatest deviations occurred at high temperatures where the calculated rate was always less than the experimental value. Slopes and intercepts for the isotherms of Figure 20 were determined using a linear least squares regression method. At temperatures about 1000°C, the coefficient of determination was less than 0.5 indicating a poor fit. For temperatures less than 1000°C, the coefficient of determination is 0.9 or greater. The least squares regression of the Arrhenius equation for k_1 and k_3 had coefficients of determination equal to 1.0.

Gasification of Pellets

Ponderosa pine pellets with diameters of 3/8, 1/2 and 3/4 inches were gasified in a stream of CO₂ at atmospheric pressure. The gasification rates for the three pellet sizes as a function of temperature are illustrated in Figure 23. Also included in Figure 23 is the rate curve for the gasification of 5 mm chips. There is virtually no difference in the rate curves for 5 mm chips and for powders (Figure 18); this shows that the mass transfer effects in powders and chips are identical. As the rates for the two particle sizes are identical, it would appear that the macropore structure of the charcoal does not affect the charcoal reactivity within the temperature limits of this study. This does not mean that the solid reaction is not diffusion

FIGURE 23
Rate vs Temperature⁻¹
for Different Pellet Diameters

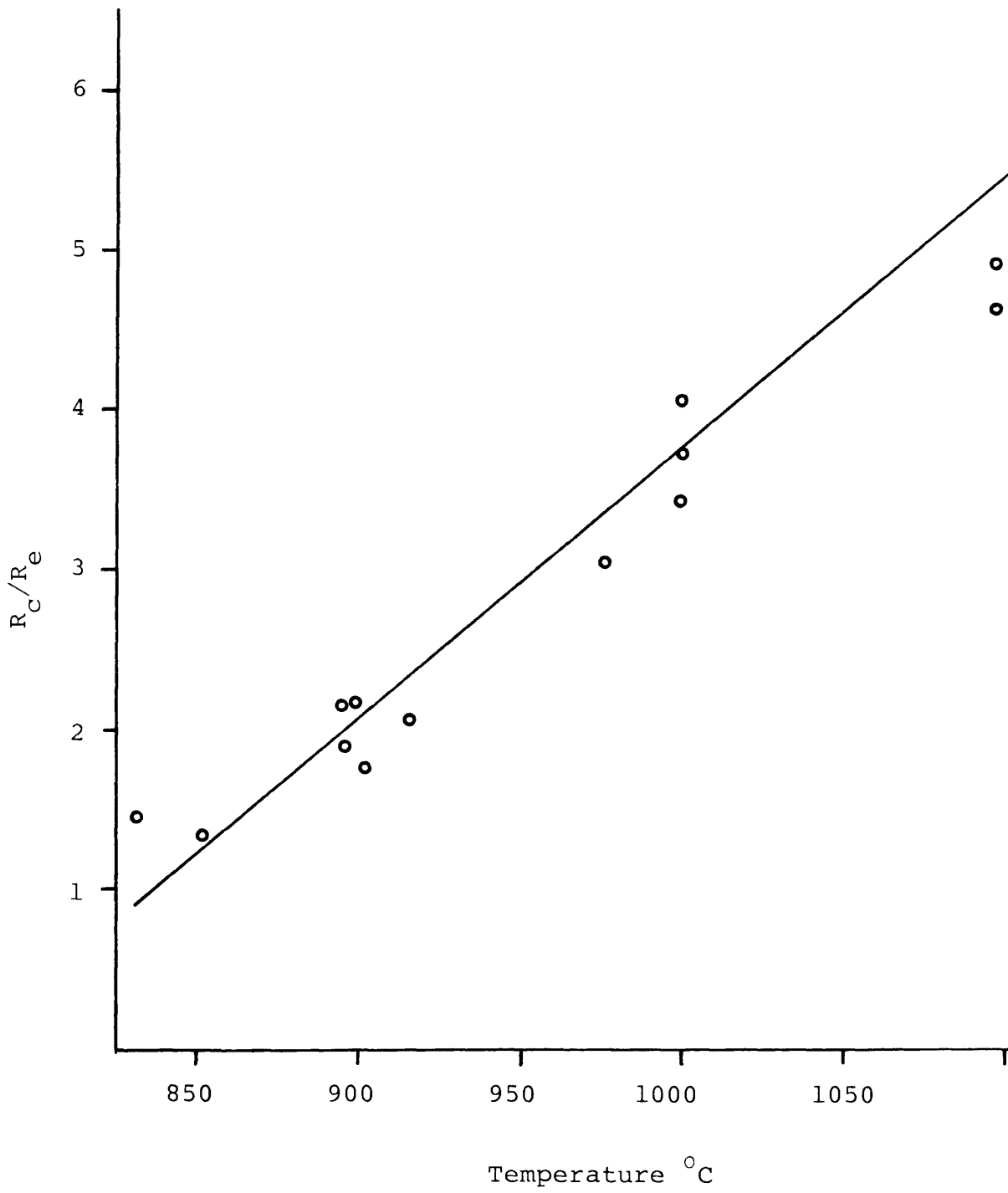


limited; the results suggest that the same micropore structure exists in the powder and the whole pyrolyzed chip.

Rate of gasification for the pellets is much lower than the rate for powders at the same conditions. For a given reaction temperature, the rate decreases as the pellet diameter increases. Runs comparing gasification rates for char powder and crushed pellets indicate that the pelletizing does not change internal structure.

Gasification conditions for the large pellets were such that the CO_2 reactant was not present in large excess. From the experimental data it is possible to calculate the partial pressure of CO in the reaction zone using a material balance around the pellet. With the partial pressure of CO_2 and CO known, it is possible to calculate the reaction rate, using equation 20, for the experimental conditions. Figure 24 represents the ratio of the calculated rate for powders at the corrected P_{CO_2} and the experimental rates as a function of temperature for $\frac{1}{2}$ inch pellets. It is apparent that the effect causing the rate reduction is temperature dependent. To further analyze pellet gasification, it is necessary to determine the significance of heat and mass transfer limitations on the global rate.

FIGURE 24
Ratio of Calculated Rate to Experimental
Rate vs Temperature for
½" pellets



Diffusion

The slope of the rate versus inverse temperature curve for pellets is about the same as that for powder. This suggests that any mass transfer effects which are present are similar and independent of particle size. Therefore, it may be postulated that any mass transfer limitations present occur in the micropores. A char pellet is made up of a large number of individual grains of char. The majority of the macropore structure exists in the void space between grains while most of the micropores are internal to the grains of char.

Effective diffusivity is determined by measuring the adsorption of CO_2 on a char sample as a function of time. As there are negligible mass transfer limitations associated with the macropore structure, the change in the amount of CO_2 adsorbed with the passage of time is related to the diffusion of CO_2 within the individual grains. Concentration of CO_2 within the individual grains is given by equation 45.

$$\frac{\partial C}{\partial t} = \frac{1}{r} \frac{\partial}{\partial r} r \frac{\partial c}{\partial r} \quad 45$$

The change in accumulated CO_2 mass is analogous to heat flow⁽²⁸⁾. The solution for transient heat flow⁽²⁹⁾ can be altered by analogy to give equation 46.

$$\frac{W_{\infty} - W_t}{W_{\infty}} = \frac{1 - \sum_{n=1}^{\infty} \frac{1}{n^2} (1 - \exp(-n^2 \pi^2 Fo))}{1.64493} \quad 46$$

The Fourier Number (Fo) is equal to the product of effective diffusivity and time divided by the square of the particle radius.

Figure 25 represents the weight fraction of CO₂ adsorbed as a function of time at 221°C. The pellet had previously been gasified at 895°C in CO₂. At 0.24 minute $(W_{\infty} - W_t)/W_{\infty} = 0.50$ and F_o equals 0.292. The problem of calculating effective diffusivity now becomes one of deciding what is the radius of the grains of char. The upper limit of particle size in the -20 mesh particle size of the wood chips used to make the pellets.

Table 11 is a tabulation of the effective CO₂ diffusivity for a number of char samples at different temperatures. Also included is the calculated Knudsen diffusivity. The pore size selected for the Knudsen diffusivity is 50 Å. The experimental diffusivities do not exhibit a temperature dependence similar to the $T^{1/2}$ of the Knudsen equation. It is possible that the experimental diffusivity is dependent on the char preparation temperature, but the evidence is inconclusive. Char preparation temperature has a direct effect on the physical properties of char such as pore size distribution and surface area which in turn have an effect on gas diffusion.

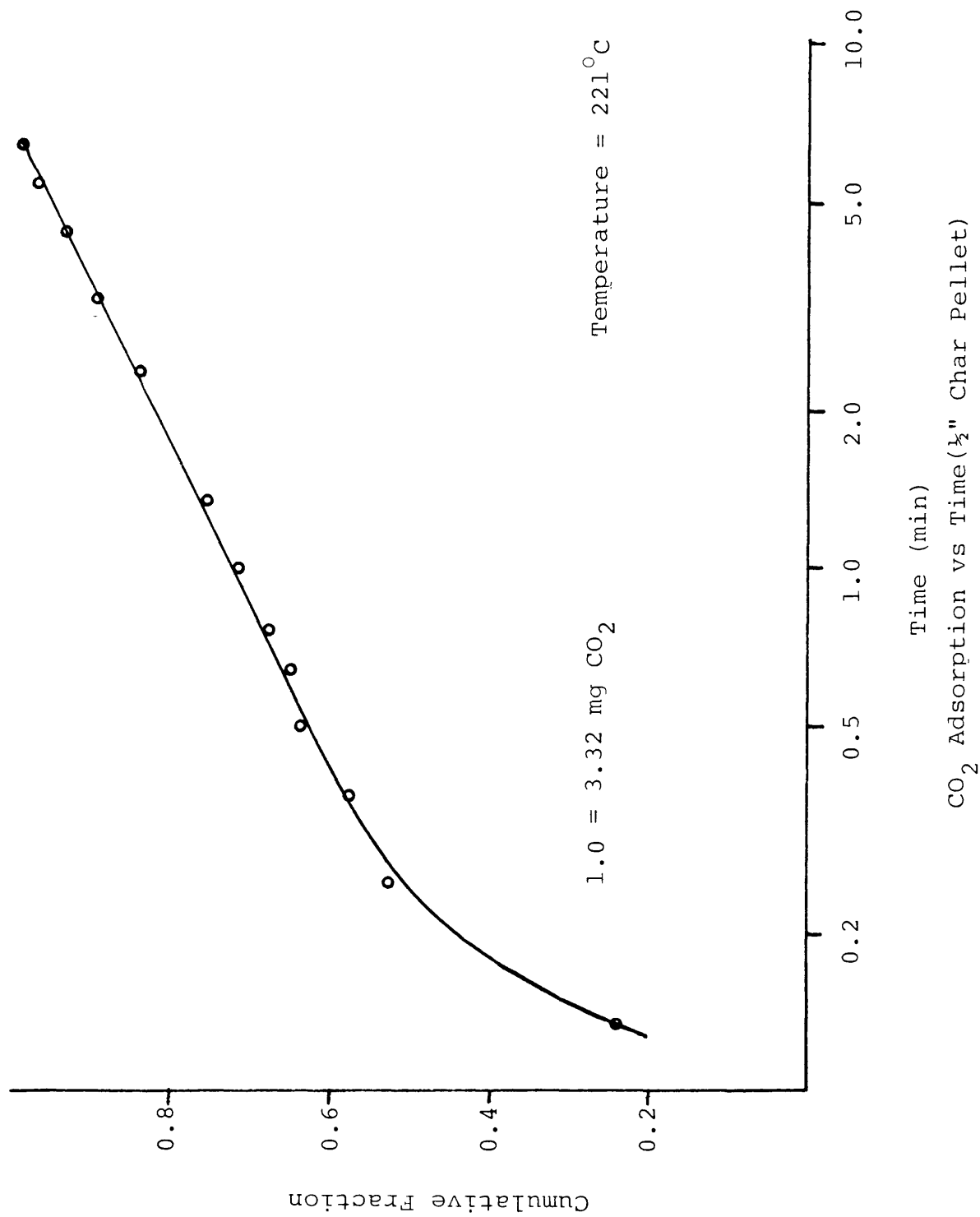


FIGURE 25

Table 11

Effective Diffusivity of CO₂ in Char

Gasification temperature °C	Mass Fraction Char remaining	CO ₂ Adsorption Temperature °C	D _e cm ² /sec	D _k cm ² /sec
740	1.00	22	1.8.10 ⁻⁶	0.013
740	1.00	240	5.5.10 ⁻⁶	0.017
740	1.00	396	3.2.10 ⁻⁶	0.019
895	0.96	221	3.4.10 ⁻⁶	0.016
895	0.96	425	3.1.10 ⁻⁶	0.019
895	0.71	18	2.5.10 ⁻⁶	0.012
895	0.71	157	8.6.10 ⁻⁶	0.015
895	0.71	406	9.2.10 ⁻⁶	0.019
895	0.50	18	3.2.10 ⁻⁶	0.012
895	0.50	160	4.8.10 ⁻⁶	0.015
1000	1.00	79	7.2.10 ⁻⁶	0.014
1000	1.00	207	9.6.10 ⁻⁶	0.016
1000	0.70	19	2.9.10 ⁻⁶	0.010
1000	0.70	150	9.4.10 ⁻⁶	0.015

Mercury intrusion porosimetry was used to determine volume distribution and surface area distribution versus pore size for a number of chars. Table 12 lists the mean pore size based on volume distribution and surface area distribution. The mean volume diameter is orders of magnitude larger than the mean surface area diameter. In Figure 26 cumulative intrusion volume and cumulative surface area have been plotted against pore size for a char pellet gasified at 1100°C to 40% of its initial mass. The major portion of the pore volume is associated with pores 10 microns or greater in diameter, while pore surface area is associated with micropores having diameters of 100 angstroms or less. Incremental pore volume versus pore size is plotted in Figure 27. The volume distribution is essentially bimodal with nodes at 25 and 1.5 microns. A third, small node exists at approximately 600 angstroms. Figure 28 is the incremental surface area distribution. This distribution is also principally bimodal with nodes at 50 and 250 angstroms.

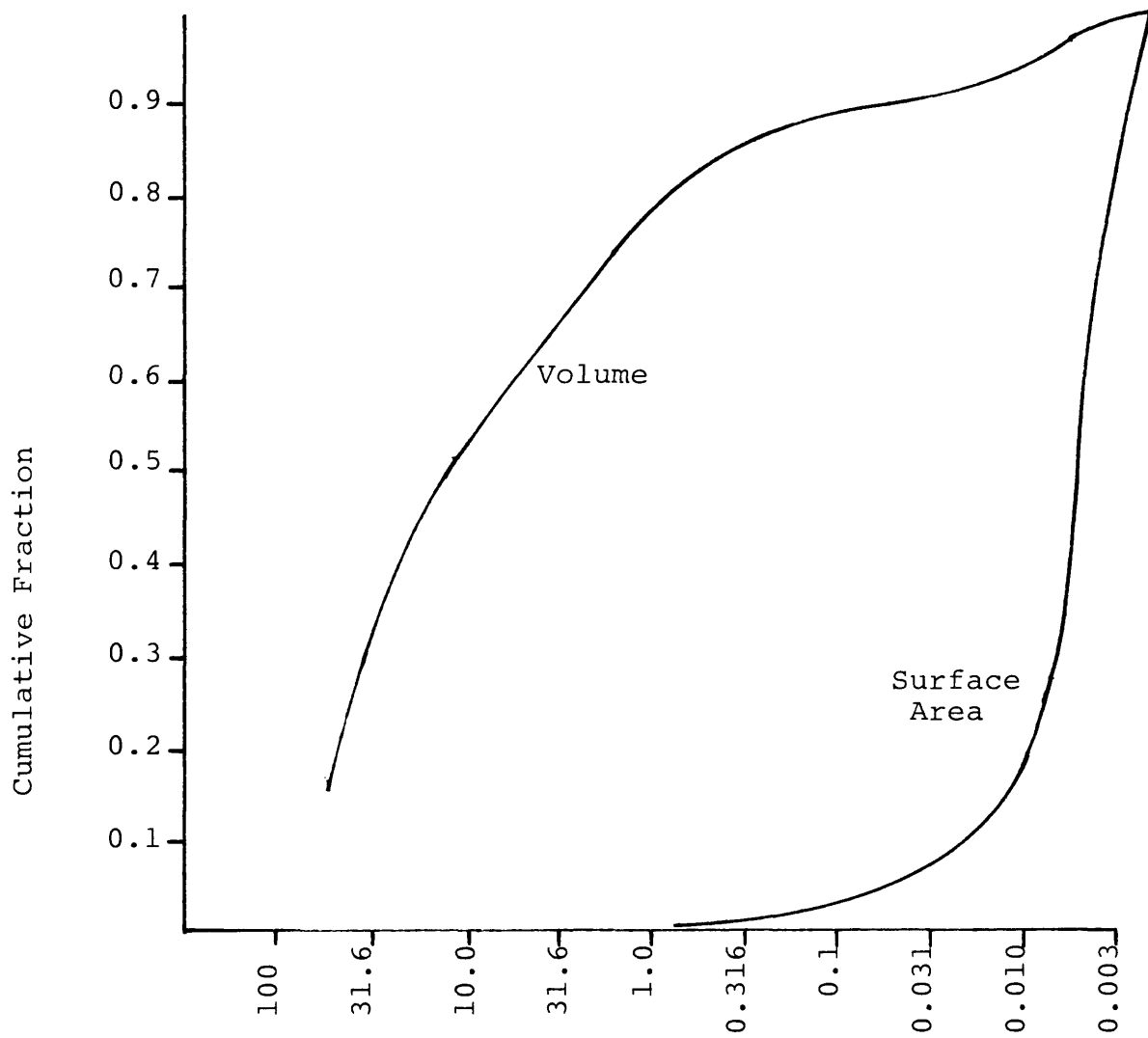
Pore size distribution as determined by intrusion volume and surface area support the assumption that diffusion within a char pellet is controlled by the micropore structure. Carbon dioxide gasification of char is made up of a series of

Table 12

Mean Pore Sizes For Different Chars

Char	Pore Area m ² /gm	Median Pore Size		Apparent Density gm/cc
		Volume	Surface Area	
		Distribution	Distribution	
		microns	microns	
1100°C				
initial				
inventory	51.1	12.4	0.0057	0.45
70%	54.3	13.2	0.0055	0.43
40%	131.8	14.1	0.0052	0.33
1000°C				
initial				
inventory	35.1	21.7	0.0058	0.45
70%	37.8	26.7	0.0045	0.36
900°C				
initial				
inventory	0.5	11.4	2.0993	0.48
50%	61.5	11.7	0.0049	0.32

FIGURE 26
 Cumulative Pore Volume and Surface Area
 vs Pore Size

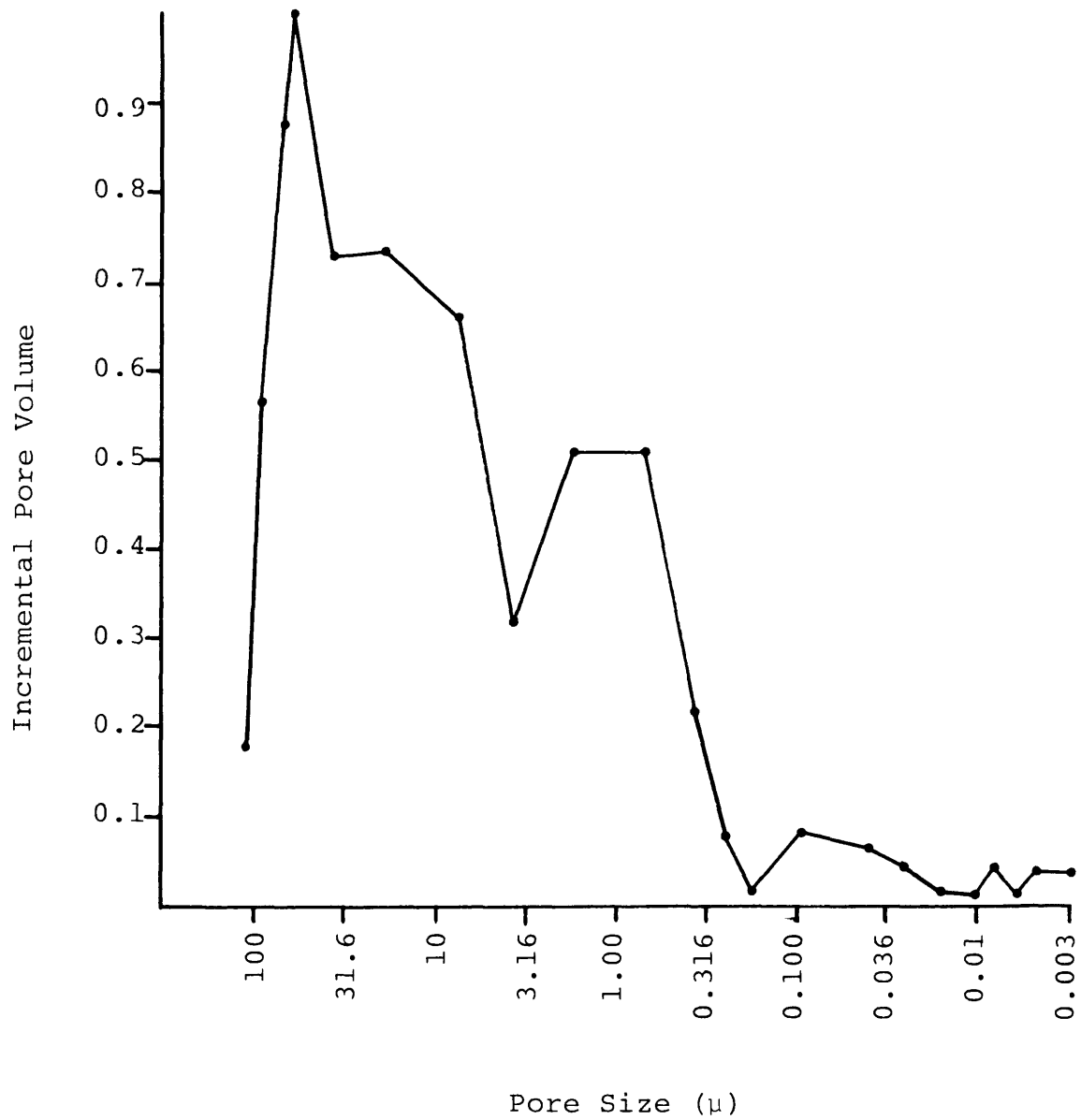


Pore size (microns)

Total Pore Volume 2.27 cm³/gm

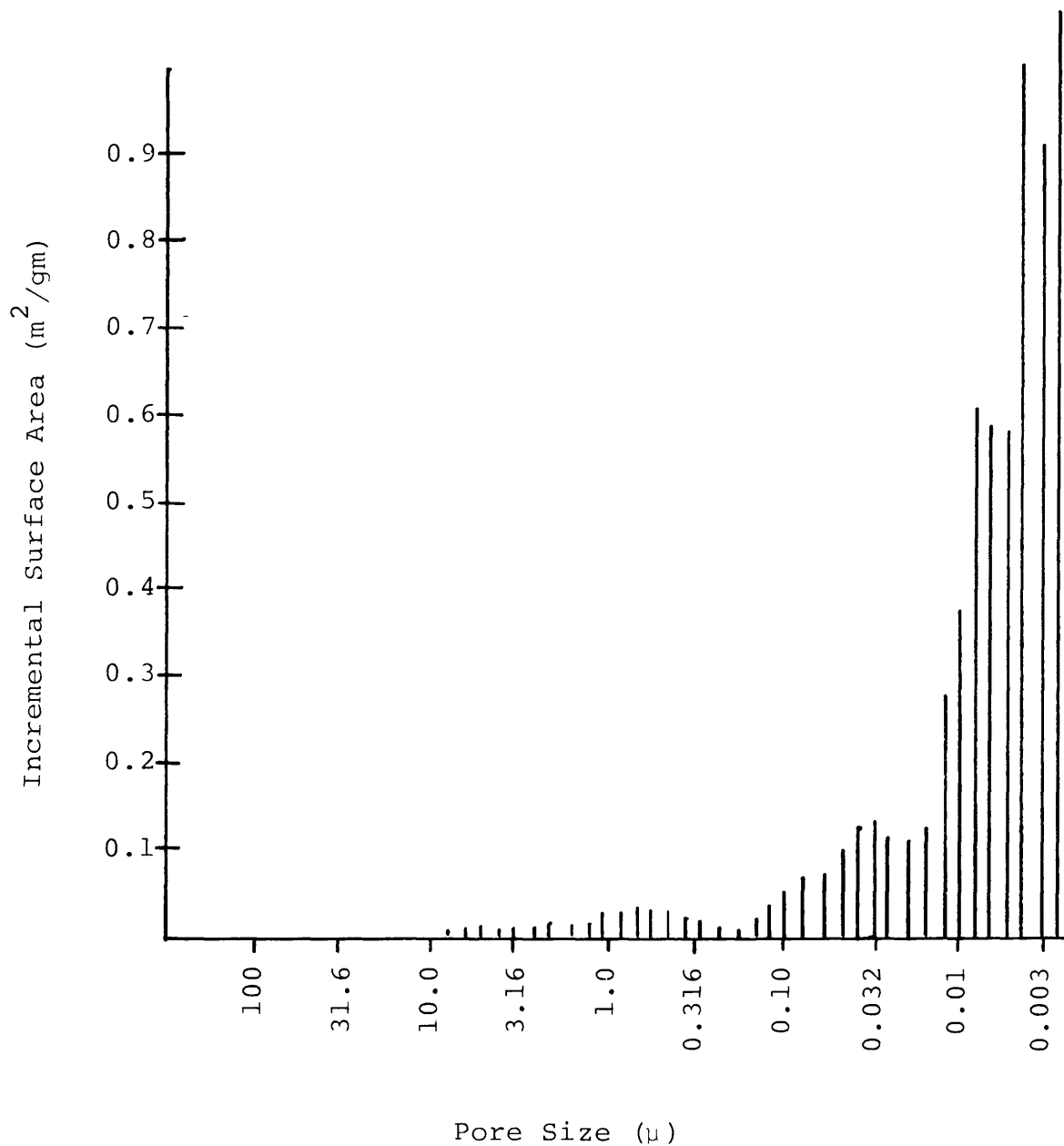
Total Surface Volume 131.8 cm²/gm

FIGURE 27
Incremental Pore Volume
vs Pore Size



Incremental Pore Volume 1.0 = $0.4165 \text{ cm}^3/\text{gm}$

FIGURE 28
 Incremental Surface Area vs Pore Size



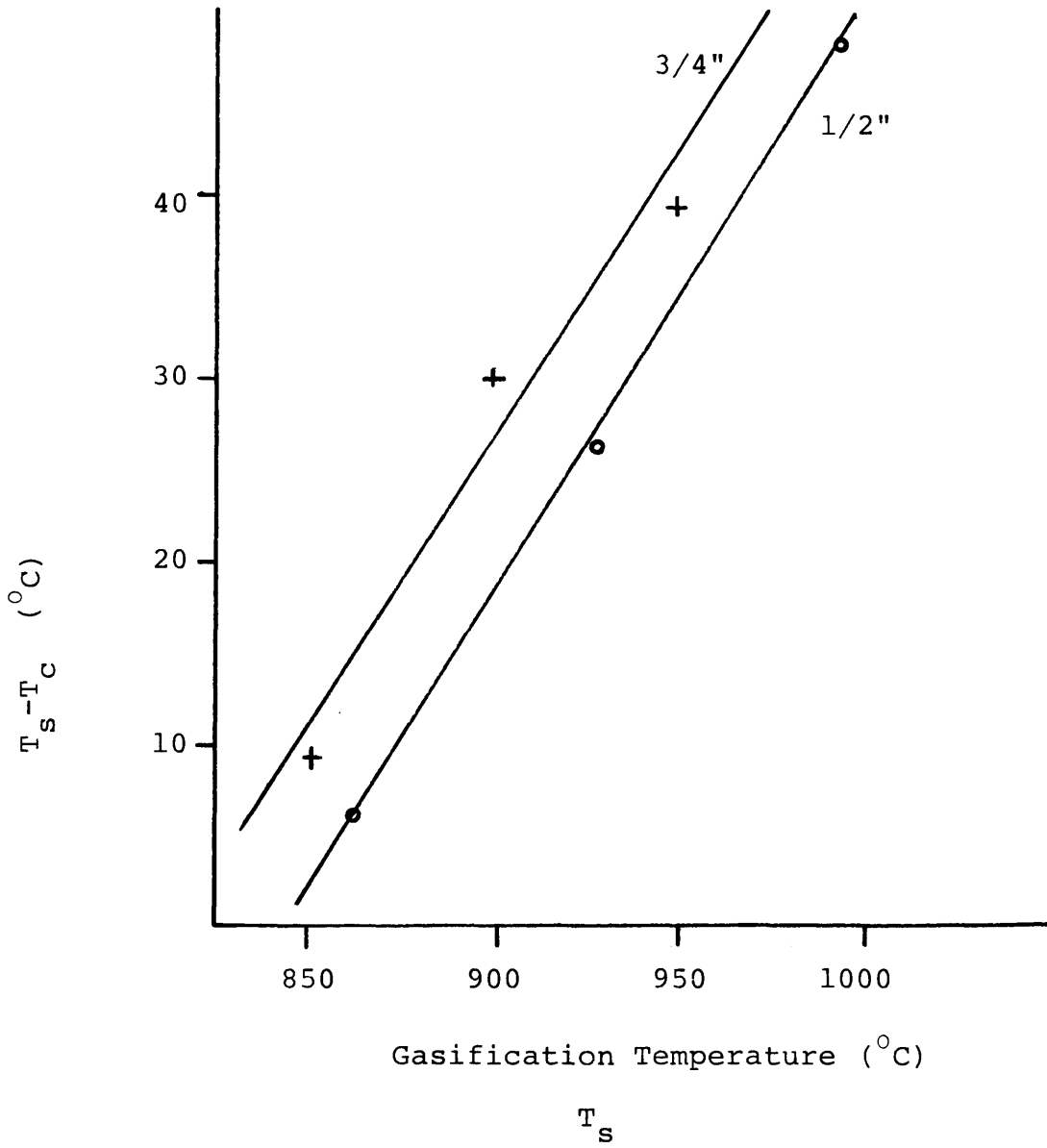
Incremental Surface Area 1.0 = 15.8 m^2/gm

steps involving adsorption, reaction and desorption occurring at active sites on the solid. If these active sites are evenly distributed over the surface, the majority of active sites for the wood char studies would be within the micropore structure. This would indicate that any mass transfer limitations present are due to micropore diffusion.

Heat Transfer

Thermal diffusivity may also affect the global gasification rate of a char pellet. The gasification of char by CO_2 is strongly endothermic. If the thermal diffusivity for a pellet is below some minimum value, the center temperature of the pellet will be less than the surface temperature. Pellet center temperatures were determined experimentally using a thermocouple embedded in the pellet. The results for 3/4 inch and 1/2 pellets are shown in Figure 30 where the temperature difference between the pellet surface and center is plotted against the surface temperature. The center temperature is consistently less than the surface temperature, and for a given temperature the difference increases with pellet diameter. Although the gasification rate at the center of a pellet may be only half the rate at the surface, the thermal gradient probably does not have a significant effect on the global rate for the pellet. This conclusion is based on the fact that the average pellet

FIGURE 29
Radial Temperature Gradient vs Temperature
for $\frac{1}{2}$ " H_e $\frac{3}{4}$ " Pellets



temperature will be higher than the center temperature and that the majority of the pellet mass is located near the surface of the pellet. Also, if the thermal gradient was significant, the apparent activation energy based on the global rate for a pellet would be very different from the activation energy for powders.

While it has been shown that heat transfer and macropore diffusion do not play a significant part in the gasification process, there is a significant difference in the gasification rates for powders and pellets. This loss of reactivity applies to the pellet structure and not to the individual grains that make up the pellet. A pellet that has been ground to a fine powder has the same rate of reaction (at equivalent conditions) as a char powder that does not have a history pelletization. This implies that it is the way the grains in a pellet come together affects the reaction rate. In the pelletization process, heat and pressure are applied which crushes the wood cell structure and redistributes the lignin when the lignin melts. It is postulated that in the pellet making process access to an amount of surface area is lost due to contact points between grains, and while the number of active sites per unit area remains the same, the total number of accessible sites per unit mass decreases.

CONCLUSIONS

1. The apparent principal activation energy for the gasification of ponderosa pine char was determined to be 34.2 kcal/mole.
2. Pretreating the char at a temperature greater than the gasification temperature will reduce the gasification rate. This reduction in rate is due to thermal annealing.
3. The true activation energy for CO₂ gasification of pine char is 53.9 kcal/mole and the pretreatment activation energy is -19.8 kcal/mole.
4. Carbon monoxide retards the CO₂ gasification of pine char. The retarding activation energy is -41.0 kcal/mole.
5. The macropore structure of the pine char does not affect the char reactivity within the temperature limits of this study.
6. The gasification rate for char pellets is lower than the rate for char powder. As pellet diameter increases, the gasification rate decreases.
7. The mass transfer limitation on the gasification rate of pine char pellets and powders is essentially the same as only micropore diffusion is significant.

8. Micropore diffusion takes place within pores in the 50 to 60 angstrom region.
9. The major portion of the pore surface area of pine char is associated with micropores having diameters of 100 angstroms or less. The majority of active sites for gasification are also associated with micropores with diameters of 100 angstroms or less.
10. There is a temperature gradient within a pine char pellet during CO₂ gasification. The temperature gradient has an insignificant effect on the global gasification rate.
11. The decrease in gasification rate when going from powders to pellets is attributed to the effect of the pelletization process on the accessible surface area of the resultant char.

Recommendations For Future Work

1. Development of a gasification model for char pellets that includes heat and mass transfer effects.
2. Investigate the gasification of pine char pellets at higher CO₂ pressures.
3. Determine the effect of catalysts, such as alkali metals, on the gasification rate of pellets.
4. Extend the study of pine char pellets to include gasification by air, oxygen and steam.
5. Optimization of the pelletization process to yield pellets with greater reactivities.
6. Investigate the diffusion mechanisms of char powders and char pellets.

References Cited

1. Freeman, S.D.; "Moving Organic Power Ahead," Proceedings Bio-Energy '80, World Congress and Exposition, 5-7, (1980).
2. Reed, T., Bryant, B.; "Energetics and Economics of Densified Biomass Fuel (DBF) Production," A.I.Ch.E Symposium Series, No. 181, Vol. 74, 26-31, (1978).
3. An Assessment of the Technical and Economic Feasibility of Converting Wood Residues to Liquid and Gaseous Fuel Products Using State-of-the-Art and Advanced Coal Conversion Technology Volume 1 (draft), Gorham International Inc., U.S. Department of Energy, Contract Number DE-AC-2-78ET20075, (1980).
4. Wan, Edward I., Cheng, Michael, "A Comparison of Thermochemical Gasification Technologies for Biomass," Symposium Paper, Energy from Biomass and Wastes, Washington D.C., 781-814, (1978).
5. Desrosiers, R., "Thermodynamics of Gas-Char Reactions," A Survey of Biomass Gasification. Solar Energy Research Institute Report No. TR-33-239. Vol. 2. Chapter 6, (1979)
6. Laurendeau, N.M., "Heterogeneous Kinetics of Coal Char Gasification and Combustion," Prog. Energy Combustion Sci., Vol 4, 221-270, (1978)

7. Menster, M., Ergun, S., U.S. Bur. Mines Bull. (644), 42 pp, (1973).
8. Johnson, J. L., Kinetics of Coal Gasification, New York John Wiley & Sons, (1979).
9. Gol'dberg, E. L. Yarorskii, I.A., "The Mechanism of the Inhibition by Carbon Monoxide of the Reaction of Carbon with CO₂," Solid Fuel Chem, V12, No. 3, 118-120, (1978)
10. Wen, C.Y., Lee, E.S., eds, Coal Conversion Technology, Reading, Massachusetts, Addison-Wesley, (1979)
11. Dutta, S., Wen, C.Y., and Belt, R. J., Am. Chem. Soc., Div. Fuel Chem., Prepr., 20(3), 103-114, (1975)
12. Bjerle, I., Eklund, Hl, Linne, M., and Svensson, O., "Thermogravimetric Analysis of Swedish Shale Char. Kinetics of the Steam-Carbon and Carbon Dioxide-Carbon Reactions," Ind. Eng. Chem. Process Des. Dev., Vol 21 No 1, 141-149, (1982).
13. Desai, N. J., Yang, R. T., "Kinetics of High-Temperature Carbon Gasification Reaction," AIChE Journal, Vol 28 No 2, 237-244, (1982).
14. Yang, R. T. Liu, R., "Gaseous Diffusion in Porous Solids at Elevated Temperatures," Ind. Eng. Chem. Fundam., Vol 21 No 3, 262-268, (1982)
15. Bird, R. B., Steward, W. E., Lightfoot, E. N., Transport Phenomena, New York, John Wiley & Sons, (1960)

16. Groeneveld, M. J., van Swaij, W.P.M., "Gasification of Char Particles with CO_2 and H_2O ," Chem. Eng. Sci., Vol. 35, 307-313, (1980).
17. Wen, C.Y., Galli, A.F., Sears, J.T., The Role of The Char- CO_2 Reaction in Coal Gasification, U.S. Dept. of Energy, Contract No. EX-76-C-01-0497, (1980).
18. Graboski, M.S., "Kinetics of Char Gasification Reactions, "A Survey of Biomass Gasification". Solar Energy Research Institute Report No. TR-33-239. Vol. 2. Chapter 7 (1979).
19. Rensfelt, E. Blomvist, G., Edstrom, C., Engstrom, S., Espenas, B.G., Liinanki, L., "Basic Gasification Studies for Development of Biomass Medium-BTU Gasification Processes, "Energy from Biomass and Waste Symposium", Washington, D.C., 465-494, (1978).
20. Baker, G. A., Oliphant, T.A., "An Implicit Numerical Method for Solving the Two Dimensional Heat Equation," Q. Appl. Math., Vol 17 No 4, P 361, (1960)
21. Srinivas, B., Amundson, N.R., "A single-Particle Char Gasification Model, "AICHE Journal, Vol 26 No 3, p 487, (1980).
22. Johnson, J.L., "Kinetics of Bituminous Coal Char Gasification with Gases Containing Steam and Hydrogen," ACS Adv. Chem. Ser., No 131, p 145, (1974)

23. Haynes, H.W., "An Improved Single Particle Char Gasification Model, "AICHE Journal, Vol 28 No 3, 517-521, (1982).
24. Deblak, K.A., Clark, M.A., Malito, S.T., "Influence of Particle Structure Changes on the Rate of Coal Char Reaction with CO₂, "ACS, Division of Fuel Chemistry Vol 27 No 2, 31-40, (1982).
25. Herman, D.R., "The Rate of Pyrolysis of Densified Ponderosa Pine, "M.S. Thesis, Golden, Colorado, Colorado School of Mines, (1981)
26. Dutta, S., Wen, C.Y., Belt, R.J., "Reactivity of Coal and Char. 1. In a Carbon Dioxide Atmosphere," Ind. Eng. Chem. Process Des. Dev., Vol 18, (1979).
27. Kosowski, G. M., Rose, G. R., Nandi, S. P., Singh, S. P., Development of Biomass Gasification to Produce Substitute Fuels, Progress Report to the Thirteenth Biomass Thermochemical Conversion Contractor's Meeting, Washington, D.C., (1981).
28. Graboski, M.S., Personal Communication, January 10, (1983).
29. Carslaw, H.S., Jaeger, J. C., Conduction of Heat in Solids, Oxford University Press, (1959).

Appendix A

Nomenclature

A	frequency factor	$\text{atm}^{-1} \text{min}^{-1}$
a	relative available surface area	
C	concentration	mole/cm^3
Cp	heat capacity	$\text{cal/gm}^{-\circ}\text{C}$
De	effective diffusivity	cm^2/sec
Dg	gas phase diffusivity	cm^2/sec
Eg	gasification activation energy	kcal/mole
Ep	pretreatment activation energy	kcal/mole
h	heat transfer coefficient	$\text{cal/cm-min}^{-\circ}\text{C}$
hi	ith species heat of formation	cal/mole
k	rate constant	
k_1	rate constant	$\text{atm}^{-1} \text{min}^{-1}$
$k_{2,3,4}$	rate constant	atm^{-1}
N	molar flux	mole/cm-sec
nt	concentration of free active sites	
$P_{\text{CO}_2}, P_{\text{CO}}$	partial pressure	atm
R	gas constant	$\text{cal/mole}^{-\circ}\text{K}$
Ra	reaction rate	$\text{mole/m}^3\text{-sec}$
r	reaction rate	min^{-1}
T	temperature	$^{\circ}\text{K}$
Tb	bulk temperature	$^{\circ}\text{K}$

T_c	pellet center temperature	$^{\circ}\text{k}$
T_g	gasification temperature	$^{\circ}\text{k}$
T_p	preparation temperature	$^{\circ}\text{k}$
T_s	pellet surface temperature	$^{\circ}\text{k}$
W	sample weight	gm
W_o	initial sample weight	gm
X	fractional conversion	
α	relative available surface area	
ϵ	total porosity	
λ	experimental constant	

Appendix B

Powder Gasification Data

Run #15
 $T_g = 1024^\circ\text{C}$
 $T_p = 1024^\circ\text{C}$
 $P_{\text{CO}_2} = 0.81 \text{ atm}$

Sample weight (mg)	Elapsed time (min)
2.55	0
2.27	0.5
1.73	1.0
0.88	1.5
0.03	2.0
0	2.2

Run #16
 $T_g = 1003^\circ\text{C}$
 $T_p = 1003^\circ\text{C}$
 $P_{\text{CO}_2} = 0.81 \text{ atm}$

Sample weight (mg)	Elapsed time (min)
5.78	0
5.43	0.40
4.88	0.80
4.23	1.20
3.57	1.60
2.92	2.00
2.18	2.40
1.49	2.80
0.28	3.40

Run #17
 $T_g = 1042^\circ\text{C}$
 $T_p = 1042^\circ\text{C}$
 $P_{\text{CO}_2} = 0.81 \text{ atm}$

Sample weight (mg)	Elapsed time (min)
3.25	0
3.10	0.28
2.75	0.40
2.41	0.60
2.12	0.80
1.72	1.00
1.37	1.20
1.03	1.40
0.67	1.60
0.34	1.80
0.0	2.00

Run #18
 $T_g = 933^\circ\text{C}$ $T_p = 933^\circ\text{C}$
 $P_{\text{CO}_2} = 0.81 \text{ atm}$

Sample weight (mg)	Elapsed time (min)
6.65	0
6.05	1.0
5.54	2.0
4.82	3.5
4.30	4.5
3.50	6.0
2.98	7.0
2.45	8.0
1.40	10.0
0.44	12.0

Run #19

 $T_g = 850^\circ\text{C}$ $T_p = 850^\circ\text{C}$ $P_{\text{CO}_2} = 0.81 \text{ atm}$

Sample weight (mg)	Elapsed time (min)
3.41	0
3.19	1.0
2.98	2.0
2.80	3.0
2.64	4.0
2.56	4.5

Run #21

 $T_g = 854^\circ\text{C}$ $T_p = 854^\circ\text{C}$ $P_{\text{CO}_2} = 0.81 \text{ atm}$

Sample weight (mg)	Elapsed time (min)
4.09	0
3.87	2.0
3.73	4.0
3.59	6.0
3.47	8.0
3.35	10.0

Run #20

 $T_g = 350^\circ\text{C}$ $T_p = 850^\circ\text{C}$ $P_{\text{CO}_2} = 0.81 \text{ atm}$

Sample weight (mg)	Elapsed time (min)
3.93	0
3.78	1.0
3.61	2.0
3.47	3.0
3.36	4.0
3.25	5.0
3.14	6.0
3.01	7.0
2.91	8.0
2.81	9.0
2.71	10.0
1.64	11.0

Run #22

 $T_g = 1114^\circ\text{C}$ $T_p = 1135^\circ\text{C}$ $P_{\text{CO}_2} = 0.81 \text{ atm}$

Sample weight (mg)	Elapsed time (min)
3.46	0
3.02	0.10
2.52	0.20
2.28	0.24

Run #23

 $T_g = 935^\circ\text{C}$ $T_p = 1105^\circ\text{C}$ $P_{\text{CO}_2} = 0.81 \text{ atm}$

Sample weight (mg)	Elapsed time (min)
3.29	0
2.95	1.0
2.76	2.0
2.57	3.0

Run #24

 $T_g = 900\text{ C}$ $T_p = 900\text{ C}$ $P_{\text{CO}_2} = \text{atm}$

Sample weight (mg)	Elapsed time (min)
14.9	0
13.5	1.0
12.0	2.0
10.6	3.0
9.4	4.0

Run #41

 $P_A = 618\text{ mmHg}$

69 mole % CO

T_g ($^{\circ}\text{C}$)	initial rate (min^{-1})
852	0.011
949	0.039
1047	0.253
1130	1.467

Run #25

 $T_g = 1125\text{ C}$ $T_p = 1125\text{ C}$ $P_{\text{CO}_2} = 0.81\text{ atm}$

Sample weight (mg)	Elapsed time (min)
8.9	0
6.4	0.5
3.4	1.0
0.85	1.5
0	1.8

Run #53

 $P_A = 615\text{ mmHg}$

17.9 mole % CO

T_g ($^{\circ}\text{C}$)	initial rate (min^{-1})
844	0.056
897	0.077
950	0.142
1007	0.431
1102	4.490

Run #28

 $T_g = 850^{\circ}\text{C}$ $T_p = 850^{\circ}\text{C}$ $P_{\text{CO}_2} = 0.81\text{ atm}$

Sample weight (mg)	Elapsed time (min)
6.56	0
6.40	1.0
5.98	2.0
5.68	3.0

Run #54

 $P_A = 613\text{ mmHg}$

31.54 mole % CO

T_g ($^{\circ}\text{C}$)	initial rate (min^{-1})
880	0.066
943	0.082
1002	0.201
1115	2.387

Run #55

 $P_A = 611$ mmHg

31.54 mole % CO

T_g ($^{\circ}\text{C}$)	initial rate (min^{-1})
919	0.064
1013	0.291
1080	0.720

Run #56

 $P_A = 611$ mmHg

45.59 mole % CO

T_g ($^{\circ}\text{C}$)	initial rate (min^{-1})
863	0.050
942	0.100
1019	0.217
1106	1.176

Appendix C

Pellet Gasification Data

Run #	Pellet diameter inch	T _g °C	CO ₂ rate mole/min	Fractional conversion	initial rate min ⁻¹
1	1/2	950	4.46.10 ⁻³	initial	0.029
2	1/2	1040	4.46.10 ⁻³	initial	0.066
3	1/2	850	4.46.10 ⁻³	initial	0.013
4	1/2	810	4.46.10 ⁻³	initial	0.010
9	1/2	993	4.46.10 ⁻³	initial	0.071
8	3/8	1000	4.46.10 ⁻³	initial	0.178
10	1/2	1130	4.46.10 ⁻³	initial	0.143
7	3/8	950	4.46.10 ⁻³	initial	0.047
11	3/8	1050	4.46.10 ⁻³	initial	0.116
12	3/8	1130	4.46.10 ⁻³	initial	0.225
5	3/8	850	4.46.10 ⁻³	initial	0.028
35	3/4	1127	4.46.10 ⁻³	initial	0.086
36	3/4	1000	4.46.10 ⁻³	initial	0.035
43	1/2	853	1.004.10 ⁻²	initial	0.026
43	1/2	928	1.004.10 ⁻²	0.96	0.051
43	1/2	993	1.004.10 ⁻²	0.93	0.072
43	1/2	1096	1.004.10 ⁻²	0.87	0.145
44	1/2	835	1.004.10 ⁻²	initial	0.018
44	1/2	975	1.004.10 ⁻²	0.96	0.064
44	1/2	1097	1.004.10 ⁻²	0.90	0.148
45	1/2	1100	1.004.10 ⁻²	initial	0.115
46	1/2	1000	1.004.10 ⁻²	initial	0.067
47	1/2	900	1.004.10 ⁻²	initial	0.039
48	1/2	900	1.004.10 ⁻²	initial	0.035
48	1/2	900	1.004.10 ⁻²	0.96	0.032
48	1/2	900	1.004.10 ⁻²	0.71	0.035
49	1/2	900	1.004.10 ⁻²	initial	0.071
49	1/2	900	1.004.10 ⁻²	0.70	0.072

Appendix D

CO₂ Adsorption Data

Run #48 A		Run #48 B	
Tp = 900°C Tg = 900°C			
Char weight 497.5 mg		Char weight 491.5 mg	
Fractional conversion-initial		Fractional conversion-initial	
P _A = 618.3 mmHg		P _A = 618.3 mmHg	
Adsorption temperature 22°C		Adsorption temperature 240°C	
Time	Weight CO ₂	Time	Weight CO ₂
(min)	(mg)	(min)	(mg)
0.125	3.10	0.0625	0.45
0.50	18.6	0.125	0.75
1.00	22.7	0.250	1.10
1.50	25.1	0.375	1.15
2.00	27.0	0.500	1.20
2.50	28.3	0.625	1.25
3.00	29.4	0.875	1.39
3.50	30.15	1.00	1.41
4.00	30.80	1.35	1.44
4.50	31.30	1.60	1.46
5.00	31.70	1.85	1.48
5.50	32.00	2.10	1.50
6.00	32.30	2.60	1.53
7.00	32.75	3.10	1.56
9.25	33.30	3.60	1.58
9.75	33.35	4.10	1.60
Final weight	33.35 mg	4.85	1.62
		5.60	1.64
		final weight	1.75 mg

Run #48 C
 Char weight 490.22 mg
 Fractional conversion initial
 $P_A = 618.3$ mmHg
 Adsorption temperature 396°C

Time Weight CO_2

(min)	(mg)
0.0625	0.40
0.125	0.58
0.250	0.72
0.375	0.78
0.500	0.88
0.625	0.99
0.750	1.04
0.875	1.09
1.000	1.12
1.125	1.16
1.500	1.21
1.750	1.25
2.250	1.28
3.250	1.31
4.250	1.35
5.250	1.36
Final weight	1.38 mg

Run #48 D
 Char weight 464.4 mg
 Fractional conversion 0.04
 $P_A = 618.3$ mmHg
 Adsorption temperature 221°C

Time Weight CO_2

(min)	(mg)
0.125	1.14
0.250	1.76
0.375	1.94
0.500	2.06
0.625	2.17
0.750	2.26
0.875	2.32
1.000	2.39
1.125	2.44
1.325	2.51
1.825	2.66
2.325	2.80
3.325	2.98
4.375	3.11
5.325	3.22
6.325	3.29
Final weight	3.32 mg

Run #49 A
 $T_g = 1000^\circ\text{C}$
 Char weight 490.5 mg
 Fractional conversion-initial
 $P_A = 618.3 \text{ mmHg}$
 Adsorption temperature 79°C

Time (min)	Weight CO_2 (mg)
0.10	3.20
0.20	7.20
0.30	8.85
0.40	9.65
0.50	10.15
0.72	10.85
0.92	11.25
1.32	11.85
1.72	12.20
2.72	12.60
3.72	12.90
5.72	13.15
6.72	13.25
7.72	13.35
8.72	13.45
Final weight	13.45 mg

Run #49 B
 Char weight 488.0 mg
 Fractional conversion - initial
 $P_A = 618.3 \text{ mmHg}$
 Adsorption temperature 207°C

Time (min)	Weight CO_2 (mg)
0.10	0.81
0.20	1.35
0.30	1.54
0.40	1.63
0.56	1.71
0.76	1.75
0.96	1.78
1.16	1.81
1.36	1.83
1.56	1.84
2.06	1.87
2.56	1.89
3.06	1.91
Final weight	1.91 mg

Run #49 C
Char weight 353.2 mg
Fractional conversion 0.30
 $P_A = 618.3$ mmHg
Adsorption temperature 19°C

Time (min)	Weight CO_2 (mg)
0.10	2.30
0.30	14.40
0.40	16.40
0.50	17.40
0.60	18.60
0.80	20.30
0.98	21.45
1.48	23.75
1.98	25.20
2.98	26.85
3.48	27.30
3.98	27.60
4.98	28.00
5.98	28.25
6.98	28.35
7.98	28.45
Final weight	28.45 mg

Run #49 D
Char Weight 348.80 mg
Fractional conversion 0.30
 $P_A = 618.3$ mmHg
Adsorption temperature 150°C

Time (min)	Weight CO_2 (mg)
0.10	1.40
0.20	2.45
0.30	2.80
0.36	3.00
0.61	3.20
0.86	3.35
1.11	3.50
Final weight	3.50 mg

Run #48 E
 Char weight 465.04 mg
 Fractional conversion 0.04
 $P_A = 618.3$ mmHg
 Adsorption temperature 425°C

Time (min)	Weight CO_2 (mg)
0.125	0.380
0.250	0.560
0.375	0.615
0.500	0.690
0.625	0.745
0.750	0.800
0.875	0.840
1.000	0.865
1.125	0.890
1.225	0.920
1.475	0.950
1.725	0.980
1.975	1.010
2.225	1.020
2.475	1.035
2.725	1.050
2.975	1.090
3.475	1.105
3.975	1.115
4.475	1.130
Final weight	1.13 mg

Run #48 F
 Char weight 360.65 mg
 Fractional conversion 0.29
 $P_A = 618.3$ mmHg
 Adsorption temperature 18°C

Time (min)	Weight CO_2 (mg)
0.10	2.95
0.20	9.95
0.30	14.85
0.40	16.55
0.44	17.10
0.64	19.05
0.84	20.55
1.04	21.75
1.24	22.75
1.44	23.65
1.64	24.45
2.14	25.75
3.14	27.40
4.14	28.25
5.14	28.70
6.64	29.05
8.14	29.20
12.14	29.35
Final weight	29.35 mg

Run #48 G
 Char weight 356.43 mg
 Fractional conversion 0.29
 $P_A = 618.3$ mmHg
 Adsorption temperature 157°C

Time (min)	Weight CO_2 (mg)
0.10	1.24
0.20	2.19
0.30	2.62
0.40	2.83
0.50	2.96
0.60	3.02
0.70	3.07
0.76	3.11
0.96	3.17
1.16	3.22
1.36	3.27
1.56	3.28
Final weight	3.28 mg

Run #48 H
 Char weight 355.09 mg
 Fractional conversion 0.29
 $P_A = 618.3$ mmHg
 Adsorption temperature 406°C

Time (min)	Weight CO_2 (mg)
0.10	0.19
0.20	0.30
0.30	0.35
0.40	0.37
0.50	0.40
0.60	0.43
0.80	0.47
1.00	0.48
Final Weight	0.48 mg

Run #48 I
 Char weight 256.2 mg
 Fractional conversion 0.50
 $P_A = 618.3$ mmHg
 Adsorption temperature 18°C

Time (min)	Weight CO_2 (mg)
0.10	3.50
0.20	9.60
0.30	11.70
0.40	12.95
0.50	13.90
0.60	14.80
0.80	16.10
1.00	17.10
1.20	18.00
1.40	18.80
1.60	18.95
2.10	20.50
2.60	21.20
3.60	22.05
4.60	22.45
5.60	22.65
7.60	22.85
10.60	22.90
Final weight	22.90 mg

Run #48 J
 Char weight 253.20 mg
 Fractional conversion 0.50
 $P_A = 618.3$ mmHg
 Adsorption temperature 160°C

Time (min)	Weight CO_2 (mg)
0.10	0.65
0.20	1.48
0.30	1.83
0.40	2.02
0.50	2.10
0.58	2.16
0.78	2.23
1.18	2.32
1.58	2.37
2.58	2.41
3.58	2.45
4.58	2.48
5.58	2.50
7.08	2.61
8.08	2.68
Final weight	2.68 mg

Run #48 K
 Char weight 252.34 mg
 Fractional conversion 0.50
 $P_A = 618.3$ mmHg
 Adsorption temperature 402°C

Time (min)	Weight CO_2 (mg)
0.10	0.18
0.20	0.24
0.30	0.26
0.40	0.27
0.50	0.29
1.00	0.30
1.50	0.34
2.00	0.36
Final weight	0.36 mg

APPENDIX E

Mercury Intrusion Porosimeter Data
 The following H_g intrusion data was determined on a micromeritics Auto-Pore 9200.
 All of the following samples were $\frac{1}{2}$ inch pellets gasified in CO_2 .

Wood Char	43	44	45	46	47	48	49
Gasification Temperature C	1100	1100	1100	1000	900	900	1000
% Initial Inventory Remaining	40	70	98	99	100	50	70
Total Intrusion Volume CC/gm	2.2707	1.6062	1.4534	1.5188	0.5620	2.2539	2.0505
Total Pore Area m^2/gm	131.83	54.30	51.08	35.06	0.50	61.54	37.78
Median Pore Diameter (Volume) microns	14.0577	13.2248	12.3644	21.6558	11.3831	11.7069	26.7151
Median Pore Diameter (Area) microns	0.0052	0.0055	0.0057	0.0058	2.0963	0.0049	0.0045
Average Pore Diameter (IV/A) microns	0.0689	0.1183	0.1138	0.1730	4.5001	0.1465	0.2171
Bulk Density gm/CC	0.3344	0.4337	0.4544	0.4450	0.4849	0.3242	0.3595
Apparent (Skeletal) Density gm/CC	1.3890	1.4292	1.3377	1.3690	0.6665	1.2034	1.3681

Wood Char 43

PRESSURE PSIA	PORE DIAMETER MICRO-M	INTRUSION VOLUME CC/G	PORE SURFACE SQ-M/G	MEAN DIAMETER MICRO-M	DV
+1.4	+126.8920	+0.0000	+0.0000	+126.8920	+0.0000
+3.0	+60.8307	+0.4165	+0.0177	+93.3112	-0.4165
+5.0	+36.2834	+0.7241	+0.0431	+48.5570	+0.0076
+9.9	+18.1551	+1.0318	+0.0883	+27.2182	+0.3077
+24.9	+7.2439	+1.3076	+0.1752	+12.6955	+0.2758
+47.8	+3.7755	+1.4402	+0.2714	+5.5097	+0.1028
+97.7	+1.8466	+1.6526	+0.5736	+2.8111	+0.2124
+247.7	+0.7286	+1.8667	+1.2387	+1.2876	+0.2141
+489.8	+0.3611	+1.9603	+1.3259	+0.5449	+0.0026
+745.8	+0.2420	+1.9956	+2.3946	+0.3015	+0.0053
+896.0	+0.1812	+2.0050	+2.5714	+0.2116	+0.0089
+1888.4	+0.0906	+2.0393	+3.5817	+0.1360	+0.0343
+4880.6	+0.0362	+2.0715	+5.6110	+0.0835	+0.0322
+7469.5	+0.0242	+2.0894	+7.9710	+0.0302	+0.0178
+8973.0	+0.0181	+2.0988	+9.7504	+0.0211	+0.0084
+11840.1	+0.0151	+2.1067	+11.6751	+0.0166	+0.0080
+13837.0	+0.0130	+2.1079	+12.0110	+0.0140	+0.0012
+15813.9	+0.0113	+2.1216	+16.5216	+0.0121	+0.0137
+18035.0	+0.0100	+2.1287	+19.1894	+0.0107	+0.0071
+20031.9	+0.0090	+2.1357	+22.0996	+0.0095	+0.0089
+20955.8	+0.0086	+2.1359	+22.1685	+0.0088	+0.0002
+21906.5	+0.0082	+2.1360	+22.2732	+0.0084	+0.0002
+23042.1	+0.0078	+2.1554	+31.9344	+0.0080	+0.0184
+23921.3	+0.0075	+2.1556	+32.0001	+0.0077	+0.0001
+24919.7	+0.0072	+2.1557	+32.0682	+0.0074	+0.0001
+25903.3	+0.0070	+2.1686	+39.3444	+0.0071	+0.0129
+26871.9	+0.0067	+2.1751	+43.1440	+0.0068	+0.0055
+27870.4	+0.0065	+2.1751	+43.1440	+0.0066	+0.0000
+28988.0	+0.0062	+2.1817	+47.2812	+0.0064	+0.0066
+29867.2	+0.0060	+2.1817	+47.3144	+0.0061	+0.0001
+30835.9	+0.0059	+2.1882	+51.6569	+0.0059	+0.0065
+31853.5	+0.0056	+2.1882	+51.6881	+0.0058	+0.0000
+32907.2	+0.0055	+2.2011	+60.9182	+0.0056	+0.0128
+33920.6	+0.0053	+2.2011	+60.9362	+0.0054	+0.0000
+34919.0	+0.0052	+2.2075	+65.2366	+0.0052	+0.0064
+38836.7	+0.0045	+2.2268	+81.6903	+0.0048	+0.0192
+44918.3	+0.0040	+2.2395	+93.5724	+0.0043	+0.0127
+49806.2	+0.0036	+2.2395	+93.5724	+0.0038	+0.0000
+54768.5	+0.0033	+2.2518	+107.8720	+0.0035	+0.0124
+58671.3	+0.0030	+2.2707	+131.8300	+0.0032	+0.0189
+50148.9	+0.0036	+2.2707	+131.8300	+0.0033	+0.0000
+40104.9	+0.0045	+2.2707	+131.8300	+0.0040	+0.0000
+29971.5	+0.0060	+2.2707	+131.8300	+0.0053	+0.0000
+20031.8	+0.0090	+2.2707	+131.8300	+0.0075	+0.0000
+10032.5	+0.0180	+2.2707	+131.8300	+0.0135	+0.0000
+5010.5	+0.0360	+2.2707	+131.8300	+0.0270	+0.0000
+1506.8	+0.1198	+2.1894	+127.6510	+0.0779	-0.0814
+1003.7	+0.1798	+2.1717	+127.1780	+0.1498	-0.0177

Wood Char 43

PRESSURE PSIA	PORE DIAMETER MICRO-M	INTRUSION VOLUME CC/G	PORE SURFACE SQ-M/G	MEAN DIAMETER MICRO-M	DV
+752.7	+0.2398	+2.1559	+126.8780	+0.2098	-0.0158
+497.8	+0.3626	+2.1397	+126.8620	+0.3012	-0.0162
+249.5	+0.7234	+2.1294	+126.5870	+0.5430	-0.0103
+100.7	+1.7929	+2.1076	+126.5170	+1.2581	-0.0218
+75.1	+2.4032	+2.1007	+126.5040	+2.0981	-0.0065
+50.6	+3.5998	+2.1002	+126.5040	+2.9865	-0.0005
+25.5	+7.0757	+2.0934	+126.4980	+5.3228	-0.0038
+15.5	+11.6109	+2.0932	+126.4980	+9.3433	-0.0002
+10.5	+17.2010	+2.0867	+126.4960	+14.4059	-0.0055

Wood Char 44

PRESSURE PSIA	PORE DIAMETER MICRO-M	INTRUSION VOLUME CC/G	PORE SURFACE SQ-M/G	MEAN DIAMETER MICRO-M	DV
+1.4	+125.6950	+0.0000	+0.0000	+125.6950	+0.0000
+3.0	+60.5318	+0.2575	+0.0111	+63.1136	+0.2575
+4.3	+36.6069	+0.4666	+0.0265	+48.5693	+0.2112
+9.9	+18.2222	+0.7030	+0.0626	+27.4145	-0.2343
+24.9	+7.2439	+0.9229	+0.1317	+12.7330	+0.0000
+47.5	+3.8000	+1.0023	+0.1896	+5.5219	+0.0766
+67.6	+1.8483	+1.1681	+0.4237	+2.6242	+0.1653
+247.2	+0.7302	+1.3486	+0.9938	+1.2863	+0.1905
+465.3	+0.3644	+1.4255	+1.5461	+0.5473	+0.0766
+745.3	+0.2422	+1.4560	+1.9476	+0.3033	+0.0304
+995.4	+0.1813	+1.4746	+2.3005	+0.2117	+0.0187
+1999.7	+0.0907	+1.4959	+2.9268	+0.1360	+0.0213
+4980.2	+0.0352	+1.5192	+4.3897	+0.0635	+0.0232
+7468.8	+0.0242	+1.5243	+5.0720	+0.0302	+0.0052
+9957.5	+0.0181	+1.5314	+6.4205	+0.0211	+0.0071
+11939.4	+0.0151	+1.5350	+7.2902	+0.0166	+0.0039
+13921.4	+0.0130	+1.5414	+8.0888	+0.0140	+0.0063
+15933.2	+0.0113	+1.5475	+11.1266	+0.0121	+0.0062
+18064.2	+0.0100	+1.5537	+13.4184	+0.0107	+0.0001
+20016.3	+0.0090	+1.5568	+14.7302	+0.0095	+0.0001
+20985.0	+0.0086	+1.5598	+16.0860	+0.0089	+0.0000
+21932.5	+0.0082	+1.5598	+16.0860	+0.0084	+0.0000
+22966.9	+0.0079	+1.5599	+16.1638	+0.0080	-0.0002
+23965.4	+0.0075	+1.5600	+16.1976	+0.0077	+0.0001
+24963.8	+0.0072	+1.5600	+16.2281	+0.0074	+0.0001
+25932.5	-0.0070	+1.5630	+17.6662	+0.0071	+0.0039
+26916.0	+0.0067	+1.5659	+19.6038	+0.0068	+0.0025
+27914.4	+0.0065	+1.5688	+21.3834	+0.0066	+0.0025
+28898.0	+0.0062	+1.5689	+21.4032	+0.0064	+0.0000
+29896.4	+0.0060	+1.5718	+23.3047	+0.0061	+0.0029
+30954.4	+0.0058	+1.5747	+25.2696	+0.0059	+0.0029
+31863.5	+0.0057	+1.5747	+25.2813	+0.0057	+0.0000
+32891.7	+0.0055	+1.5776	+27.3675	+0.0056	+0.0029
+33864.7	+0.0053	+1.5776	+27.3757	+0.0054	+0.0000
+34863.1	+0.0052	+1.5776	+27.3817	+0.0052	+0.0000
+36836.1	+0.0045	+1.5979	+44.0926	+0.0046	+0.0202
+44917.7	+0.0040	+1.5979	+44.0926	+0.0043	+0.0000
+49775.7	+0.0036	+1.5979	+44.0926	+0.0039	+0.0000
+54812.6	+0.0033	+1.6005	+47.1408	+0.0035	+0.0025
+59700.5	+0.0030	+1.6062	+54.2997	+0.0032	+0.0057
+50193.0	+0.0036	+1.6062	+54.2997	+0.0033	+0.0000
+40029.7	+0.0045	+1.6062	+54.2997	+0.0041	+0.0000
+29955.9	+0.0060	+1.6062	+54.2997	+0.0053	+0.0000
+20046.0	+0.0050	+1.6062	+54.2997	+0.0075	+0.0000
+10046.8	+0.0120	+1.6062	+54.2997	+0.0135	+0.0000
+5024.8	+0.0359	+1.6062	+54.2997	+0.0289	+0.0000
+1506.1	+0.1198	+1.5897	+53.4526	+0.0779	-0.0165
+1002.1	+0.1601	+1.5759	+53.0850	+0.1500	-0.0136

Wood Char 44

PRESSURE PSIA	PORE DIAMETER MICRO-M	INTRUSION VOLUME CC/G	PORE SURFACE SQ-M/G	MEAN DIAMETER MICRO-M	DV
+751.1	+0.2403	+1.5698	+52.9497	+0.2102	-0.0071
+500.1	+0.3609	+1.5586	+52.8140	+0.3006	-0.0102
+201.0	+0.8878	+1.5536	+52.7822	+0.6293	-0.0050
+100.0	+1.8057	+1.5412	+52.7455	+1.3517	-0.0124
+74.9	+2.4101	+1.5412	+52.7455	+2.1079	+0.0000
+49.8	+3.6211	+1.5412	+52.7455	+3.0156	+0.0000
+24.8	+7.2428	+1.5412	+52.7455	+5.4319	+0.0000
+14.8	+12.1896	+1.5412	+52.7455	+9.7162	+0.0000
+9.8	+18.1940	+1.5404	+52.7453	+15.1917	-0.0008

Wood Char 45

PRESSURE PSIA	PORE DIAMETER MICRO-M	INTRUSION VOLUME CC/G	PORE SURFACE SQ-M/G	MEAN DIAMETER MICRO-M	DV
+1.4	+125.6950	+0.0030	+0.0001	+125.6950	+0.0030
+3.0	+60.5318	+0.2497	+0.0107	+93.1138	+0.2467
+4.9	+36.6069	+0.4142	+0.0242	+48.5693	+0.1645
+8.9	+18.2222	+0.6169	+0.0538	+27.4145	+0.2027
+24.9	+7.2439	+0.8227	+0.1185	+12.7330	+0.2057
+47.6	+3.7899	+0.8992	+0.1740	+5.5169	+0.0766
+97.3	+1.8455	+1.0436	+0.3789	+2.9177	+0.1444
+247.3	+0.7297	+1.2093	+0.8936	+1.2876	+0.1657
+495.5	+0.3643	+1.2904	+1.4895	+0.5470	+0.0311
+745.5	+0.2421	+1.3163	+1.8556	+0.3032	+0.0280
+995.6	+0.1613	+1.3314	+2.1030	+0.2117	+0.0131
+1989.9	+0.0907	+1.3530	+2.7391	+0.1360	+0.0216
+4980.4	+0.0362	+1.3707	+3.8545	+0.0635	+0.0177
+7469.0	+0.0242	+1.3819	+5.3254	+0.0302	+0.0111
+9957.7	+0.0181	+1.3832	+5.5835	+0.0211	+0.0014
+11939.6	+0.0151	+1.3669	+6.4667	+0.0166	+0.0037
+13921.6	+0.0130	+1.3504	+7.4565	+0.0140	+0.0035
+15933.4	+0.0113	+1.3366	+9.5259	+0.0121	+0.0063
+18064.4	+0.0100	+1.4028	+11.8529	+0.0107	+0.0062
+20016.5	+0.0090	+1.4060	+13.1855	+0.0095	+0.0032
+20965.2	+0.0086	+1.4061	+13.2283	+0.0089	+0.0001
+21969.7	+0.0082	+1.4062	+13.2691	+0.0084	+0.0011
+22967.1	+0.0079	+1.4092	+14.7674	+0.0080	+0.0030
+23965.6	+0.0075	+1.4093	+14.8016	+0.0077	+0.0001
+24964.0	+0.0072	+1.4123	+16.4243	+0.0074	+0.0031
+25932.6	+0.0070	+1.4152	+18.1082	+0.0071	+0.0003
+26916.2	+0.0067	+1.4153	+18.1330	+0.0066	+0.0000
+27914.6	+0.0065	+1.4183	+19.9403	+0.0066	+0.0030
+28898.2	+0.0062	+1.4212	+21.8086	+0.0064	+0.0030
+29896.6	+0.0060	+1.4242	+23.7366	+0.0061	+0.0030
+30854.6	+0.0058	+1.4242	+23.7553	+0.0059	+0.0000
+31863.7	+0.0057	+1.4272	+25.8117	+0.0057	+0.0030
+32891.9	+0.0055	+1.4301	+27.9294	+0.0056	+0.0030
+33864.8	+0.0053	+1.4301	+27.9379	+0.0054	+0.0000
+34863.3	+0.0052	+1.4331	+30.1672	+0.0052	+0.0029
+39836.3	+0.0045	+1.4390	+35.0350	+0.0048	+0.0059
+44917.8	+0.0040	+1.4418	+37.7335	+0.0043	+0.0029
+49775.6	+0.0036	+1.4418	+37.7335	+0.0039	+0.0000
+54812.8	+0.0033	+1.4534	+51.0808	+0.0035	+0.0115
+59700.7	+0.0030	+1.4534	+51.0808	+0.0032	+0.0000
+50193.2	+0.0036	+1.4534	+51.0808	+0.0033	+0.0000
+40029.9	+0.0045	+1.4534	+51.0808	+0.0041	+0.0000
+29956.1	+0.0060	+1.4534	+51.0808	+0.0053	+0.0000
+20046.2	+0.0090	+1.4534	+51.0808	+0.0075	+0.0000
+10047.0	+0.0160	+1.4534	+51.0808	+0.0135	+0.0000
+5025.0	+0.0359	+1.4534	+51.0808	+0.0269	+0.0000
+1506.3	+0.1198	+1.4306	+49.6118	+0.0779	-0.0228
+1002.3	+0.1801	+1.4225	+49.6952	+0.1499	-0.0081

Wood Char 45

PRESSURE PSIA	PORE DIAMETER MICRO-M	INTRUSION VOLUME CC/G	PORE SURFACE SQ-M/G	MEAN DIAMETER MICRO-M	DV
+751.3	+0.2402	+1.4153	+49.5577	+0.2102	-0.0072
+500.2	+0.3608	+1.4079	+49.4590	+0.3005	-0.0074
+201.2	+0.8969	+1.3969	+49.3892	+0.6288	-0.0110
+100.1	+1.8023	+1.3902	+49.3694	+1.3496	-0.0067
+75.1	+2.4038	+1.3902	+49.3694	+2.1031	+0.0000
+50.0	+3.6074	+1.3898	+49.3688	+3.0056	-0.0004
+25.1	+7.1891	+1.3898	+49.3688	+5.3983	+0.0000
+15.0	+12.0323	+1.3898	+49.3688	+9.6136	+0.0000
+10.1	+17.8643	+1.3898	+49.3688	+14.9517	+0.0000

Wood Char 46

PRESSURE PSIA	PORE DIAMETER MICRO-M	INTRUSION VOLUME CC/G	PORE SURFACE SQ-M/G	MEAN DIAMETER MICRO-M	DV
+1.4	+125.0580	+0.0052	+0.0002	+125.3770	+0.0052
+3.0	+61.1326	+0.3644	+0.0156	+93.0952	+0.3562
+5.0	+36.3369	+0.5893	+0.0341	+48.7347	+0.2245
+9.9	+18.1684	+0.7986	+0.0648	+27.2526	+0.2093
+24.9	+7.2460	+0.9678	+0.1180	+12.7072	+0.1662
+46.7	+3.8611	+1.0241	+0.1586	+5.5535	+0.0533
+66.6	+1.8637	+1.1360	+0.3148	+2.8649	+0.1116
+247.7	+0.7297	+1.2936	+0.8003	+1.2967	+0.1576
+465.4	+0.3643	+1.3766	+1.1077	+0.5465	+0.0830
+743.4	+0.2428	+1.4037	+1.7642	+0.3036	+0.0271
+992.5	+0.1819	+1.4184	+2.0420	+0.2123	+0.0147
+1984.8	+0.0908	+1.4382	+2.5236	+0.1363	+0.0199
+4964.3	+0.0364	+1.4592	+3.3426	+0.0636	+0.0210
+7467.9	+0.0242	+1.4658	+4.1154	+0.0303	+0.0066
+9941.6	+0.0182	+1.4701	+5.6270	+0.0212	+0.0043
+11923.6	+0.0151	+1.4740	+6.5695	+0.0166	+0.0035
+13935.3	+0.0130	+1.4761	+7.1582	+0.0140	+0.0021
+15932.2	+0.0113	+1.4798	+8.3866	+0.0121	+0.0037
+18048.3	+0.0100	+1.4835	+9.7670	+0.0101	+0.0037
+20000.5	+0.0090	+1.4866	+12.0238	+0.0095	+0.0054
+20998.9	+0.0086	+1.4886	+12.0238	+0.0089	+0.0006
+21982.4	+0.0082	+1.4888	+12.0238	+0.0084	+0.0006
+22936.2	+0.0079	+1.4890	+12.0983	+0.0080	+0.0001
+23934.6	+0.0075	+1.4908	+13.0236	+0.0077	+0.0019
+24933.0	+0.0072	+1.4925	+13.9861	+0.0074	+0.0016
+25901.7	+0.0070	+1.4926	+14.0025	+0.0071	+0.0000
+26900.1	+0.0067	+1.4926	+14.0174	+0.0068	+0.0000
+27863.6	+0.0065	+1.4944	+15.0691	+0.0066	+0.0018
+28857.0	+0.0062	+1.4961	+16.1679	+0.0064	+0.0018
+29880.5	+0.0060	+1.4979	+17.3436	+0.0061	+0.0019
+30978.9	+0.0058	+1.4979	+17.0726	+0.0059	+0.0006
+31862.5	+0.0057	+1.5066	+20.0198	+0.0058	+0.0087
+32905.6	+0.0055	+1.5066	+23.4198	+0.0056	+0.0000
+33963.7	+0.0053	+1.5066	+23.4198	+0.0054	+0.0000
+35006.8	+0.0052	+1.5066	+23.4198	+0.0052	+0.0000
+36279.8	+0.0045	+1.5067	+23.4361	+0.0048	+0.0000
+44797.5	+0.0040	+1.5084	+25.0363	+0.0043	+0.0017
+49834.4	+0.0036	+1.5118	+28.6285	+0.0038	+0.0034
+54826.6	+0.0033	+1.5118	+28.6285	+0.0035	+0.0006
+59714.4	+0.0030	+1.5169	+35.0648	+0.0032	+0.0051
+49968.4	+0.0036	+1.5169	+35.0648	+0.0033	+0.0000
+40058.6	+0.0045	+1.5169	+35.0648	+0.0041	+0.0000
+30118.9	+0.0060	+1.5169	+35.0648	+0.0052	+0.0000
+20045.1	+0.0090	+1.5169	+35.0648	+0.0075	+0.0000
+10030.9	+0.0180	+1.5169	+35.0648	+0.0135	+0.0000
+5023.8	+0.0359	+1.5169	+35.0648	+0.0270	+0.0000
+1504.2	+0.1200	+1.5069	+34.5547	+0.0760	-0.0099
+1000.2	+0.1805	+1.5004	+34.3799	+0.1502	-0.0066

Wood Char 46

PRESSURE PSIA	PORE DIAMETER MICRO-M	INTRUSION VOLUME CC/G	PORE SURFACE SQ-M/G	MEAN DIAMETER MICRO-M	DV
+752.1	+0.2400	+1.4844	+34.2653	+0.2102	-0.0060
+499.1	+0.3616	+1.4917	+34.2299	+0.3008	-0.0027
+218.8	+0.8248	+1.4905	+34.2218	+0.5922	-0.0012
+99.1	+1.8211	+1.4847	+34.2043	+1.3230	-0.0058
+74.0	+2.4397	+1.4846	+34.2041	+2.1304	-0.0001
+48.9	+3.6886	+1.4809	+34.1993	+3.0641	-0.0036
+23.9	+7.5592	+1.4808	+34.1992	+5.6239	-0.0001
+13.9	+12.9725	+1.4808	+34.1992	+10.2658	-0.0001
+8.9	+20.2010	+1.4790	+34.1988	+16.5867	-0.0018

Wood Char 47

PRESSURE PSIA	PORE DIAMETER MICRO-M	INTRUSION VOLUME CC/G	PORE SURFACE SQ-M/G	MEAN DIAMETER MICRO-M	DV
+1.4	+125.6960	+0.0000	+0.0000	+125.6960	+0.0000
+3.0	+60.3834	+0.0619	+0.0027	+93.0396	+0.0619
+4.9	+35.3069	+0.1123	+0.0068	+48.4951	+0.0505
+9.9	+18.1551	+0.2005	+0.0197	+27.3809	+0.0832
+24.9	+7.2439	+0.3302	+0.0606	+12.6995	+0.1297
+47.0	+3.8420	+0.3868	+0.1014	+5.5429	+0.0586
+96.6	+1.8636	+0.5067	+0.2654	+2.8553	+0.1200
+246.3	+0.7327	+0.5568	+0.4234	+1.3006	+0.0501
+495.5	+0.3642	+0.5587	+0.4377	+0.5485	+0.0020
+747.5	+0.2414	+0.5606	+0.4628	+0.3028	+0.0019
+995.6	+0.1813	+0.5610	+0.4693	+0.2114	+0.0003
+1391.0	+0.0907	+0.5620	+0.4995	+0.1360	+0.0010
+4964.6	+0.0364	+0.5620	+0.4995	+0.0635	+0.0000
+7468.2	+0.0242	+0.5620	+0.4995	+0.0303	+0.0000
+9956.8	+0.0181	+0.5620	+0.4995	+0.0211	+0.0000
+11923.9	+0.0151	+0.5620	+0.4995	+0.0166	+0.0000
+13935.7	+0.0130	+0.5620	+0.4995	+0.0140	+0.0000
+15902.6	+0.0113	+0.5620	+0.4995	+0.0121	+0.0000
+17969.0	+0.0100	+0.5620	+0.4995	+0.0107	+0.0000
+19956.1	+0.0090	+0.5620	+0.4995	+0.0095	+0.0000
+20909.9	+0.0086	+0.5620	+0.4995	+0.0088	+0.0000
+21906.3	+0.0082	+0.5620	+0.4995	+0.0084	+0.0000
+22906.7	+0.0079	+0.5620	+0.4995	+0.0081	+0.0000
+23890.3	+0.0076	+0.5620	+0.4995	+0.0077	+0.0000
+25007.9	+0.0072	+0.5620	+0.4995	+0.0074	+0.0000
+25672.3	+0.0070	+0.5620	+0.4995	+0.0071	+0.0000
+26669.9	+0.0067	+0.5620	+0.4995	+0.0068	+0.0000
+27869.2	+0.0065	+0.5620	+0.4995	+0.0066	+0.0000
+28971.6	+0.0062	+0.5620	+0.4995	+0.0064	+0.0000
+29880.9	+0.0060	+0.5620	+0.4995	+0.0061	+0.0000
+30939.0	+0.0058	+0.5620	+0.4995	+0.0059	+0.0000
+31937.4	+0.0057	+0.5620	+0.4995	+0.0057	+0.0000
+32891.2	+0.0055	+0.5620	+0.4995	+0.0056	+0.0000
+33919.4	+0.0053	+0.5620	+0.4995	+0.0054	+0.0000
+34873.1	+0.0052	+0.5620	+0.4995	+0.0052	+0.0000
+39969.6	+0.0045	+0.5620	+0.4995	+0.0048	+0.0000
+44812.8	+0.0040	+0.5620	+0.4995	+0.0043	+0.0000
+49805.0	+0.0036	+0.5620	+0.4995	+0.0038	+0.0000
+54797.2	+0.0033	+0.5620	+0.4995	+0.0035	+0.0000
+59700.0	+0.0030	+0.5620	+0.4995	+0.0032	+0.0000
+50192.5	+0.0036	+0.5456	-19.3635	+0.0033	-0.0164
+40029.2	+0.0045	+0.5456	-19.3635	+0.0041	+0.0000
+30119.3	+0.0060	+0.5456	-19.3635	+0.0053	+0.0000
+20075.3	+0.0090	+0.5456	-19.3635	+0.0075	+0.0000
+10046.2	+0.0180	+0.5456	-19.3635	+0.0135	+0.0000
+5009.3	+0.0360	+0.5456	-19.3635	+0.0270	+0.0000
+1504.6	+0.1200	+0.5456	-19.3635	+0.0780	+0.0000
+999.6	+0.1806	+0.5456	-19.3635	+0.1503	+0.0000

PRESSURE PSIA	PORE DIAMETER MICRO-M	INTRUSION VOLUME CC/G	PORE SURFACE SQ-M/G	MEAN DIAMETER MICRO-M	DV
+748.5	+0.2411	+0.5456	-19.3635	+0.2108	+0.0000
+499.4	+0.3614	+0.5456	-19.3635	+0.3012	+0.0000
+247.6	+0.7289	+0.5456	-19.3635	+0.5451	+0.0000
+99.1	+1.8219	+0.5456	-19.3635	+1.2754	+0.0000
+74.0	+2.4386	+0.5456	-19.3635	+2.1302	+0.0000
+49.0	+3.6813	+0.5456	-19.3635	+3.0600	+0.0000
+24.1	+7.5040	+0.5456	-19.3635	+5.5926	+0.0000
+14.2	+12.7443	+0.5456	-19.3635	+10.1241	+0.0000
+9.2	+19.6530	+0.5456	-19.3635	+16.1986	+0.0000

Wood Char 48

PRESSURE PSIA	PORE DIAMETER MICRO-M	INTRUSION VOLUME CC/G	PORE SURFACE SQ-M/G	MEAN DIAMETER MICRO-M	DV
+1.4	+126.3410	+0.0075	+0.0002	+126.3400	+0.0075
+3.0	+60.3834	+0.3444	+0.0147	+93.3519	+0.3368
+5.0	+36.3908	+0.6587	+0.0407	+48.3870	+0.3144
+9.9	+19.1634	+0.9937	+0.0857	+27.2795	+0.3069
+14.9	+12.1123	+1.1155	+0.1232	+15.1404	+0.1498
+19.9	+9.0708	+1.2016	+0.1578	+10.3916	+0.0861
+24.9	+7.2460	+1.2633	+0.1890	+8.1584	+0.0637
+27.5	+6.5731	+1.2653	+0.1890	+6.9096	+0.0000
+32.4	+5.3723	+1.3158	+0.2222	+6.0727	+0.0505
+37.5	+4.8151	+1.3570	+0.2540	+5.1937	+0.0412
+47.4	+3.8082	+1.4357	+0.3270	+4.3121	+0.0787
+72.2	+2.4983	+1.5857	+0.5172	+3.1539	+0.1500
+87.2	+1.8538	+1.6982	+0.7238	+2.1777	+0.1125
+147.1	+1.2233	+1.8410	+1.0943	+1.5418	-0.1427
+197.0	+0.9131	+1.9123	+1.3616	+1.0715	-0.0716
+246.3	+0.7303	+1.9430	+1.5035	+0.8235	+0.0304
+297.3	+0.6039	+1.9734	+1.6916	+0.6384	+0.0304
+348.7	+0.5176	+1.9984	+1.8548	+0.5618	+0.0229
+399.5	+0.4552	+2.0135	+2.0123	+0.4864	+0.0191
+446.3	+0.4044	+2.0309	+2.1557	+0.4298	+0.0154
+497.1	+0.3631	+2.0428	+2.2772	+0.3837	+0.0117
+595.7	+0.3030	+2.0921	+2.5117	+0.3330	+0.0135
+595.4	+0.2596	+2.0741	+2.3623	+0.2913	+0.0120
+795.0	+0.2270	+2.0786	+2.7353	+0.2433	+0.0045
+894.6	+0.2017	+2.0888	+2.6084	+0.2144	+0.0082
+894.3	+0.1815	+2.0986	+3.1564	+0.1816	+0.0119
+1194.5	+0.1511	+2.1073	+3.3660	+0.1663	+0.0087
+1391.8	+0.1297	+2.1084	+3.3372	+0.1404	-0.0011
+1594.0	+0.1132	+2.1244	+3.3240	+0.1215	+0.0160
+1799.4	+0.1003	+2.1244	+3.9240	+0.1071	+0.0000
+1990.6	+0.0907	+2.1244	+3.9240	+0.0953	+0.0000
+2484.3	+0.0726	+2.1353	+4.4672	+0.0817	+0.0111
+2681.1	+0.0605	+2.1443	+5.0086	+0.0663	-0.0090
+3482.1	+0.0518	+2.1488	+5.3683	+0.0562	+0.0050
+3663.7	+0.0455	+2.1544	+5.7645	+0.0487	+0.0048
+4680.0	+0.0382	+2.1600	+6.3091	+0.0409	+0.0056
+5373.5	+0.0302	+2.1614	+6.4750	+0.0332	+0.0014
+5373.8	+0.0259	+2.1624	+6.6305	+0.0260	+0.0011
+7360.4	+0.0227	+2.1671	+7.3604	+0.0243	+0.0046
+8953.9	+0.0201	+2.1713	+8.2248	+0.0214	+0.0045
+8957.3	+0.0181	+2.1733	+9.1331	+0.0191	+0.0043
+14318.7	+0.0121	+2.1833	+14.5976	+0.0151	+0.0206
+20001.3	+0.0080	+2.2049	+17.7831	+0.0106	+0.0084
+24918.0	+0.0072	+2.2031	+19.8585	+0.0081	+0.0042
+26881.3	+0.0060	+2.2189	+24.5130	+0.0066	+0.0077
+39910.4	+0.0045	+2.2232	+33.0687	+0.0053	+0.0113
+49745.8	+0.0036	+2.2332	+43.9340	+0.0041	+0.0110
+59700.4	+0.0030	+2.2339	+61.5485	+0.0033	+0.0146

Wood Char 48

PRESSURE PSIA	PORE DIAMETER MICRO-M	INTRUSION VOLUME CC/G	PORE SURFACE SQ-M/G	MEAN DIAMETER MICRO-M	DV
+50133.2	+0.0036	+2.2539	+61.5485	+0.0033	+0.0000
+40104.1	+0.0045	+2.2539	+61.5485	+0.0041	+0.0000
+30104.8	+0.0060	+2.2539	+61.5485	+0.0052	+0.0000
+20105.5	+0.0090	+2.2539	+61.5485	+0.0075	+0.0000
+10046.3	+0.0180	+2.2539	+61.5485	+0.0135	+0.0000
+5024.7	+0.0359	+2.2539	+61.5485	+0.0269	+0.0000
+2511.2	+0.0719	+2.2367	+60.2711	+0.0539	-0.0170
+1505.0	+0.1199	+2.2176	+59.4744	+0.0959	-0.0191
+1003.0	+0.1800	+2.2072	+59.1986	+0.1499	-0.0103
+500.9	+0.3603	+2.1848	+58.8671	+0.2701	-0.0224
-249.8	+0.7224	+2.1751	+58.7950	+0.5414	-0.0098
+99.5	+1.8136	+2.1699	+58.7784	+1.2380	-0.0053
+74.6	+2.4190	+2.1659	+58.7708	+2.1163	-0.0040
+49.9	+3.6204	+2.1618	+58.7635	+3.0197	-0.0040
+24.7	+7.2999	+2.1573	+58.7625	+5.4596	-0.0040
+14.7	+12.2826	+2.1539	+58.7609	+9.7908	-0.0039
-9.7	+18.5623	+2.1539	+58.7609	+15.4324	-0.0001

Wood Char 49

PRESSURE PSIA	PORE DIAMETER MICRO-M	INTRUSION VOLUME CC/G	PORE SURFACE SQ-M/G	MEAN DIAMETER MICRO-M	DV
+1.4	+125.3330	+0.0013	+0.0001	+125.3330	+0.0016
+3.0	+80.2358	+0.5838	+0.0255	+92.9658	+0.5920
+5.0	+38.4444	+0.8014	+0.0510	+48.3400	+0.3078
+9.5	+13.1933	+1.1333	+0.0850	+27.3133	+0.2324
+15.0	+12.0707	+1.2230	+0.1099	+15.1330	+0.0942
+19.9	+8.0708	+1.2348	+0.1313	+10.5708	+0.0568
+24.8	+7.2366	+1.3270	+0.1521	+8.1552	+0.0424
+25.8	+6.9552	+1.3270	+0.1521	+7.0974	+0.0000
+31.0	-5.8175	+1.3492	+0.1650	+6.3863	+0.0222
+35.8	+5.0208	+1.3790	+0.1881	+5.4192	+0.0239
+45.7	+3.8525	+1.4293	+0.2329	+4.4867	+0.0503
+70.4	+2.5524	+1.5346	+0.3622	+3.2574	+0.1053
+85.7	+1.8881	+1.6184	+0.5093	+2.2242	+0.0815
+145.0	+1.2447	+1.7265	+0.7907	+1.5654	+0.1101
+155.0	+0.8257	+1.7827	+1.0348	+1.0852	+0.0862
+245.1	+0.7384	+1.8239	+1.1943	+0.8311	+0.0332
+285.8	+0.6100	+1.8497	+1.3355	+0.6732	+0.0235
+345.8	+0.5222	+1.8750	+1.5144	+0.5661	+0.0253
+388.5	+0.4587	+1.8883	+1.6311	+0.4904	+0.0143
+445.2	+0.4054	+1.9036	+1.7637	+0.4321	+0.0143
+494.0	+0.3653	+1.9132	+1.8633	+0.3854	+0.0068
+592.7	+0.3045	+1.9277	+2.0382	+0.3349	+0.0145
+683.3	+0.2603	+1.9343	+2.1297	+0.2824	+0.0068
+782.8	+0.2275	+1.9440	+2.2362	+0.2440	+0.0067
+883.5	+0.2020	+1.9474	+2.3531	+0.2148	+0.0034
+882.1	+0.1819	+1.9324	+2.4570	+0.1820	+0.0050
+1180.4	+0.1516	+1.9592	+2.6193	+0.1668	+0.0033
+1380.8	+0.1268	+1.9823	+2.7224	+0.1407	+0.0036
+1588.8	+0.1136	+1.9984	+2.8393	+0.1217	+0.0036
+1787.2	+0.1010	+1.9713	+3.0295	+0.1072	+0.0051
+1988.4	+0.0898	+1.9713	+3.0448	+0.0955	+0.0004
+2484.6	+0.0726	+1.9789	+3.3899	+0.0817	+0.0071
+2874.1	+0.0607	+1.9842	+3.7107	+0.0667	+0.0053
+3473.8	+0.0519	+1.9848	+3.7469	+0.0563	+0.0006
+3884.5	+0.0453	+1.9813	+4.3031	+0.0467	+0.0067
+4882.3	+0.0381	+1.9834	+4.6333	+0.0408	+0.0033
+5881.2	+0.0301	+1.9882	+5.1332	+0.0331	+0.0037
+6874.7	+0.0258	+2.0012	+5.4235	+0.0280	+0.0020
+7858.3	+0.0227	+2.0013	+5.4836	+0.0243	+0.0004
+8858.7	+0.0202	+2.0034	+5.8336	+0.0214	+0.0013
+8855.1	+0.0181	+2.0069	+6.5429	+0.0161	+0.0034
+14832.4	+0.0121	+2.0186	+8.3337	+0.0151	+0.0118
+20014.0	+0.0089	+2.0206	+10.4039	+0.0106	+0.0020
+24813.6	+0.0072	+2.0255	+12.8238	+0.0081	+0.0048
+28884.1	+0.0060	+2.0272	+13.8328	+0.0066	+0.0017
+38833.0	+0.0045	+2.0335	+18.8230	+0.0053	+0.0063
+48788.3	+0.0038	+2.0397	+24.7186	+0.0041	+0.0062
+58713.1	+0.0030	+2.0505	+37.7833	+0.0033	+0.0109

Wood Char 49

PRESSURE PSIA	PORE DIAMETER MICRO-M	INTRUSION VOLUME CC/G	PORE SURFACE SQ-M/G	MEAN DIAMETER MICRO-M	DV
-50041.3	+0.0036	+2.0505	+37.7833	+0.0033	+0.0000
+40012.5	+0.0045	+2.0505	+37.7833	+0.0041	+0.0000
+30102.6	+0.0060	+2.0505	+37.7833	+0.0053	+0.0000
+20073.3	+0.0080	+2.0505	+37.7833	+0.0073	+0.0000
+10044.4	+0.0180	+2.0505	+37.7833	+0.0135	+0.0000
+5022.5	+0.0353	+2.0505	+37.7833	+0.0270	+0.0000
+2513.1	+0.0718	+2.0418	+37.1310	+0.0539	-0.0033
+1504.8	+0.1189	+2.0322	+36.7310	+0.0859	-0.0038
+889.8	+0.1805	+2.0247	+36.5319	+0.1502	-0.0075
+498.7	+0.3613	+2.0200	+36.4627	+0.2712	-0.0047
+247.1	+0.7304	+2.0128	+36.4097	+0.5462	-0.0072
+85.3	+1.3841	+2.0050	+36.3891	+1.3073	-0.0038
+72.5	+2.4885	+2.0073	+36.3851	+2.1866	-0.0017
+47.5	+3.7980	+2.0056	+36.3829	+3.1437	-0.0017
+22.5	+8.0050	+2.0024	+36.3607	+5.8015	-0.0033
+12.3	+14.3233	+1.9845	+36.3379	+11.1651	-0.0078
+7.3	+23.3343	+1.9697	+36.3363	+18.3848	-0.0047

APPENDIX F

Effective Diffusivity Calculation

The following is the derivation of the solution (equation 46) to equation 45 which is used to determine effective diffusivity from experimental data. The solution is arrived at by analogy to the heat transfer problem for a sphere where it is desired to know what fraction of the energy transferred at time equals infinity has been transferred at a given time t .

$$\frac{1}{r} \frac{\partial}{\partial r} r \frac{\partial C}{\partial r} = \frac{\partial C}{\partial t} \quad 45$$

$$@ \quad r = 0 \quad \frac{\partial C}{\partial r} = 0$$

$$@ \quad r = R \quad C = C_0$$

Analogous heat transfer problem is:

$$\frac{1}{r} \frac{\partial}{\partial r} r \frac{\partial T}{\partial r} = \frac{\partial T}{\partial t}$$

$$@ \quad r = 0 \quad \frac{\partial T}{\partial r} = 0$$

$$@ \quad r = R \quad T = T_0$$

The solution to the heat transfer problem is:

$$\Theta = \frac{T - T_{\infty}}{T_0 - T_{\infty}} = 2 \sum_{n=1}^{\infty} (-1)^{n+1} e^{-\beta^2 Fo} \frac{\sin \beta r^*}{\beta r^*}$$

$$\beta = n\pi \quad r^* = r/R \quad Fo = \frac{\alpha t}{R^2}$$

Cumulative heat absorbed up to time t is:

$$Q(t) = \int_0^t -k \frac{\partial T}{\partial r} \Big|_{r=R} dF_0$$

Expressed in terms of θ , the cumulative heat becomes:

$$Q(t) = \frac{-k(T_0 - T_{\infty})}{R^2} \int_0^{Fo} \frac{\partial \theta}{\partial r^*} \Big|_{r^*=1} dF_0$$

The fraction of the heat absorbed at time t is:

$$\frac{Q(t)}{Q(\infty)} = \frac{\int_0^{Fo} \frac{\partial \theta}{\partial r^*} \Big|_{r^*=1} dF_0}{\int_0^{\infty} \frac{\partial \theta}{\partial r^*} \Big|_{r^*=1} dF_0}$$

Surface flux in terms of θ is:

$$\frac{\partial \theta}{\partial r^*} \Big|_{r^*=1} = 2 \sum_{n=1}^{\infty} (-1)^{n+1} e^{-\beta^2 Fo} \frac{\cos \beta - \sin \beta}{\beta}$$

which reduces to

$$\frac{\partial \theta}{\partial r^*} \Big|_{r^*=1} = 2 \sum_{n=1}^{\infty} e^{-\beta^2 Fo}$$

Cumulative heat transferred at time t is now:

$$Q(t) = \sum_{n=1}^{\infty} \frac{2}{\beta^2} e^{-\beta^2 Fo} - 1$$

and cumulative heat transfer at time ∞ is:

$$Q(\infty) = \sum_{n=1}^{\infty} \frac{-2}{\beta^2}$$

$$\frac{Q(t)}{Q(\infty)} = \frac{\sum_{n=1}^{\infty} \frac{2}{\beta^2} e^{-\beta^2 Fo} - 1}{\sum_{n=1}^{\infty} \frac{-2}{\beta}}$$

$$\frac{Q(t)}{Q(\infty)} = \frac{\sum_{n=1}^{\infty} \frac{2}{\beta} e^{-\beta^2 Fo} - 1}{1.64493}$$

This final equation is used to calculate the effective diffusivity where

$$Fo = \frac{D_e t}{R^2}$$

To calculate the effective diffusivity, a point is picked off the plot cumulative fraction CO_2 absorbed versus time (Figure 25) and then the dimensionless time (Fo) is found that corresponds to the fractional mass accumulation. Knowing t and R, the effective diffusivity can be calculated.